MODELING AND CONTROL OF LINEAR MOTOR FEED DRIVES FOR GRINDING MACHINES

A Dissertation
Presented to
The Academic Faculty

By

Qiulin Xie

In Partial Fulfillment
of the Requirements for the Degree
of Doctor of Philosophy in the
George W. Woodruff School of Mechanical Engineering

Georgia Institute of Technology
May, 2008

MODELING AND CONTROL OF LINEAR MOTOR FEED DRIVES FOR GRINDING MACHINES

Approved by:

Dr. Steven Y. Liang, Advisor
George W. Woodruff School of
Mechanical Engineering
Georgia Institute of Technology

Dr. Shreyes N. Melkote
George W. Woodruff School of
Mechanical Engineering
Georgia Institute of Technology

Dr. David Taylor
School of Electrical and Computer
Engineering
Georgia Institute of Technology

Dr. Chen Zhou
H. Milton Stewart School of
Industrial and Systems Engineering
Georgia Institute of Technology

Dr. Min Zhou
George W. Woodruff School of
Mechanical Engineering
Georgia Institute of Technology

Date Approved: 12/05/2007

To my family

ACKNOWLEDGEMENTS

I would, first of all, like to thank my advisor Dr. Steven Liang for all the support, guidance and encouragement throughout the course of my graduate study. I would also like to thank the members of my thesis committee, Professors Shreyes Melkote, David Taylor, Chen Zhou and Min Zhou.

Thanks are also due to Kyle French, Steven Sheffield, and John Graham for their assistance in conducting my experiments. I would also like to thank all the support staff in MARC and ME for all their help especially John Morehouse, Pam Rountree, Dr. Jeffrey Donnell, Glenda Johnson, Trudy Allen and Wanda Joefield.

I would like to thank my colleagues, Ramesh Singh, Kuan-Ming Li, Sivaramakrishnan Venkatachalam, Carl Hanna, Hyung-Wook Park, Jing-Ying Zhang, Jiann-Cherng Su, and Adam Cardi for their help and support during my stay at Georgia Tech. Finally, I am indebted to my family especially my wife, Jinfeng Zhao, for their love, support, encouragement and understanding throughout my graduate study. This thesis would not be possible without them.

TABLE OF CONTENTS

LIST OF TABLES

LIST OF FIGURES

SUMMARY

One of the most common goals in manufacturing is to improve the quality and accuracy of the parts being fabricated without reducing productivity. Aiming at this goal, many different manufacturing processes have been developed. Among them, machining plays a major role in increasing product accuracy. As an important machining process, grinding is a vital step that can produce both fine finish and dimensional accuracy for applications in which the workpiece material is either hard or brittle. Currently, the ball screw is the most frequently used setup for grinding machine tool feed drive. However, the existence of transmission components induces wear, high friction, backlash, and also lower system stiffness; therefore, applications of conventional feed drives for high speed and high accuracy machining are very limited. As a promising technology, a linear motor feed drive discards the transmission system; therefore, it eliminates transmission induced error, such as backlash and pitch error, and avoids stiffness reduction as well. As a result, a linear motor drive can achieve both high speed and high accuracy performance. A linear motor feed drive will be subject to external disturbances such as friction, force ripple and machining force. Due to the lack of a transmission unit, the tracking behavior of a linear motor feed drive is prone to be affected by external disturbances and model parameter variations. Thus, in order to deliver high performance, a controller should be capable of achieving high accuracy in the presence of external disturbance and parameter uncertainty. This dissertation proposes a general robust motion control framework for the CNC design of a linear motor feed drive to achieve high speed/high precision as well as low speed/high precision. An application to the linear motor feed drives in grinding

machines was carried out. One of the developed algorithms is the HSMC, which combines the merits of a reaching law based sliding mode control and a modified disturbance observer for precision tracking to address the practical issues of friction, force ripple, and grinding force disturbances. Another algorithm presented is ASMC, which combines the reaching law based sliding mode control with adaptive disturbance estimation to achieve an adaptive robust motion control.

CHAPTER 1

INTRODUCTION

1.1 Overview of Grinding

One of the most common goals in manufacturing is to improve the quality and accuracy of the parts being fabricated without reducing productivity. Aiming at this goal, many different manufacturing processes have been developed. Among them, machining plays a major role in increasing product accuracy. Figure 1.1 shows that, in the past several decades, significant breakthroughs have pushed machining accuracy down to a nanometer level.

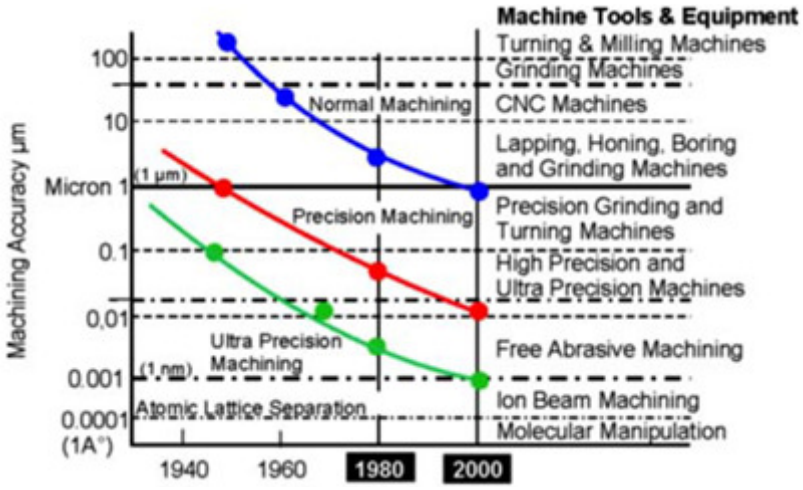

Figure 1.1 The development of achievable machining accuracy (Byrne et al. 2003)

As an important machining process, grinding is a vital step that can produce both fine finish and dimension accuracy for applications in which the workpiece material is either hard or brittle. Some grinding applications, such as ball and roller bearings, pistons, valves, cylinders, cams, gears, cutting tools and dies, etc, are shown in Figure 1.2. The position of grinding in producing roll bearing gears and shafts is shown in Figure 1.3.

Figure 1.2 Applications of grinding process

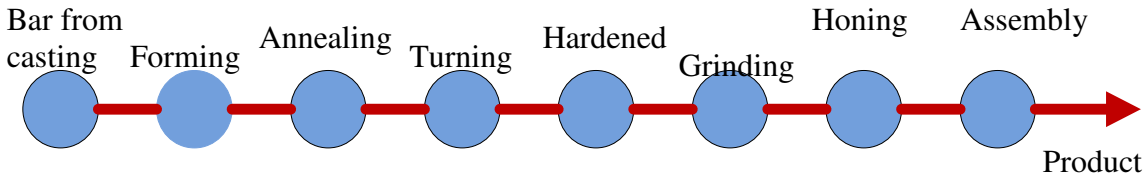

Figure 1.3 Production procedures of roller bearing gear and shaft

Grinding is a machining process that uses abrasive grains distributed around a grinding wheel to machine hard or brittle materials in order to achieve both accuracy and surface finish (Malkin 1989). Figure 1.4 relates the capability of grinding to that of other processes such as laser machining, EDM, micromachining and the LIGA process.

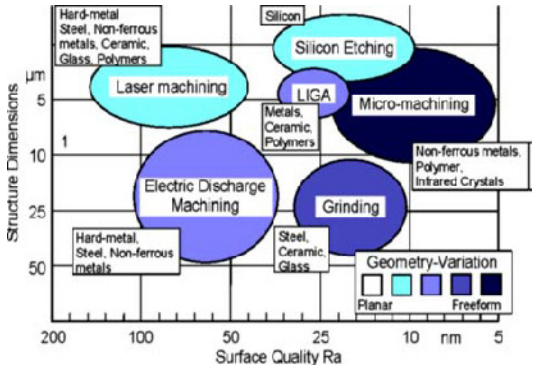

Figure 1.4 Grinding relate to other machining processes (Byrne et al. 2003)

Figure 1.5 is a schematic view of the grinding mechanism. Unlike single-point cutting, the grinding process has the following characteristics: (1) particles with irregular shapes and random distribution along the periphery of the wheel are used as abrasive grains, (2) the average rake angle of the grain is highly negative, such as negative sixty degree or even lower, and (3) grinding speeds are very high, typically 30m/s (Kalpakjian 2001).

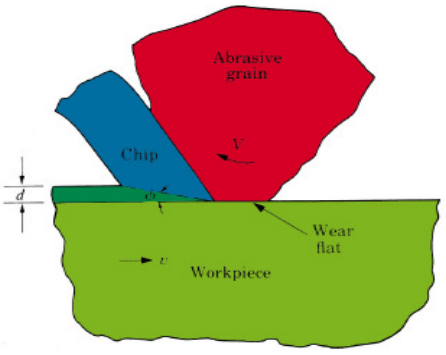

Figure 1.5 Chip forming in grinding process (Kalpakjian 2001)

1.2 Progress of Grinding Process and Machine

In the past decades significant advances have pushed the capability grinding processes to improve both product quality and throughput. One example is high speed grinding (HSG). According to Kopac and Krajnick (2006), the meaning of HSG is twofold: (1) it describes a high-productivity grinding processes that maintain the same level of quality as traditional processes, and (2) it can also be a high-quality grinding with a constant material removal rate. Advances in HSG grow in large part from the continuous progress of the abrasive industry.

As can be seen from Figure 1.6 both the circumferential speed of the grinding wheel and the material removal rate per unit grinding width have been increased. Using electro-plated bonding, it is possible for the grinding wheel to reach a circumferential speed of almost 300m/s, which is 10 times faster than the typical speed.

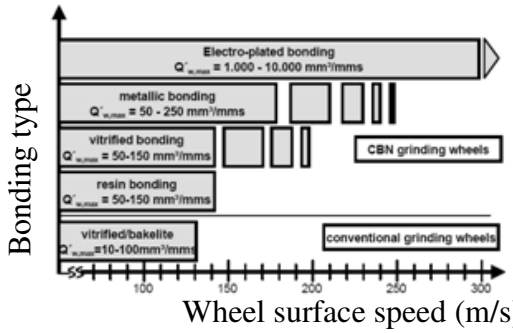

Figure 1.6 Bond system speed and material removal rate limitation (Webster and Tricard 2004)

The increase in grinding wheel speed has had an important impact on the grinding process. The effect of HSG can be examined in terms of the following equation:

$$A_g = \frac{v_w}{v_s}\frac{1}{N_A}\sqrt{\frac{a_e}{d_e}} \tag{1-1}$$

where A_g is the average chip cross section, v_w is the workpiece speed, v_s is the surface speed of grinding wheel, N_A is the number of cutting edges on the unit area of the wheel surface, a_e is the depth of cut, and d_e is the equivalent wheel diameter (Toenshoff et al. 1998).

From Equation (1-1) it can be seen that the chip cross section can be controlled by, v_s, the wheel surface speed. The advantages of HSG are illustrated in Figure 1.7. For the constant removal rate case, the wheel wear, the surface roughness and the grinding force decrease as the wheel surface speed increases. If the average chip cross section remains constant, the grinding force and the roughness and the wheel wear will also remain constant regardless of the increase of wheel surface speed; whereas the material removal rate increases proportionally with the increase of the wheel surface speed.

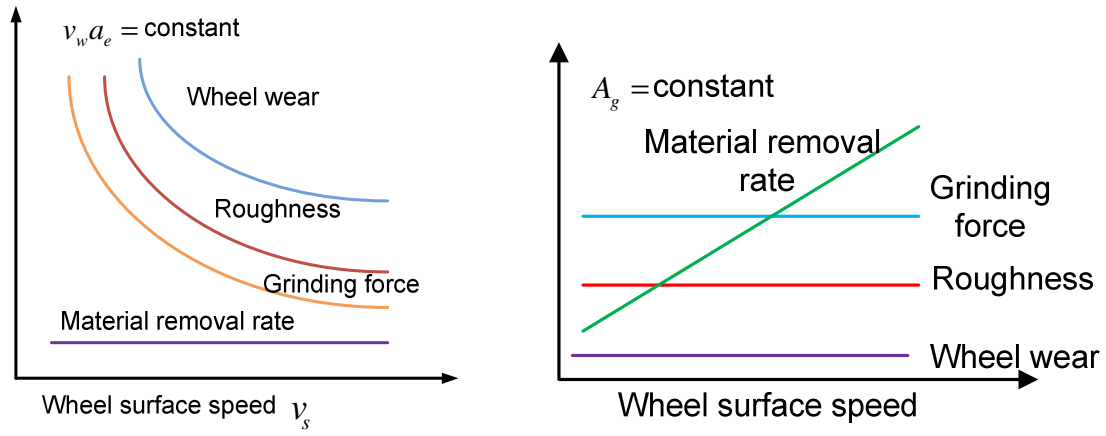

Figure 1.7 Effect of high speed grinding (Toenshoff et al. 1998)

Another example of advances in grinding is the invention of speed-stroke grinding (SSG) for ceramics by the Japanese in the 1980s. Aiming at improved die manufacture and achieving high stock removal rates while keeping the depth of cut in the ductile grind regime, SSG is characterized by very high table speeds of 50 to 100 m/min and shallow depths of cut of the order of 1 µm or less (Marinescu 2007). For SSG, the effects of work feed speed on grinding process parameters are shown in Figure 1.8.

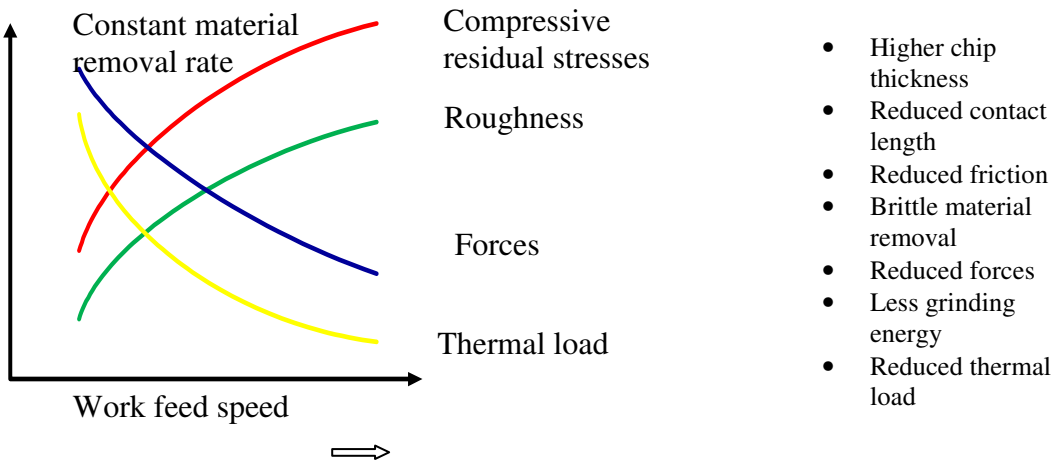

Figure 1.8 Effect of a speed stroke grinding (SSG) (Toenshoff et al. 1998)

The aforementioned technical achievements in grinding processes have posed challenges to the design of grinding machines. One such challenge is how to meet the performance requirement of increased feed. On one hand, a higher feed rate is required. For HSG, when the grinding wheel surface speed is raised, the material removal rate can be increased by increasing the workpiece speed without compromising product quality; For SSG, the high feed rate will be as high as 100m/min (Marinescu 2007), which pushes the conventional drives using ball-screws to reach their limits (Toenshoff et al. 1998; Marinescu 2007). On the other hand, there is also a low feed rate requirement imposed by other grinding processes such as the creep feed grinding process. In this case, the feed rate will be as slow as 0.05 m/min.

For a machine tool, feed rate is manipulated by a linear axis drive called a machine tool feed drive. As the lowest level of the motion control hierarchy in a machine tool, a machine tool feed drive controls the positions and velocities of machine tool slides or axes according to commands issued by a CNC interpolator. In order to achieve both high product accuracy and high productivity, many requirements are imposed on a feed drive system. These are summarized by (Srinivasan and Tsao 1997) as follows: (1) Control over a wide range of speeds, which may range from a few mm/min in precision machining to tens of m/min in rapid transverse machining centers, (2) Precise control of position (currently a position accuracy of a few microns in normal machining and submicron in precision machining is not atypical), (3) Ability to withstand machining loads while maintaining accuracy of position control, (4) Rapid response of drive system

to command inputs from the machine tool CNC system, and (5) Precise coordination of the control of multiple axes of the machine tool in contouring operations.

Continuous improvements in feed drive performance have occurred as a result of progress in drive actuation, sensing, and drive control. Prior to about 1980, nearly all machine tools were hydraulically driven (Marinescu 2007); Currently, indirect drives, which contain a rotary motor with a ballscrew transmission to the slide, are the most widely used setup for grinding machine tool feed drives (Slocum 1992). However, there are some disadvantages associated with this kind of setup, which include (1) Transmission errors due to pitch tolerances of the leadscrew, (2) Dead zone and friction induced backlash, additional large inertias, and (3) Position, velocity and acceleration limitations due to the mechanical characteristics of the leadscrew (stiffness, critical velocity) and wear, Therefore, the application of conventional feed drive for high speed and high accuracy machining is very limited (Pritschow 1998).

The origin of linear motors is traced in the book to a reluctance type, invented by Charles Wheatstone in 1845**,** while the first full-size working model did not appear until the late 1940s owning to Professor Eric Laithwaite of Imperial College in London (McLean 1988). Currently, linear motors are widely use in different areas, such as maglev propulsion, aircraft propulsion (Wikipedia 2007) , and motion control equipments as well.

Linear motor can be envisioned as a rotary motor cut axially and unrolled flat. It actually consists only of the primary part "stator" and secondary part “rotor" as illustrated in Fig. 9. The thrust is directly applied to the slide or to the object to be moved. For almost every

kind of rotary motor, there is a counterpart in linear motors. The same basic technologies used to produce torque in rotary motors are used to produce force in linear motors. Similar to its rotary counterpart, a linear motor can be classified as either a DC or AC motor which can then be further classified as induction motors, linear synchronous motors, or linear variable reluctance motors (Boldea and Nasar 1997)**.** Among all the available linear motors, synchronous permanent linear motors (PMLMs) are probably the most naturally related to applications involving high speed and/or high precision motion control due to their benefits such as availability of high force density, low thermal loss, etc. Therefore, only PMLM will be investigated in this research.

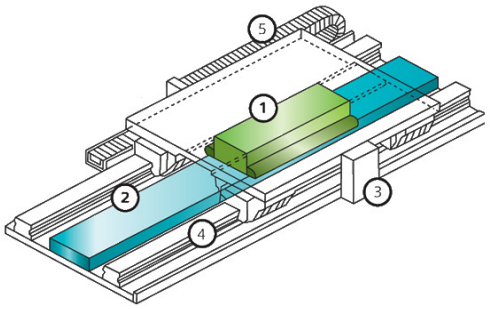

1) Primary part
2) Secondary part
3) Linear encoder
4) Guide
5) Power cable

Figure 1.9 Schematic of a linear motor (Siemens 2007)

As a promising technology, a linear motor direct feed drive discards the transmission system required for a conventional feed drive and therefore there exists no transmission associated error such as backlash, pitch error, etc. Also, the friction problem is greatly alleviated by the application of direct drive. As a result, direct linear drives can achieve high accuracy. The main limitation on the final accuracy is the feedback device. Currently an incremental linear encoder with a resolution of 1nm is commercially available [Heidenhan GMBH].

In addition, direct drive motors are capable of achieving high acceleration and velocity, which is hard to obtain using a conventional feed drive. Linear motor acceleration rates are limited by the linear bearings, most of which will tolerate 2 or 3Gs, and those that will take 5Gs are now available. A linear motor regularly travels up to 5m/s where a lead-screw typically limits velocity to less than 1.5m/s (Denkena et al. 2004).

In short, the characteristics of a machine tool axis are widely enhanced due to the specific characteristics of the direct linear drives. Therefore, a linear direct feed drive is an excellent choice to meet the requirements of higher speeds, great accuracies and improved reliability due to its mechanical simplicity. So far, the direct linear drive based linear motor has been widely used for high speed machining and ultra-precision machining. Machine tools equipped with linear direct drives have been displayed at the EMO (Exposition Mondiale de la Machine Outil) of 2002 in Hanover, Germany. In 2000, among the total 25,000 machining centers manufactured by global manufacturer, 1,100 applied linear motor technology. By 2001, this amount had more than doubled to reach 3, 000 (Byrne et al. 2003). Linear motors have been successfully applied to Landis LTI and Toyoda GC32M, both of which are camshaft grinders.

Significant advancements have recently been made in grinding technology, leading to both high accuracy and increased productivity (Inasaki 1999). In order to fully exploit the advantages of advanced grinding technologies, the requirements on the feed drive in terms of axis speed, acceleration, accuracy, and available static and dynamic stuffiness are continuously rising (Toenshoff et al. 1998).

Currently, the ball screw is the most frequently used setup for grinding machine tool feed drives (Slocum 1992). However, the existence of transmission components induces wear, high friction, backlash, and also lower system stiffness; therefore, applications of conventional feed drives for high speed and high accuracy machining are very limited (Pritschow 1998; Denkena et al. 2004). As a promising technology, a linear motor feed drive discards the transmission system; therefore, it eliminates transmission induced error, such as backlash and pitch error, and avoids stiffness reduction as well. As a result, a linear motor drive can achieve both high speed and high accuracy performance (Weidner and Quickel 1999).

1.3 Objectives and Research Plan

In spite of these advantages over rotary counterparts, linear motors have not been able to totally replace conventional techniques. Resistance to utilizing linear motors may be ascribed to the following drawbacks: (1) Force ripple which originates from cogging, reluctance force and commutation error, (2) Grinding force disturbances directly acting on linear motor, and (3) Friction is still a problem although it has been reduced in comparison to that found on conventional drives. To become a viable feed drive technology, all of these factors should be overcome by explicitly taking them into account in the controller's design.

The successful implementation of an advanced feed drive that meets the above requirements will hinge largely upon the following two factors: (1) advanced hardware, which may include actuators and precise sensors which can be used in machine tools in a

true manufacturing environment to generate accurate relative motion between tool and workpiece, and (2) state of the art software, including a sophisticated control algorithm, is crucial to minimize tracking errors under the disturbance of various factors including friction, force/torque ripple, grinding force, unmodeled plant dynamics, and inherent uncertainties associated with a complicated machining process. The proposed research will focus on surface grinding because it is suitable for linear motor application.

The overall objective of the proposed research is to develop a systematic methodology to enhance the direct feed drive performance for grinding machines under the effect of force ripple, friction and grinding force by systematic experiments, simulation, and sophisticated controller design. To this end, this project:

- Investigates the application of linear motors in grinding machines to achieve high speed and high quality grinding.
- Focuses on CNC controller design. In particular, modeling, simulation, robust servo control algorithm development, and experimental evaluation were performed to achieve high-performance tracking in terms of robustness, adaptability and accuracy.

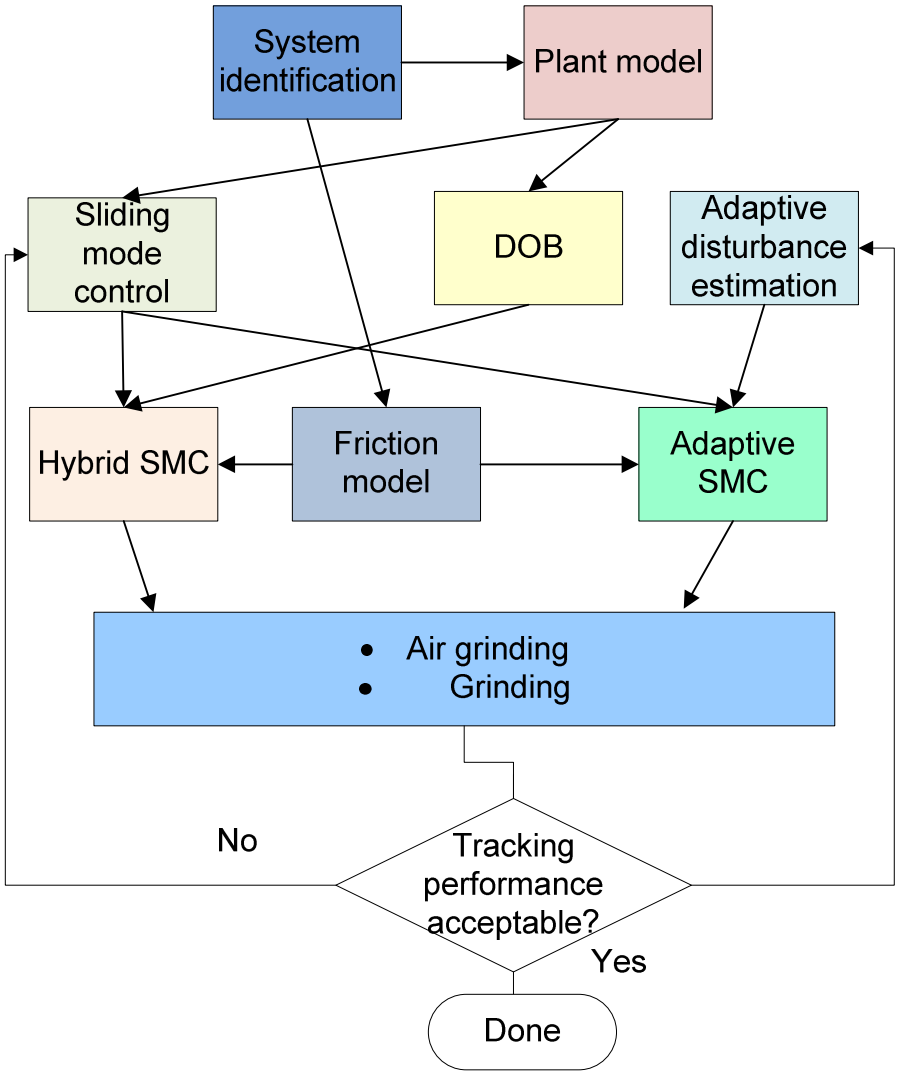

Figure 1.10 outline of research plan

The outline of the research plan is presented in Figure 1.10. The time domain based step response is utilized to obtain a rough second order plant model as a basis of controller design. A series of constant velocity experiments will be performed to get friction forces at different velocities. And then nonlinear least square optimization is implemented to produce friction parameters. Based on the obtained model, friction feedfoward is carried out. A hybrid sliding mode control (HSMC) which combines the reaching law based sliding mode control (SMC) with disturbance observer (DOB) is proposed. An adaptive

sliding mode control (ASMC) is also employed to achieve both adaptive and robust performance. A large variety of grinding and air grinding experiments will be conducted to validate the performance of proposed control algorithm. Parameter tuning is required to get the best performance.

1.4 Thesis Organization

The thesis begins by reviewing the past and present literature on modeling and control techniques directly related to servo control of linear motor feed drives, great attentions are paid to the modeling of disturbances and servo control of motion in the presence of external disturbances (Chapter 2).

A comprehensive model is developed to model the open-loop dynamics of a liner motor feed drive system with an application to cylindrical grinding. This model is then utilized for the simulation study of the linear motor feed drive system in order to provide useful information for controller design (Chapter 3). The proposed model is very good for a simulation study and it also holds prospects of directly incorporation into a model-based controller design for real time implementation provided that enough computational capacities are available, which is not the case in this study. Therefore, a simplified but still effective model will be pursued, whose parameters will be systematically indentified on experimental setup fabricated for this study (Chapter 4).

Chapter 5 proposes a general robust motion control framework for the CNC design of a linear motor feed drive to achieve high speed/high precision as well as low speed/high

precision. An application to the linear motor feed drives in grinding machines was carried out. One of the developed algorithms is the HSMC, which combines the merits of a reaching law based sliding mode control and a modified disturbance observer for precision tracking to address the practical issues of friction, force ripple, and grinding force disturbances. Another algorithm presented is ASMC, which combines the reaching law based sliding mode control with adaptive disturbance estimation to achieve an adaptive robust motion control. To validate developed motion control algorithms, extensive experiments including low feed rates, high feed rates, air grinding and part grinding are conducted. The experimental results have verified the effectiveness of the proposed motion control framework (Chapter 6). Finally conclusions of this research and recommendations for future work are presented (Chapter 7).

CHAPTER 2

LITERATURE REVIEW

Linear motors can achieve high speed and high accuracy. However, linear motor feed drives are very sensitive to disturbances. In order to develop the proposed high performance controller, a clear understanding of these disturbances will be indispensible. In grinding machine applications, disturbances consist of force ripple, grinding force, and friction. In this chapter, first of all, several aspects of linear motor feed drives which would aid in modeling linear motor feed drives will be reviewed. And then a review of controller design for machine tools in general and for linear motor feed drives with a focus on robust high performance tracking controllers will be presented.

2.1 Modeling of Linear Motor Feed Drives

Modeling linear motor feed drives is crucial to the successful design of a high performance controller. Unfortunately, there have been few efforts to systematic ally model linear motor feed drives for grinding machines in a way that puts all aspects under one framework (Xie et al. 2006). In view of this, this review will focus on different aspects related to linear motors.

2.1.1 Friction Modeling

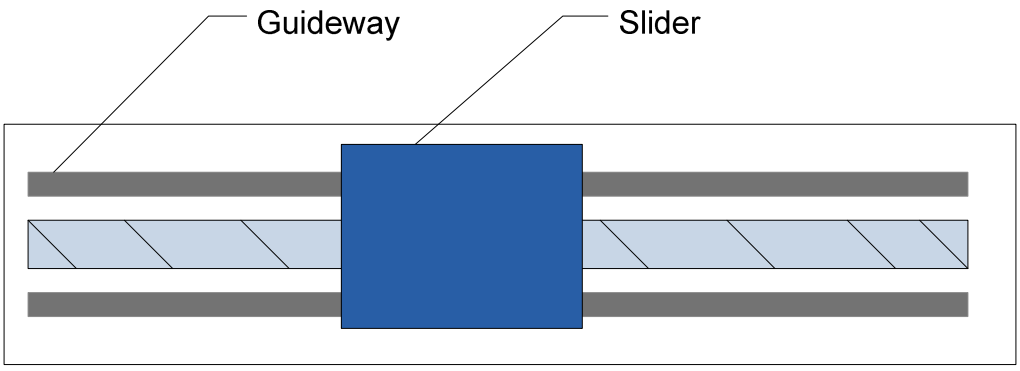

Figure 2.1 Schematic of a linear motor stage

For a linear motor feed drive system as shown in Figure 2.1, the relative movement between the slider and guideway incurs friction. Uncompensated friction in a machine tool feed drive system causes static state error, limit cycle, and stick-slip, all of which impose constraints on the positioning and tracking performance of the machine, and limit the product quality that can be achieved (Armstrong-Helouvry et al. 1994). In order to make valid friction compensation possible, an authentic friction model is desirable. Compared to a ball screw feed drive system, the friction exhibited in a linear motor feed drive is alleviated but not completely eliminated. Thus, friction still remains as a major factor influencing the precision of the linear motor system, particularly when the precision requirement on the feed drive system reaches to the submicron regime.

As an important physical phenomenon, friction has been intensively researched by experiments, modeling, and simulation studies. An exhaustive survey has been made by Armstrong et al. (1994) on the physics behind the friction phenomenon, as well as

compensation techniques of dealing with it. Some of the important aspects of friction will be summarized.

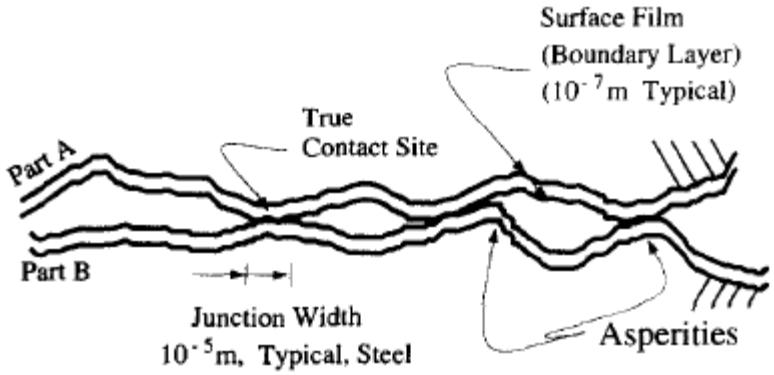

Figure 2.2 Part-to-part contact occurs at asperities, the small surface features (Armstrong-Helouvry et al. 1994)

To understand the tribology of engineering surfaces it is necessary to consider the surface topography as shown in Figure 2.2. There are four regimes of lubrication for lubricated metallic surfaces in contact: static friction (presliding), boundary lubrication, partial fluid lubrication, and full fluid lubrication as, illustrated in Figure 2.3

In the presliding regime, the asperity junctions deform elastically. Once the tangential force exceeds a certain threshold, referred to as the static friction value, the junctions will break, causing sliding to start; the transition from presliding to sliding is called breakway. It is noted in tribology literature that static friction level will be a function of dwell time, which is the duration that the surfaces are at rest before sliding occurs.

In the boundary lubrication regime, sliding occurs at a very low velocity. Though it is not always true, the friction in this regime is often assumed to be less than that found in fluid lubrication cases,

In the partial fluid lubrication regime, the film is not thick enough to completely separate the two surfaces, and the contacts at some asperities still affect the friction force. As partial fluid lubrication increases, solid to solid contact between the boundary layers decreases, which results in the reduction of friction force with increasing velocity. This regime is the most difficult to model of the four regimes. Furthermore, there is a phase lag between the change in friction and the changes in velocity or load conditions; referred to as frictional memory this phase lag may be in the order of milliseconds to seconds.

After sliding velocity reaches a certain level, a continuous fluid film is formed which completely separates the two surfaces. In this regime, referred to as full fluid lubrication, the viscosity of the lubricant is dominant on the friction force.

Friction properties can be classified into two categories: static characteristics, which include the kinetic and viscous force and the Stribeck effect as shown Figure 2.3; and dynamic characteristics, which comprise pre-sliding displacement, varying breakaway force, Dahl effect, and a frictional lag (Armstrong-Hâelouvry 1991; Armstrong-Helouvry et al. 1994).

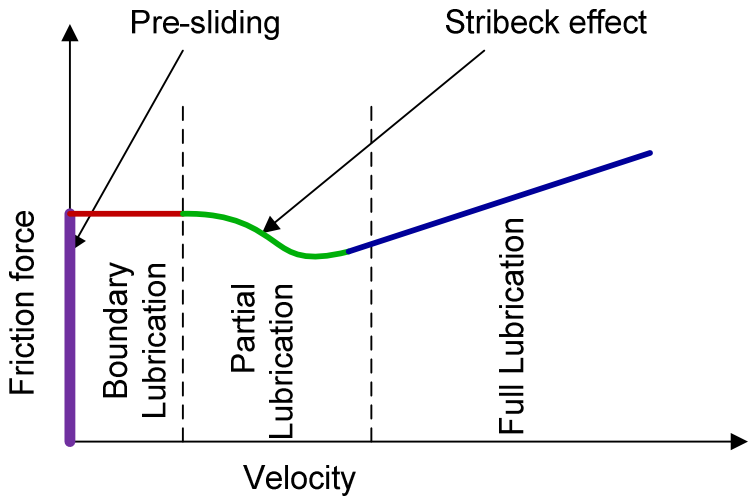

Figure 2.3 Stribeck Curve (Armstrong-Helouvry et al. 1994).

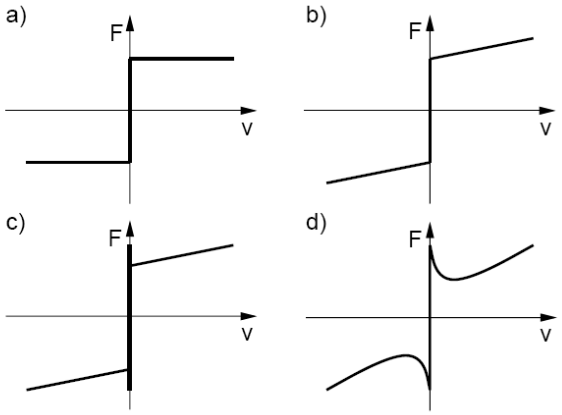

Figure 2.4 Examples of static friction models. a) Coulomb friction model. b) Coulomb plus viscous friction model. C) Stiction plus Coulomb and viscous friction model. d) Stiction plus Coulomb and viscous friction model with Stribeck effect. (Olsson et al. 1998)

To interpret those observed friction properties, many models have been proposed. All of the existing models can be boiled down to static and dynamic models that try to explain the observed friction characteristics.

In static models, friction is modeled as a static map between velocity and friction force.

$$F=\begin{cases} F(v) & if\ v \neq 0 \\ F_e \quad if\ v = 0\ and\ |F_e| < F_s \\ F_s sgn(F_e)\ otherwise \end{cases} \tag{2-1}$$

A common form of $F(v)$ (Armstrong-Helouvry et al. 1994) is

$$F(v) = F_c + (F_s - F_c)e^{-\left|\frac{v}{v_s}\right|^{\delta_s}} \tag{2-2}$$

The main disadvantage when using a model such as that in Equation 2-1 is the detection of zero velocity. To overcome this problem, a remedy is suggested by Karnopp (1985). This model defines a zero velocity interval. For velocities within this interval the output of the block is maintained at zero by a dead-zone. The drawback with the model is that it is strongly coupled with the rest of the system, which is not always given such as the external force. Therefore, the model has to be tailored for each configuration. Despite this, variations of the Karnopp model are widely used since they allow efficient simulations.

Due to the simplicity of the static models, they have been extensively used for both the ball screw feed drives and the linear motor feed drives control (Yang and Tomizuka 1988; Tung et al. 1993; Tan et al. 2002; Yao and Xu 2002; Elfizy et al. 2004).

Static models assume there is no motion while sliding. However, Dahl (1976) has observed that there is a pre-sliding displacement on the order of 2-5 microns in steel junctions, which is approximately a linear function of the applied force until breakaway occurs. Pre-sliding displacement is believed to be dominant in extremely high precision

positioning applications and is of significant interest to the control community (Dahl 1976; Futami et al. 1990; Ro and Hubbel 1993). To capture static and dynamic characteristics such as pre-sliding displacement, the Dahl effect and friction lag, Dahl (1976) developed a comparatively simple model that was used extensively to simulate systems with ball bearing friction. The friction model is an extension of Coulomb friction, but it produces a smooth transition.

One of the shortcomings of the Dahl model lies in its inability to model the steady state friction characteristic in the sliding regime, as is seen in the Stribeck curve. To overcome this deficiency, a joint effort between Lund and Grenoble has been made which led to the derivation of a new nonlinear analytical friction model, i.e., the LuGre model (Canudas de Wit et al. 1995; De Wit and Lischinsky 1997). The LuGre model combines the pre-sliding behavior of the Dahl model with the steady state friction characteristic of the sliding regime, as in the Stribeck curve. The strength of the dynamic LuGre friction model is the ability to capture a large number of practically observed friction phenomena as described in (Canudas de Wit et al. 1995; De Wit and Lischinsky 1997). Therefore, the LuGre model serves as a good friction model for machine tool feed drives, especially for applications where position accuracy requirements may be down to submicron regime.

The application of the LuGre model for friction modeling and compensation in conventional ball screw feed drive systems has been demonstrated by Ro et al. (2000). However, static friction models which cannot capture the pre-sliding effect are still widely used in the control community to model the friction for linear motor feed drives

(Tan et al. 2002; Yao and Xu 2002). Since it is common that the precision requirements on linear motor feed drives often are in the submicron regime, a more accurate dynamic friction such as the LuGre model should be a better choice when modeling friction for linear motor feed drives. However, an immeasurable inner state should be observed in order to use LuGre model.

2.1.2 *Force Ripple Modeling*

Among all the available linear motors, synchronous permanent linear motors (PMLMs) are probably the most closely related to applications involving high speed and/or high precision motion control owing to their benefits such as high force density available, low thermal loss, etc. Due to these advantages, the PMLM is a very good candidate for machine tool feed drives. However, in addition to thrust force, PMLMs generate undesired force ripples which cause thrust to be position dependent; this must be compensated to achieve high positioning and tracking performance (Otten et al. 1997). One of the sources of force ripple is the cogging force which results from the mutual attraction between the magnets and iron cores of the translator (Van Den Braembussche et al. 1996). It is present even when there is no motor current. Another source of force ripple is the reluctance force, which is caused by the variation of the self inductance of the windings with respect to the related position between the translator and the magnets. The modeling force ripple for linear motors can be found in the literature (Van Den Braembussche et al. 1996; Van Brussel and Van den Braembussche 1998).

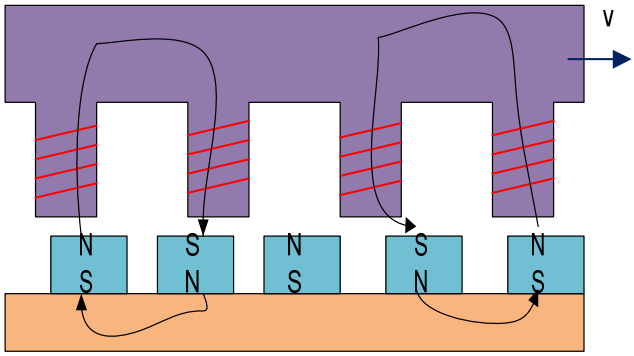

Figure 2.5 The principle of linear motor (Otten et al. 1997)

The most common method of controlling the current applied to the stator windings is through six-step commutation. Commutation is the powering of the three-phases of the motor stator with three different waveforms, each 120 degrees out of phase with the others. In six-step commutation, the three phases of the stator windings (designated A, B, and C) are energized using one of three states - either "fully positive", "fully negative" or zero. As the rotor rotates, the three phases of the stator are energized in a six-step, square wave pattern. As shown in Figure 2.6, Phase A goes positive, zero, negative, negative, zero then positive in the six-step cycle while Phase B goes negative, negative, zero, positive, positive, zero and Phase C goes zero, positive, positive, zero, negative, negative.

The "positive" or "negative" current applied to the phases generates an electric field that creates either a repelling force in one direction or an attracting force in the other direction. These fields interact with the rotor's field magnets to generate the desired torque. Six-step commutation works very well in a stalled motor situation since the torque generated is proportional to the current being applied to the windings. In a dynamic situation when the rotor is moving, six-step commutation can generate undesirable torque ripple. This

disturbance torque results from the discontinuous switching between states. Therefore, the forces which generate torque on the rotor are not constant throughout the full rotation.

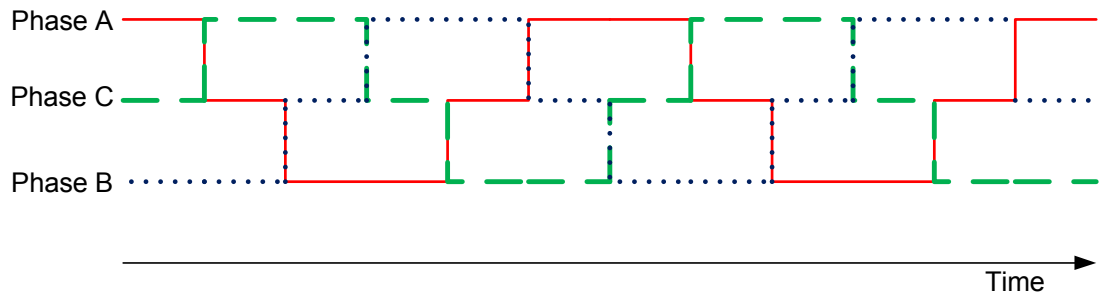

Figure 2.6 Six step commutation

2.2 Servo Control for Machine Tool Feed Drives

Control of machine tools originated with the invention of Numerical Controlled (NC) machines in the 1950s and was advanced to Computer Numerical Control (CNC) in the early 1970s (Liang et al. 2004). Servo control of machine tool feed drives is one of the major functions of a CNC and it stays at the lowest level of the machine tool control hierarchy as shown in Figure 2.7.

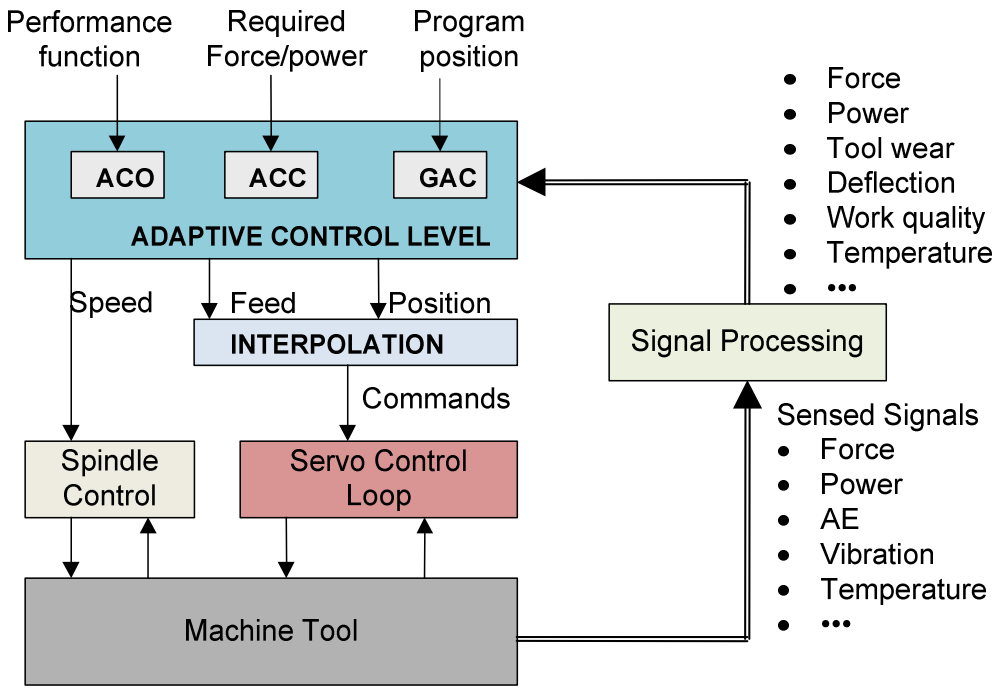

Figure 2.7 Machine Tools Control and Monitoring - General Scheme (Koren 1997)

The main objective of a servo control is to make the output, y, to follow the reference signal, r, at sufficient accuracy, which can be defined in terms of performance specifications, by manipulating the control signal as shown in Figure 2.8 (Dorf and Bishop 2001).

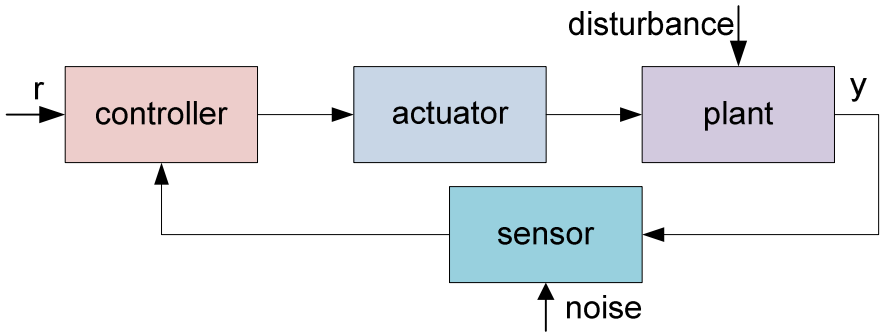

Figure 2.8 Block diagram of a servo control system (Dorf and Bishop 2001)

A general servo controller structure for a single axis is a cascade type compensator with an inner velocity loop and an outer position loop as shown in Figure 2.9. Design criteria are based on achieving a certain closed position control loop bandwidth, steady state accuracy, and rejection of disturbances.

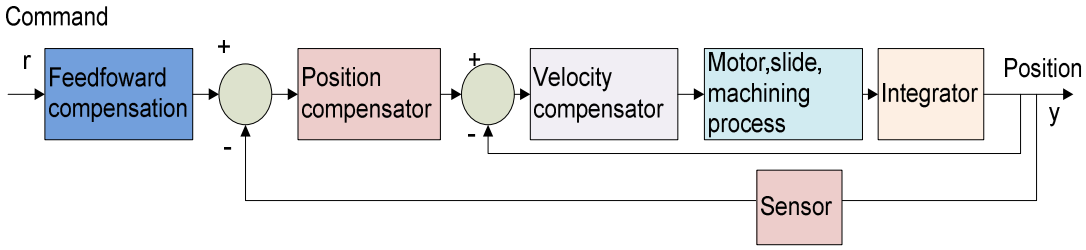

Figure 2.9 General single axes control structure (Koren 1997)

Traditionally, the dynamics of each axis in a machine tool are represented as a second order system for which well-known feedback controllers can be applied, such as PID (Proportional-Integral-Derivative) controllers (Koren 1997). In a PID controller, the correction signal consists of three components: a proportional, an integral, and a derivative of the position. The integral controller is utilized to eliminate the steady state error for ramp tracking and to reject external disturbances. However, the integral will easily cause actuator saturation and thus significant overshoot. In addition, the action of simple controllers such as PID can be degraded by process perturbations, model uncertainties and non-linearities. In these cases, sophisticated techniques to achieve higher control requirements are needed.

When the reference trajectory is known, the future reference points can be used to improve tracking accuracy. This idea has led to active research in feedfoward controller

design. The basic philosophy behind feedfoward controller design is to force the closed-loop transfer function to approach unity by compensating for uncancellable components and delays in axis dynamics. A feedfoward control is often combined with a feedback controller such as PID to achieve disturbance and parameter variation robustness, whereas a feedforward compensator is utilized to reduce the tracking error.

A major approach to feedforward control is the Zero Phase Error Tracking Controller (ZPETC) based on zero pole cancellation with special care for non-minimum phase systems (Tomizuka 1987). The ZPETC increases closed-loop bandwidth and therefore the tracking error can be reduced significantly. However, one of the major drawbacks of ZPETC is its sensitivity to modeling errors and plant parameter variations. Another issue with ZPETC is that the resulting controller signal includes high-frequency components and thus easily reaches saturation (Tung and Tomizuka 1993). In order to limit the generation of high-frequency content, a zero phase low-pass filter can be added before ZPETC (Weck and Ye 1990; Tung and Tomizuka 1993).

For applications that require multi-axes cooperation, contour error, defined as the orthogonal deviation from the desired tool path, is often the major concern of servo control. One of the approaches works to reduce the single axis tracking error and thereby to reduce the contour error. By contrast, a Cross-Coupling Controller (CCC) (Koren and Lo 1992) combines feedback information from all the axes and the interpolator to obtain an optimal compensating law, and then issues a feedback correction signal to individual axes.

Besides the above controllers, there are also other algorithms, such as optimal control (Srinivasan and Kulkarni 1990), predictive control (Boucher et al. 1990; Boucher et al. 1993; Dumur and Boucher 1994; Dumur et al. 1996), and repetitive control (Tung et al. 1993), etc. The use of repetitive control is limited to repetitive tasks. Moreover, a large memory is often required to store previous data for the machining of a highly complex part (Koren and Lo 1992).

2.3 Design of Robust Control System

The design of a control system often assumes knowledge of the plant. A linear motor feed drive will be subject to external disturbances such as friction, force ripple and machining force. Due to the lack of a transmission unit, the tracking behavior of a linear motor feed drive is prone to be affected by external disturbances and model parameter variations (Van Den Braembussche et al. 1996; Srinivasan and Tsao 1997). Both physics and empirically based methodology can be employed to model the plant as reviewed before. However, no matter how faithful the models are, there will always be an inaccurate representation of the actual physical system because of unavoidable parameter changes, unmodeled dynamics, unmodeled time delays, changes in equilibrium point, sensor noise and unpredicted disturbance inputs, etc. (Dorf and Bishop 2001).

Another issue with linear motor feed drives is machining instability. For linear motor feed drive systems, there exists a strong dynamic feedback interaction between the machining process and the servo loop which can lead to excessive vibration or chatter.

Therefore besides tracking performance, a linear motor feed drive should also establish enough dynamic stiffness in order to maintain machining stability and to reduce the effect of disturbances on the tracking performance (Alter and Tsu-Chin 1996). Thus, in order to deliver high performance, a controller should be capable of achieving high accuracy in the presence of external disturbances and parameter uncertainty.

In many cases PID controller design techniques lead to a perfectly satisfactory solution and thus it is unnecessary to utilize more powerful tools. However, the plant dynamics may be complex and poorly modeled, or the performance specifications may be particularly stringent; both cases are true for linear motor feed drives. In these cases, difficulties arise. Even if a solution is eventually found, the process is likely to be expensive in terms of the design engineer's time (Green and Limebeer 1995). In order to satisfy performance requirements, more powerful design tools are required.

A significant amount of research has been published in pursuit of performance over a wide range of uncertainty and disturbances, and this has lead to the theory of linear robust control (Zames 1996). One of linear robust design technique is H_∞ optimal controllers, which is essentially a constrained optimization method in frequency domain. It takes into consideration the worst case scenario on the expected behavior of the closed loop (Doyle et al. 1992).

H_∞ loop-shaping is another design methodology (Zhou and Doyle 1998). It combines the intuition of classical control methods with H_∞ optimization techniques to achieve

controllers whose stability and performance properties hold good in spite of small differences between the nominal plant assumed in the design and the true plant encountered in practice. By weighting the plant transfer function in the frequency domain, the resulting loop-shape is then rendered more robust through optimization to maximize the system's stability margins.

However, H_∞ design may be conservative for high speed/high accuracy tracking control and there is no systematic way to quantize practical information about plant uncertainty and modeling inaccuracy for application of the H_∞ technique.

2.4 Sliding Mode Control

In contrast to H_∞, Sliding Mode Control (SMC) provides a simple and systematic way to achieve robust control. SMC is essentially a variable structure control law characterized by high-speed discontinuous switching operation (Utkin 1977; DeCarlo et al. 1988). There are several advantages to this approach. First, the dynamic behavior of the system may be tailored by the particular choice of switching function. Second, superb system performance includes insensitivity to parameter variations, and even complete rejection of disturbances. Third, there exist simple and systematic procedures to design SMC systems. In addition, due to the ability to specify performance, SMC is attractive from the design perspective (Slotine and Li 1991; Edwards and Spurgeon 1998; Young et al. 1999). Because of these characteristics, SMC provides a simple, but meaningful approach to robust control.

Although, in theory, SMC features excellent robustness properties in the face of parametric uncertainty, classical SMC suffers from chattering, and therefore, its practical applicability is limited (Slotine and Coetsee 1986). Chattering describes the phenomenon of finite-frequency, finite-amplitude oscillation appearing in many sliding mode implementations. Chattering results in low control accuracy, high heat loss in electrical power circuits, and high wear of moving mechanical parts. It may also excite unmodelled high-frequency dynamics, which degrade the performance of the system (Khalil 2002). In addition, the high actuator frequency may be manifested in the form of audible noise that may propagate and have deleterious effects elsewhere in the system (Friedland 1996). Chattering therefore presents a major obstacle to the practical implementation of SMC. To remedy this problem, several smoothing techniques for sliding control were suggested. Continuous approximation of the switching control law, called boundary layer control, uses a continuous high gain control law in the boundary with saturation outside the boundary. However, if the acceptable gain has to be reduced sufficiently to avoid instability in the boundary layer, the resulting system performance may be significantly worse than that achieved by the ideal sliding mode control (Slotine and Li 1991). From the different perspective of boundary layer control, the reaching law method suppresses chattering by directly tuning the reaching mode characteristics based on the consideration that chattering is caused by nonideal reaching at the end of the reaching phase. Another important merit of the reaching law method is that it easily allows the SMC control law to be obtained (Gao and Hung 1993).

2.5 Disturbance Estimation

When designing a control system, a number of requirements need to be satisfied. The control system must track changes in the set point accurately and with sufficient speed in the presence of external disturbances. Since a linear motor feed drive is more prone to external disturbances than a ball-screw feed drive, the control system of a linear motor feed drive should be able to provide additional disturbance rejection.

A basic approach to providing disturbance rejection is to estimate the equivalent disturbance and then cancel it (Ohnishi et al. 1996). To realize this approach, the disturbance estimation is of critical importance. Many methods for disturbances estimation were reviewed recently (Radke and Gao 2006).

One disturbance estimation method is time-delayed control (TDC) (Elmali and Olgac 1992; Youcef-toumi and Reddy 1992) , which uses a nominal model and one-step delayed input/output signal to estimate perturbation. However, the second derivative of the position signal required by TDC generates noises in practical implementation.

A more common method for disturbance estimation is a disturbance observer (DOB) (Umeno and Hori 1991; Lee and Tomizuka 1996; Schrijver and van Dijk 2002). The merit of the DOB is that it can estimate a disturbance and reject it without affecting performance. The separation property enables two independent design stages to be used for the overall controller design: one for performance and one for disturbance rejection. Another benefit of DOB is that it makes the real plant behave like the nominal plant for a

certain frequency range and, thus, the robustness of the system is improved (Umeno and Hori 1991; Lee and Tomizuka 1996).

Disturbance can also be obtained by on-line parameter identification (Yao et al. 1997). In this approach, the uncompensated external disturbance is assumed to be constant and to remain between an upper and lower bound. By an adaptation mechanism, the disturbance can be obtained.

2.6 Control of Linear Motors

A significant amount of research has been devoted to solving the difficulties in controlling linear motors. To reduce the nonlinear effect of disturbances such as friction and force ripple, feedforward compensation is often employed, and this can be very effective if disturbance models can be obtained. Classical static friction models, in which friction force is modeled as a static map of moving velocity (Armstrong-Helouvry et al. 1994), are often utilized for controller design. More sophisticated friction models, such as the LuGre model (Canudas de Wit et al. 1995; De Wit and Lischinsky 1997), are recommended for any application where position accuracy requirements may be down to the submicron regime. Since it is very complicated to physically model force ripple, an empirically based model provides a feasible alternative for feedforward compensation (Van Den Braembussche et al. 1996). In literature, a neural-network-based feedforward controller was presented to improve positioning performance in the presence of force ripple (Otten et al. 1997). However, overall system stability is not guaranteed.

The implementation of feedforward control requires a precise disturbance model to totally eliminate the effects of disturbance. However, it is often impractical, if not impossible, to obtain such a perfect model. Moreover, it is possible that, in operation, the plant will be subject to varying disturbances and model uncertainties. Thus, a robust feedback control is essential. Alter and Tsao (1996; Alter and Tsu-Chin 1998) applied an H_∞ optimal feedback controller to a linear motor feed drive for cutting in order to provide high dynamic stiffness. Meanwhile, feedforward control was employed to improve tracking performance. In another study, a MIMO H_∞ controller was proposed to improve the tracking accuracy of a linear motor feed drive for an end milling process (Choi and Tsao 2005). An H_∞ controller using an improved weighting function was also examined and applied to linear motor feed drive axis to deal with the load uncertainty problem (Van den Braembussche et al. 2001).

2.7 Summary

From the above literature review, it is evident that modeling and control of linear motor feed drives for grinding machines is very challenging. Although different aspects of linear motors feed drives are scattered throughout the literature, its systematic modeling is rarely touched. Also, a breakthrough in controller design for linear motor feed drives should be achieved in order to obtain robust performance.

The chapter will address the issue of modeling of linear motor feed drives in a systematic way to facilitate a simulation study and the design of controller. A nonlinear robust high

performance controller design with learning capability will be developed on the basis of sliding mode control.

CHAPTER 3

OPEN-LOOP SIMULATION STUDY OF LINEAR MOTOR FEED DRIVES FOR GRINDING MACHINES

Controller design often assumes knowledge of plant characteristics. In the course of a controller design cycle, modeling is often the first step (Doyle et al. 1992). A model allows the dynamics of a system to be simulated and analyzed without building the system, thus providing a basis for the design of a control system. A reliable model is essential for the successful implementation of a control algorithm. Any discrepancy between the real system and the model may lead to a failure to meet the design speciation and may also cause instability in the closed loop system (Ninness and Goodwin 1995).

In the case of motion control for a machine tool feed drive, the accuracy of the axis dynamics model is crucial for the reduction of tracking error or contour error. A feedfoward controller such as ZPETC is very effective in reducing tracking error. However, an inaccurate plant model will degrade the performance significantly (Tomizuka 1987). On the other hand, robust feedback control was suggested to address the issue of model discrepancy. The basic philosophy of robust control is to address the worst case scenario; therefore, optimal performance is not pursued (Green and Limebeer 1995). Although advanced adaptive control can be used to deal with unknown parameters by using online learning, the transient performance is often hard to guarantee (Ioannou and Sun 1996). In addition to knowledge about the plant, the knowledge of

nonlinear disturbances, such as friction should also be captured, so that model-based friction compensation can be used to improve the tracking or contouring performance (Armstrong-Helouvry 1991).

When a linear motor feed drive is applied to a grinding application, it will be subject to the influence of friction, grinding force, and force ripple. All of these factors will have adverse effects on the closed-loop performance if axis dynamics alone are considered. Consequently these factors should be studied comprehensively for simulation purpose and eventually to facilitate of controller design for the linear motor feed drive.

Several approaches to modeling linear motor stages (Tan et al. 2002; Denkena et al. 2004) have been presented in literature, and these models are good enough for many applications. However, difficulties must be addressed if the potential of linear motor feed drive is to be realized. These are in large part due to following:

(1) Although the linear motor is targeted to high precision motion, the conventional static friction models, which cannot handle presliding displacement, were used. This is not satisfying because presliding displacement is essential for motion control where the accuracy requirement may be down to the submicron level (Ro et al. 2000), as is the case of linear motor feed drives (Schuffenhauer 1996; Gao et al. 2004).

(2) From the simulation point of view, a dynamics force model considering the coupling nature between the grinding force and the feed drive output is much better than lumpping the cutting force as a part of external disturbances.

To solve these problems, first, a dynamic friction model will be presented. This model can capture not only observed static but also dynamic friction phenomena such as presliding displacement, which is the dominant friction contribution for high precision applications. Then, a cylindrical grinding operation is assumed to show how grinding force can be integrated in the model. For other grinding processes, such as surface grinding, the same methodology can be employed. A grinding force model based on the relation between the radial infeed velocity and grinding force is employed. In addition to friction and grinding force, force ripple is also modeled. Moreover, all of the three factors that have influences on the direct feed drive positioning and tracking have been taken into account under one framework.

In this chapter, analytical or empirical models for functionality-critical features of a linear motor, including friction, grinding force, and force ripple will be discussed. First, a dynamic friction model, based on the LuGre approach, will be used in order to describe not only observed static friction but also dynamic friction phenomena such as presliding displacement, which is the prevailing friction phenomenon for high precision application. Then, in order to study the influence of grinding force on a linear motor feed drive's positioning performance, an analytical grinding force model proposed by Hahn and Lindsay is employed. After friction and grinding force have been considered, force ripple is taken into account, in view of its importance to machine tool applications, based on empirical modeling. To validate the force ripple model, a

simulation result has been compared with the experimentally measured open velocity response of a linear motor motion system. The effectiveness of the model has been shown by agreement between the simulation and experimental results. The friction model has also been validated through the comparison of simulation results to experimentally measured responses obtained by frequency domain identification on an electromechanical motion system.

3.1 System Modeling

A linear motor can be envisioned as a rotary motor that has been cut axially and unrolled flat. The thrust is directly applied to the slide or to the object to be moved. For almost every kind of rotary motor, there is a counterpart in linear motors. The same basic technologies used to produce torque in rotary motors are used to produce force in linear motors. In this chapter, a voltage controlled linear motor will be considered for simulation study. The body diagram of the liner motor feed drive system is shown in Figure 3.1.

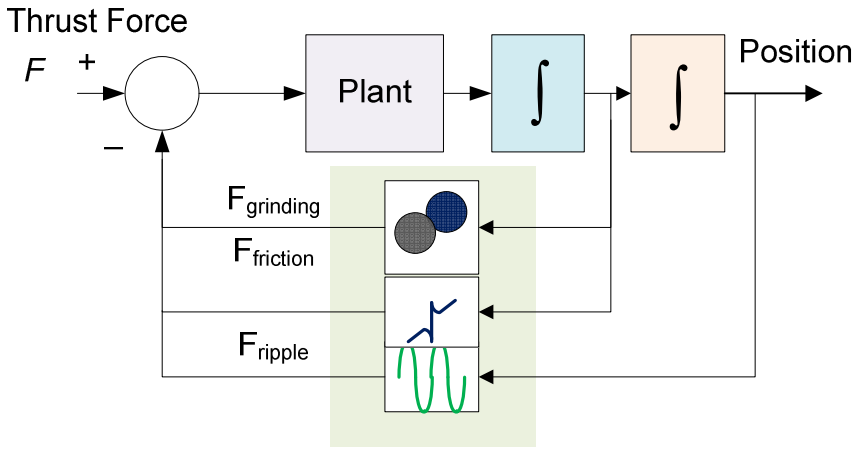

Figure 3.1 Block diagram of the linear motor feed drive system

According to Newton's law, the following equation can be obtained

$$F(t) = m\ddot{x} + f_{friction} + f_{ripple} + f_{grinding} \tag{3.1}$$

where m is the moving thrust mass, f_{ripple} , $f_{friction}$, and $f_{grinding}$ are force ripple, friction force and grinding force, respectively.

3.2 Friction Modeling

The LuGre model combines the presliding behavior of the Dahl model with the steady state friction characteristic in sliding regimes such as the Stribeck effect. The strength of the dynamic LuGre friction model is its ability to describe a large number of practically observed friction phenomena as described in (Armstrong-Helouvry et al. 1994). For high precision motion, a friction model that can address both presliding and sliding behavior will be desirable.

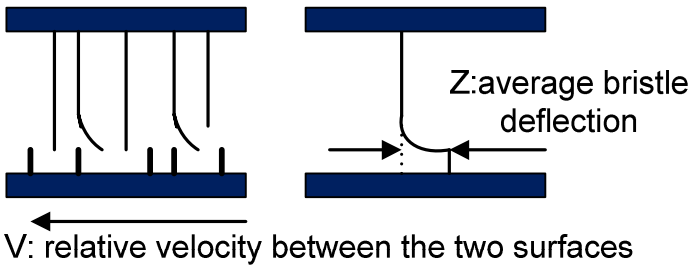

Figure 3.2 Bristle deflection (Ro et al. 2000)

The LuGre friction model (Canudas de Wit et al. 1995) will be adopted since it combines the presliding behavior and the steady state friction characteristic in sliding regimes such as the Stribeck curve, which plays an important role in describing the lower velocity motion of a linear motor. According to the LuGre friction model, the friction force can be modeled as a function of the state variable z as illustrated in Figure 3.2 and velocity v :

$$F_f = \sigma_0 z + \sigma_1 \frac{dz}{dt} + \sigma_2 v \tag{3.2}$$

where the parameters σ_0, σ_1 and σ_2 are the asperity stiffness, the micro-viscous friction coefficient, and the viscous friction coefficient, respectively. The interpretation of the internal state is linked to the bristle friction model; viz. the state variable z represents the average deflection of the contacting asperities:

$$\frac{dz}{dt} = v - \sigma_0 \frac{|v|}{g(v)} z \tag{3.3}$$

where $g(v)$ is a decreasing function for increasing velocity with an upper limit equal to the stiction force F_s and a lower limit equal to the Coulomb friction force F_c:

$$g(v) = \mathrm{sgn}(v)(F_c + (F_s - F_c)e^{-|v/v_s|^{\delta v_s}}) \tag{3.4}$$

where v_s is the Stribeck velocity and δv_s is the Stribeck shape factor.

3.3 Grinding Force Modeling

Grinding force models consist of a physical part which includes the speed ratio, the depth of cut, and the equivalent diameter, as well as empirical constants for grinding force and workpiece materials (Denkena et al. 2004). A grinding force model developed by Hahn and Lindsay (Bhateja and Lindsay 1982) is very straightforward and will be used to model the grinding force. This model assumes there is linear relationship between the material removal rate and the normal force. In general, the total specific grinding energy is composed of chip formation, plowing, and the sliding components as shown in Figure 3.3 (Malkin 1989).

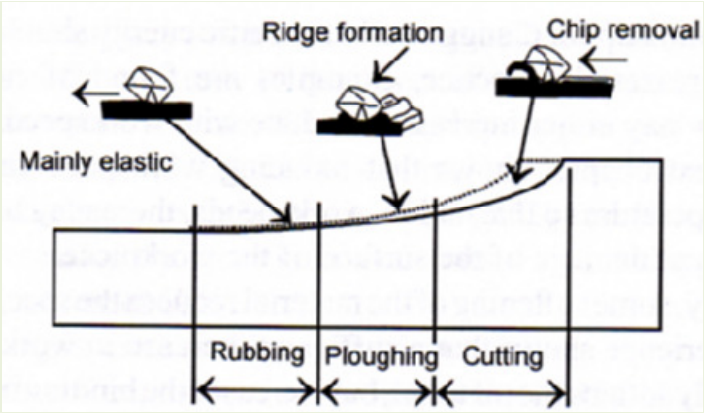

Figure 3.3 Three stages of chipping forming (Marinescu 2004)

Correspondingly, there are three grinding force components. Among them, a threshold force can represent the sum of plowing and sliding force components. Only when the threshold force value is above the threshold will it contribute to material removal. For easy to grind material, the energy consumption associated with sliding and plowing will be insignificant compared to chipping energy, and hence almost all energy is used for material removal and the threshold force can be ignored. Therefore, the grinding force can be modeled to be proportional to the material removal rate.

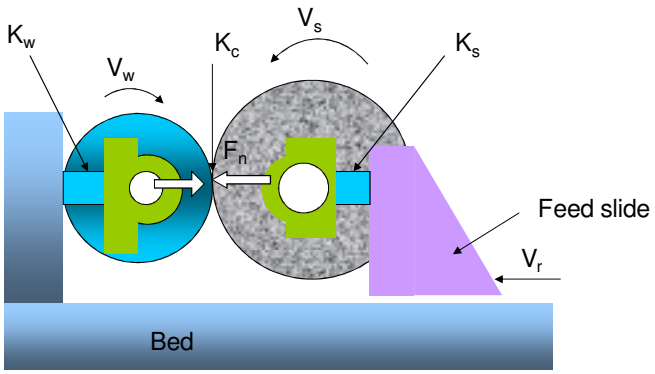

Figure 3.4 Schematic of cylindrical grinding (Bhateja and Lindsay 1982)

For cylindrical plunge grinding as illustrated in Figure 3.4, the material removal can be computed as

$$\pi b_s d_w v \tag{3.5}$$

where b_s is the grinding wheel width, d_w is the diameter of workpiece and v is the actual infeed velocity. However, because of the final stiffness associated with work, wheel and contact, the actual radial infeed velocity will be different from the commanded radial infeed velocity (Malkin 1989). Neglecting wheel wear for the moment, continuity requires that the difference between the controlled $u(t)$ and the actual $v(t)$ infeed velocities be equal to the time rate change of the radial elastic deflection of the grinding system:

$$u(t) - v(t) = \dot{\varepsilon} \tag{3.6}$$

$$\varepsilon = \frac{F_n}{k_e} \tag{3.7}$$

where F_n is the normal force component and k_e is the effective stiffness. For cylindrical plunge grinding with a constant radial speed, there is a relationship between the control feed rate V_r and the actual velocity V_{reff} as described by

$$V_r - V_{reff} = \frac{d}{dt}\left(\frac{F_n}{K_{eq}}\right) \tag{3.8}$$

As shown in (Denkena et al. 2004) for cylindrical plunge grinding, the grinding normal force can be approximated to be proportional to the material removal rate as depicted by

$$F_n = c\pi d_w b_s V_{reff} \tag{3.9}$$

where c is the proportionality constant describing the dullness of the grinding wheel. Combining (3.11) and (3.12), the transfer function from V_r to F_n can be obtained as:

$$\frac{F_n(s)}{V_r(s)} = \frac{c\pi d_w b_s}{1+(c\pi d_w b_s / k)s} \tag{3.10}$$

where s is the Laplace operator.

3.4 Force Ripple Modeling

As mentioned earlier, cogging is a magnetic disturbance force, which is due to the mutual attraction between the magnets and iron cores of the translator. It depends merely on the relative position of the motor coils with respect to the magnets, and is independent of the motor current. The reluctance force is caused by the variation of the self inductance of the windings with respect to the related position between the translator and the magnets. Thus, the reluctance force also has a periodic relationship with the translator-magnet position .The reluctance force exists only when the motor current is non zero, and its absolute value depends on the required force and the relative position of the carriage. Cogging and reluctance force are commonly called force ripple.

From motion control considerations, force ripple is highly undesirable. This can be minimized or even eliminated by an alternative design of the motor structure or the spatial layout of the magnetic materials, such as skewing the magnet, optimizing the disposition and width of the magnets, etc. However, these mechanisms often increase the complexity of the motor structure. A control algorithm aimed at eliminating the effects of force ripples is therefore highly desirable. For that purpose, a model of the force ripple is much desired. Ripple models suggested by P.V.

Braembussche et al. (1996) will be utilized in this research. In his model, the reluctance force is described as:

$$F_{reluctance} = F_{desired}[a_f \sin(\frac{2\pi}{p}x + \phi_{11}) + b_f \sin(3\frac{2\pi}{p}x + \phi_{12})] \quad (3.11)$$

and the cogging force is modeled as:

$$F_{cogging} = a_c \sin(\frac{2\pi}{p}x) + b_c \sin(3\frac{2\pi}{p}x + \phi_c) \quad (3.12)$$

where $F_{desired}$ represents the desired force, p is the average pitch of the magnets for the considered stroke, x represents the position of the motor carriage, a_f , b_f , a_c and b_c are estimated coefficients, and ϕ_{11} , ϕ_{12} and ϕ_c are the estimated phase shift.

3.5 Experimental Validation

In this section, experimental results obtained from the literature are provided to illustrate the effectiveness of the proposed modeling strategy. Since experimental results a system with exactly the same parameters as our simulations cannot be found from literature, those parameters that are given are utilized in the corresponding experiments to perform simulations that will yield a valid comparison.

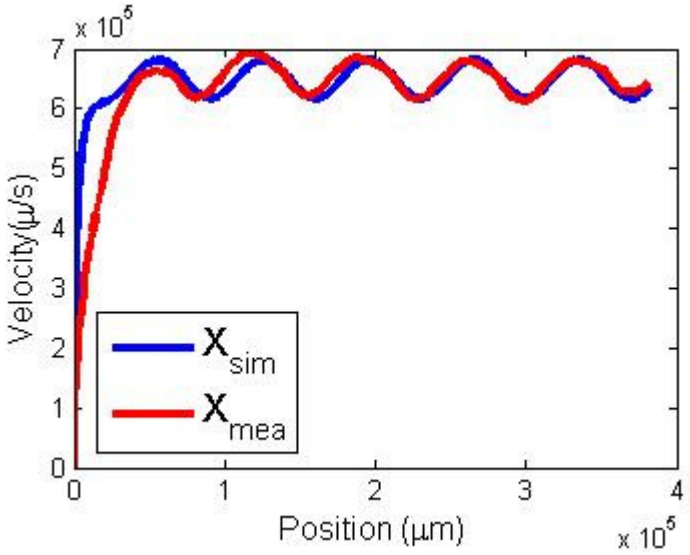

Figure 3.5 Comparison of simulation and measured velocity response of a linear motor

Figure 3.5 depicts the simulated and experimental velocity response for a permanent magnet linear motor with both friction and force ripple using parameters documented in (Tan et al. 2002). Since the dynamic friction parameters are not given, they were based on data presented in (Lampaert et al. 2004). From Figure 3.5, it can be seen that the simulation results match the experimental values reasonably very well, which means our model can predict the response of a real linear motor system.

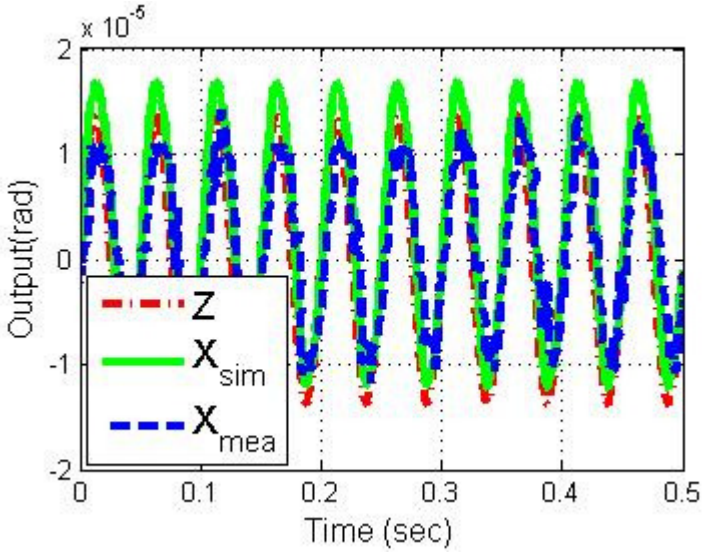

Figure 3.6 Sinusoidal input u=0.01sin (40*pi*t) (N)

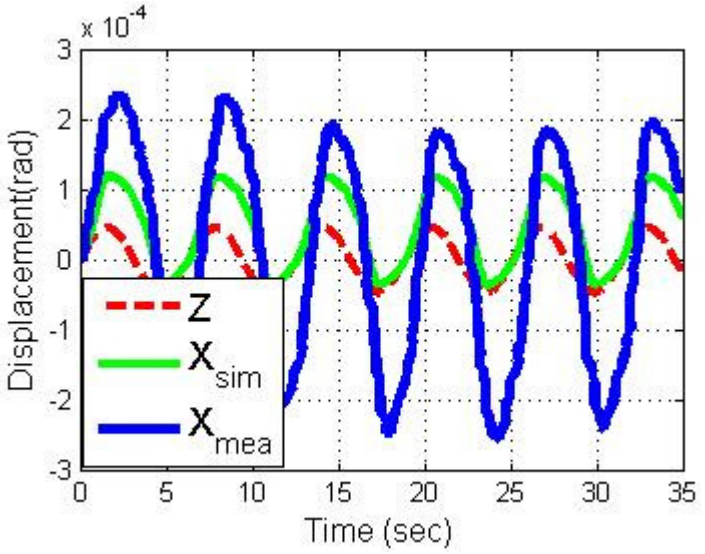

Figure 3.7 Sinusoidal input u=0.035sin (t) (N)

Figure 3.6 and Figure 3.7 illustrate the system response achieved from both simulation and experiments. The simulation parameters used and the experimental results are documented in (Hensen et al. 2002). In Figure 3.6, it is evident that the motion is in the stiction regime since the displacement is very close to bristle deflection. From this figure, it can also be seen that the simulated presliding displacement matched the measured response very well, which means that

the LuGre model can capture the presliding behavior accurately. Figure 3.7 describes results obtained using another sinusoidal excitation with higher amplitude and period. It can be seen that the measured response is higher than both the macroscopic and presliding displacements obtained from simulations. The possible reasons are given in (Hensen et al. 2002) .

3.6 Simulation Results and Discussion

Numerical simulations were carried out to investigate the effects of friction, force ripple, and grinding force on the system response. Only open loop simulations were performed since our focus in this chapter is to model the motion behavior of a linear motor feed drive under the influence of friction, force ripple, and grinding force. In this part, the friction effects are studied first. The dynamic presliding behaviors and the varying breakaway force under inputs with different rates are examined. Then, the effect of force ripple combined with friction was studied. Finally, motion behaviors of the linear motor feed drive system with all the three factors combined are investigated. The friction parameters used for simulation are listed in Table 1. F_s represents static friction which is assumed to be 50% larger than Coulomb friction. The bristle stiffness σ_0 is chosen to be the same quantitative order as listed in (Lampaert et al. 2004). The value of the damping coefficient σ_1 was chosen to give a damping ζ =0.7 for the linearized system equation in the stiction regime (Canudas de Wit et al. 1995). Without losing the illustration effects of force ripple on linear motor feed drives, only the cogging force is considered for simulations. For the cogging force, the higher order harmonic term is ignored because of the dominance of the first harmonic term.

Table 1 Friction parameters used for simulation

parameter	value	units
F_s	120	(N)
F_c	80	(N)
υ_s	0.1	(m/s)
σ_0	$2*10^6$	(N/m)
σ_1	$2*10^4$	(Ns/m)
σ_2	0.4	(Ns/m)

3.6.1 Effects of Friction

To study the friction behavior, two kinds of input were considered. The first is step input, the second is sinusoidal input. For step input, we have considered two cases: one input is below the stiction value, the other is larger than the stiction value. Figure 3.8 shows the response of a step input with a magnitude of 12, which is 10% of the stiction. From this figure, it can be seen that the motion is in the stiction regime where macroscopic displacement is almost equal to the presliding displacement, which is about $6\,\mu m$. This is in the same order of magnitude as reported in literature (Armstrong-Helouvry et al. 1994). Figure 3.9 shows the case when input is 10% larger than the stiction. The upper part demonstrates that the motion is away from the stiction regime since the presliding displacement is much smaller than the macro displacement. This

conclusion is confirmed by the lower part because it is very clear that the friction decreased gradually and eventually stopped at the Coulomb friction.

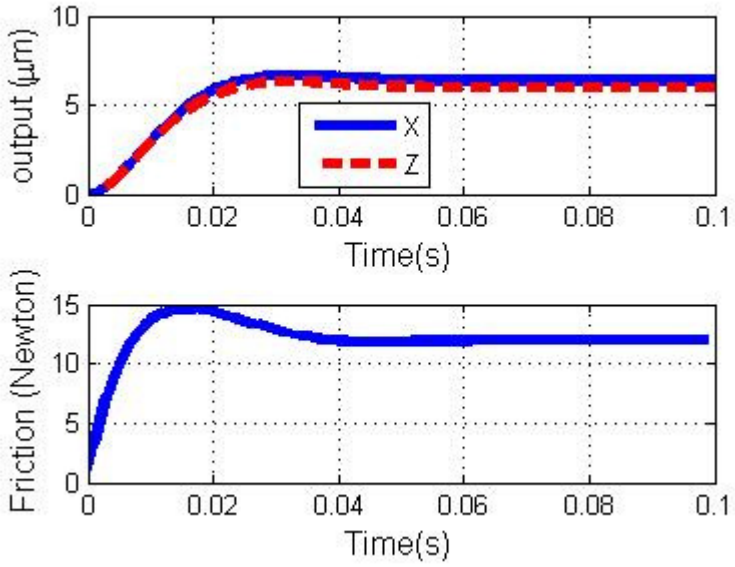

Figure 3.8 Open loop step response (u=12 N)

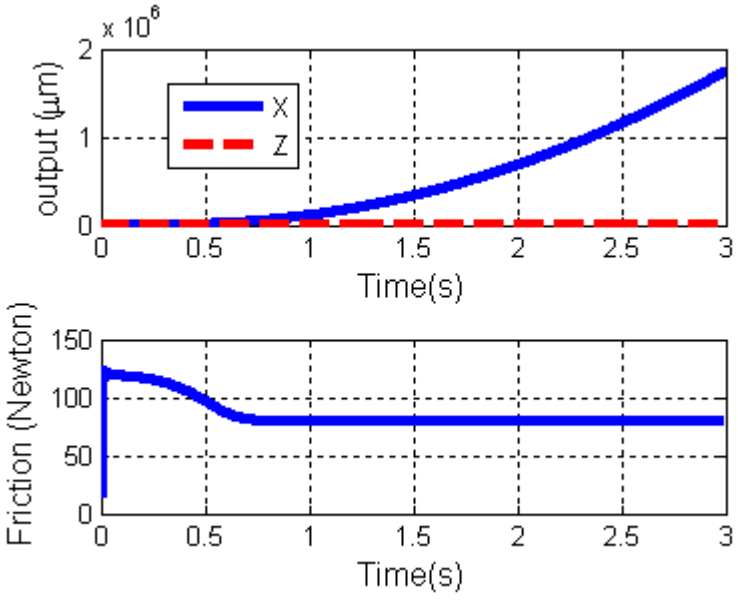

Figure 3.9 Open loop step response (u=130 N)

Figure 3.10 (a) and (b) show the system response with three sinusoidal inputs with amplitude of 12 but with different frequencies, which are 0.1, 1, and 10, respectively. These first two inputs did not show distinguishable differences regardless of the different input frequency. For the case of input frequency 10, again the response amplitude is the same as the former two; however, there is a phase shift.

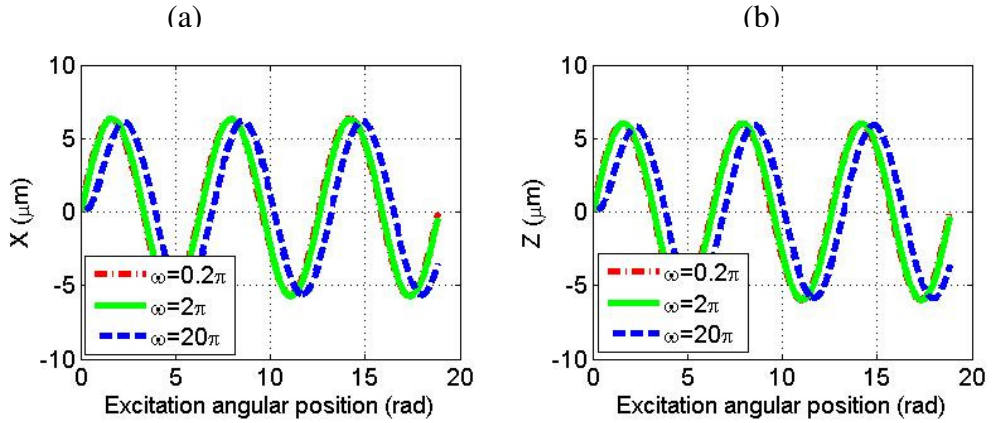

Figure 3.10 Open loop sinusoidal responses with the same magnitude but different frequencies presliding displacement; (b) bristle deflection

When the amplitude is 120, the system response varies with input frequency as shown in Figure 3.11. It can be seen that higher frequency responds to lower macroscopic displacement. Although an explanation cannot be given , it is possible that this phenomenon is related to friction lag phenomena (Canudas de Wit et al. 1995).

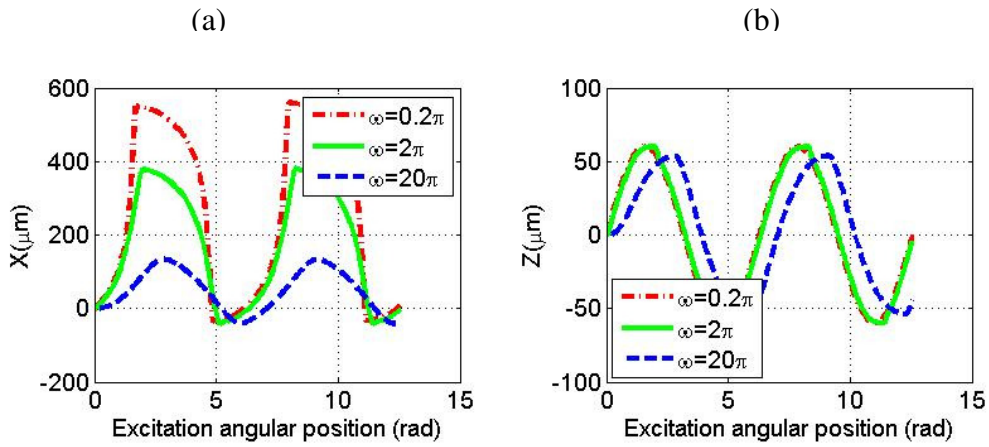

Figure 3.11 Comparison of open loop response excited by sinusoidal inputs having the same magnitude (stiction) but different frequencies. (a) Macroscopic displacement. (b) Presliding displacement.

Figure 3.12 (a) demonstrates the breakaway phenomena. To show the breakaway points, the transition region is zoomed to Figure 3.12 (b). From this figure, we can tell how breakaway points vary with different input rates. A higher rate will result in a lower breakaway critical point. This matches the findings in the literature (Canudas de Wit et al. 1995).

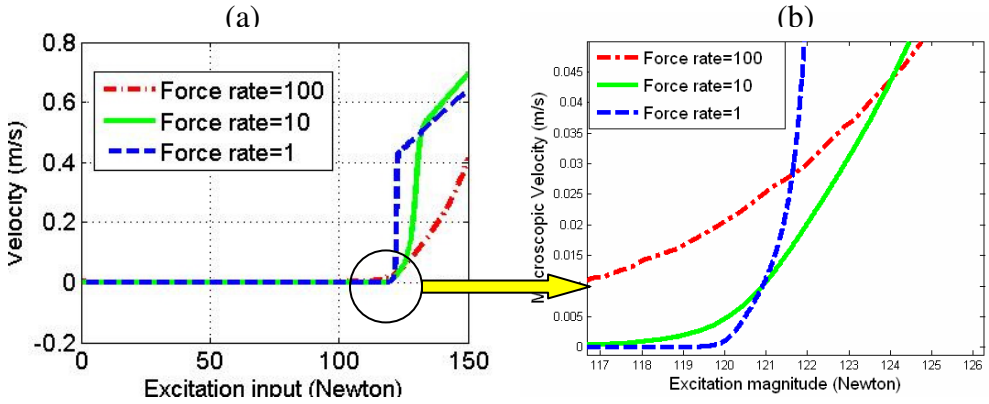

Figure 3.12 Breakaway response

3.6.2 Effects of Friction and Force Ripple

Figure 3.13 shows the system response that is obtained when both friction and force ripple are taken into consideration. The curve of macroscopic displacement as shown in Figure 3.13 (a) looks very similar to that of the no force ripple case as shown in Figure 3.9; however, the

macroscopic displacement of the case with force ripple is smaller. The friction force is shown in Figure 3.13 (b), which indicates that a transition from stiction to sliding occurred, as can also be seen from the friction curve in Figure 3.9 for the no force ripple case. A close examination of friction curves as shown in Figure 3.9 and Figure 3.13 (b) reveals that the transition from stiction to sliding occurred earlier than was the case with force ripple. This is because the force ripple acts as an obstacle to the motion at the beginning stage, as can be seen from the force ripple curve shown in Figure 3.13 (c).

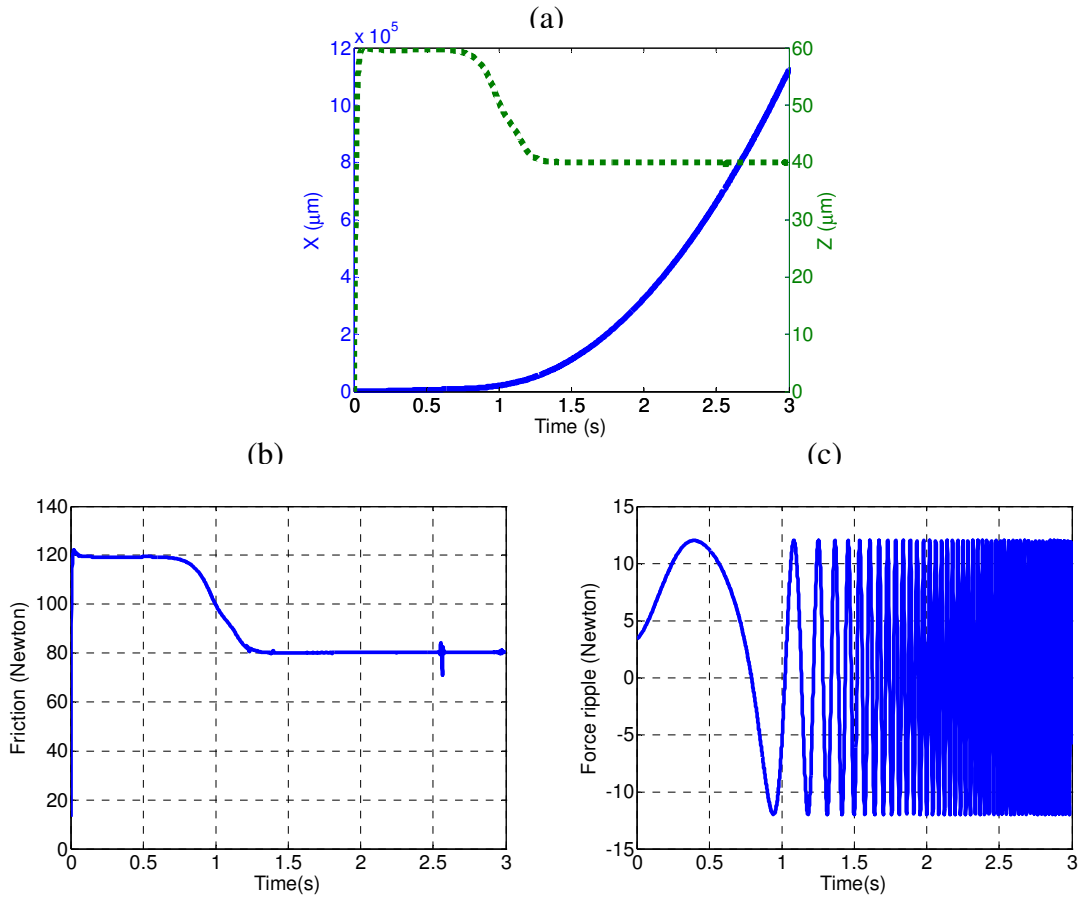

Figure 3.13 Open loop step response (u=130 N)

Figure 3.14 shows the system response with amplitude of 130 and a period of 1. From Figure 3.14 (a), it can be seen that the macroscopic displacement is shifted as time advances which is reasonable because the force ripple is decreasing with shift as shown in Figure 3.14 (b).

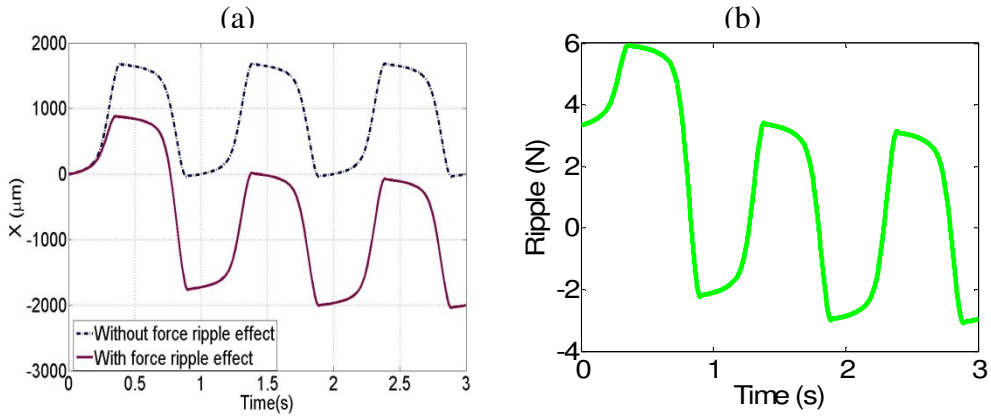

Figure 3.14 Open loop sinusoidal response

3.6.3 Effects of Combined Friction, Force Ripple, and Grinding Force

Figure 3.15 shows the system response when all of the three factors: friction, force ripple, and grinding force are taken into account. In Figure 3.15, (a) shows both the macroscopic and presliding displacement, (b) illustrates the change of three force components. It can be seen that the force ripple is negligible among all of the three force components. Although the friction is increasing during the simulation period, the grinding force is dominant in the whole simulation period.

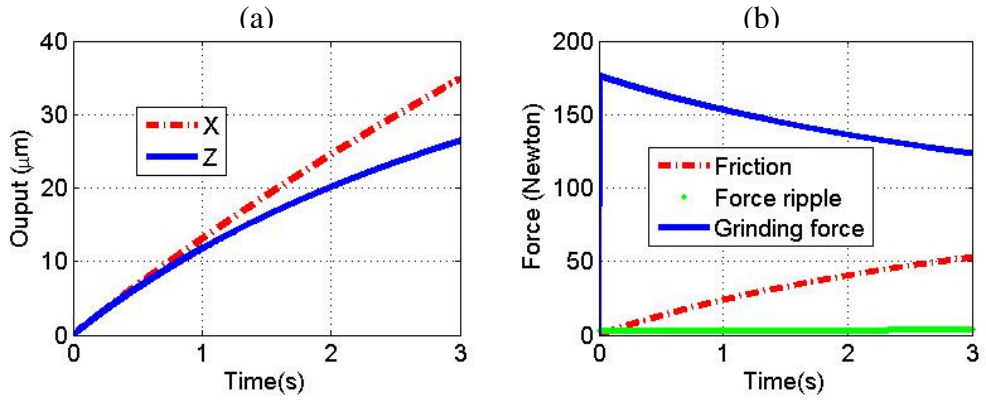

Figure 3.15 Step response with the consideration of friction, force ripple, and grinding force (u=180 N)

3.7 Summary

This chapter presents a dynamic model of linear motor feed drives for grinding machines. In this work, a dynamic friction model (LuGre model) is used to capture not only observed static friction phenomena but also dynamic friction phenomena such as presliding displacement, which is the prevailing friction phenomenon for high precision applications. Friction behaviors under step input and sinusoidal input are investigated. Both the stiction regime and the sliding regime are examined. It has been found that the presiding displacement is very close to the bristle deflection in the stiction regime. However, macroscopic displacement is much larger than the bristle deflection in the sliding regime. The varying breakaway phenomena are captured by simulation. It has been found that larger force rate will result in a smaller breakaway point. Force ripple was also studied based on the periodical nature of force ripple with respect to position. It was discovered under some circumstances the effect of force ripple is insignificant, while in other cases it will induce a shift of macroscopic displacement. To study the influence of grinding force on a linear motor feed drive's positioning performance, an analytical grinding

force model proposed by Hahn and Lindsay is employed. When all of the three force components are taken into account in one simulation, it was found that the grinding force is the most important component, followed by friction. The effect of force ripple is not important.

CHAPTER 4

EXPERIMNETAL SETUP AND PARAMETER IDENTIFICATION

The chapter has two major parts. The first part is the experimental setup. This part, discusses the mechanical and electrical aspects of the experimental setup, which is a linear motor feed drive test rig implemented on a surface grinding machine. The motion control architecture which is employed for this study is also presented. The second part of this chapter is concerned with modeling the identification for the linear motor feed drive. Experimental results are used to validate the effectiveness of the proposed method for modeling and identifying the dynamics of feed drives.

4.1 Experimental Setup

4.1.1 Description of Experimental Setup

The studies in this work are tested on a linear motor feed drive. The linear motor stage was mounted and fixed on the bed of a Chevalier FSG1224AD 3-axis auto surface grinder. The experimental setup is shown in Figure 4.1.

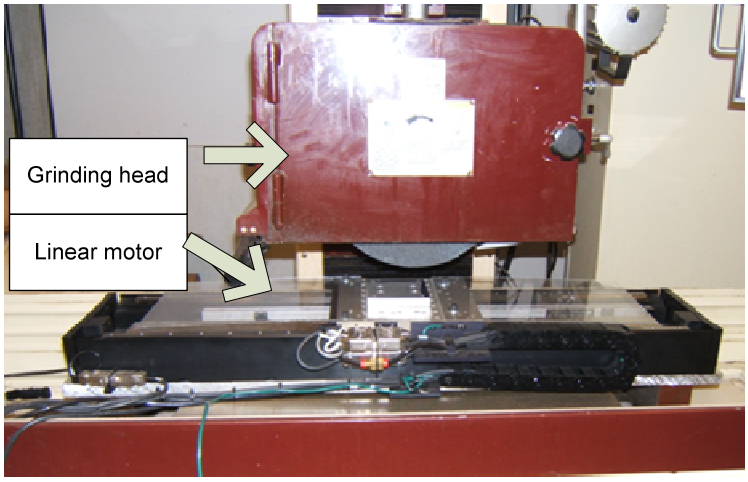

Figure 4.1 Experimental setup

The linear stage used for the X table is an ALS20060 (Aerotech 2006) equipped with Aerotech brushless linear servo motor BLM-142-A, which has a peak force of 673 N and a continuous force of 109 N, respectively (Aerotech 2002). BLM series motors are direct drive devices that consist of a noncontacting forcer coil and U-channel rare-earth magnet track. The noncontact design of the forcers and the magnet track generates a maintenance-free design. The compact moving forcer coil assembly contains Hall Effect devices, and a thermal sensor, and is constructed of reinforced ceramic epoxy while the stator is a rail of magnets. This ironless design eliminates eddy-current losses that otherwise would limit speed and produce additional heat. For the highest RMS force, optional air cooling is available. The BLM series nonmagnetic forcer eliminates cogging and magnetic attraction to allow for extremely smooth motion and very tight velocity and position control. These linear motors are ideal for any application that requires high levels of positioning resolution and accuracy.

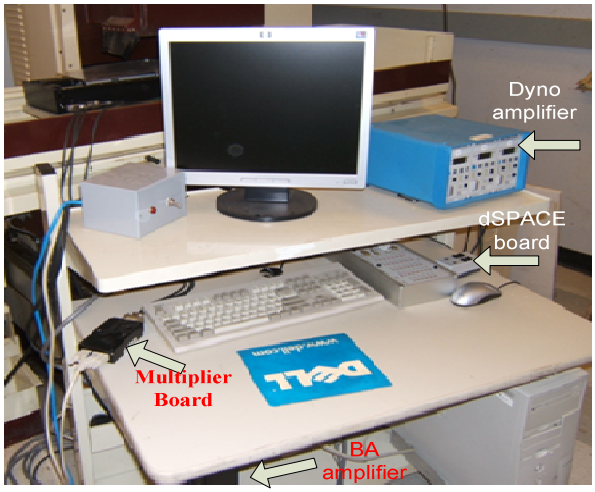

Figure 4.2 Electrical system of experimental setup

The linear motor in this study is controlled and powered by the electrical systems shown in Figure 4.2. The Aerotech BA20 amplifier (Aerotech 2000) is used as a current loop controller. The BA series amplifiers are Aerotech's stand-alone drive for three-phase AC brushless and single-phase DC brush motors. This amplifier is set to run in current mode using a self-commutation by the modified six-step algorithm; this switches the motor phase current based on three Hall Effect signals that are spaced at intervals of 120 electrical degrees beginning at 0 electrical degrees. Although this is slightly more difficult to implement than the standard 6-step algorithm, it closely approximates the motor's back EMF. Therefore it causes less ripple. This BA20 amplifier accepts standard ±10 VDC current as a command from the motion controller. The BA amplifier is based on a 20 kHz IGBT for reliable operation in a compact package.

A RSF MSA670 sealed linear encoder is used as the position sensor. It has a signal period of 20 μm with high signal quality for reliable interpolation. A MX10 multiplier board is shown in Figure 4.2; it provides a multiplication factor of 10 and is used with the sine wave encoder to

increase its resolution. When used with an appropriate controller, the quadrature of the output signal provides a multiplication of 4 to yield the effective multiplication of 40. And thus a resolution of 0.5 μm can be reached by interpolation for the MSA linear encoder.

The RSF MSA670 sealed linear encoders for linear motors generally have a natural frequency higher than 2 kHz in the measuring direction, which in most applications exceeds the mechanical natural frequency of the machine and therefore has practically no limiting effect on the position and speed control loops.

Force measurements are made with a Kistler 9256C2 MiniDyn (Kistler 2007) as shown in Figure 4.2; this is a piezoelectric 3-axis dynamometer up to 250N. The top plate is made of titanium. This achieves natural frequencies of 4 kHz in all three force directions. The extremely high sensitivity (three times that of quartz dynamometers) means that very small machining forces can be reliably measured. It is mounted between the workpiece and the matching plate used to mount the dynamometer on the linear motor stage. A Kistler 5010 charge amplifier, which is shown in Figure 4.2 is used to convert the piezoelectric force signal into high level output voltage for acquisition.

Figure 4.3 Kistler 9256C2 dynamometer (Kistler 2007)

4.1.2 Motion Control Architecture

The motion controller architecture is presented in Figure 4.4. This structure conforms to the requirement of an open controller architecture (Pritschow et al. 2001), by separating the different motion control functionalities into different levels. The current controller and the power amplifier are implemented in the BA20 drive, and the position and tracking controller are implemented with a dSPACE DS1102 DSP controller board. The controller board is hosted by a DELL Pentium III 500 MHZ PC running Windows 2000. The controller board combines the high computing performance of a TI TMS320C31 floating-point DSP with a set of I/O modules frequently required in control systems. With its 24 bit incremental encoder interface and four 12-bit D/A output interfaces configured at ±10 V output voltage range, it is possible to read in the digital encoder position signal of the X axis of the feed table, and send the control command to the motor amplifiers.

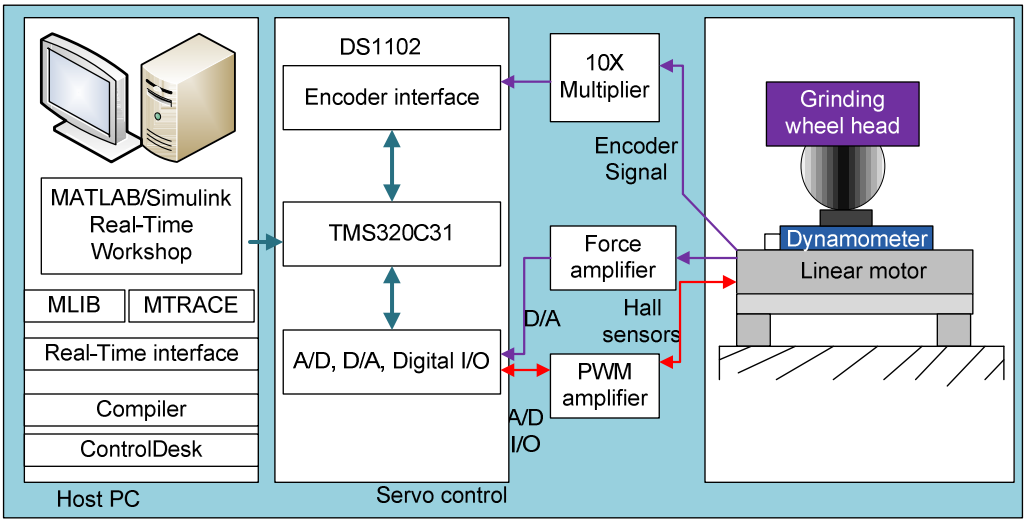

Figure 4.4 Schematic of experimental setup

The controller is developed in Simulink and the C language. MATLAB Real-Time Workshop compiles the Simulink code to C and uploads the file into the dSPACE DS1102 system. The experimental data acquisition is realized by calling library functions supplied by MLIB and MTRACE. The human-machine interface, which is used for starting and stopping the program and which also provides a means to view the controller signals in real time, is provided by ControlDesk 2.2, also from dSPACE, and is running on the host computer. The DS1102 has two 16-bit and two 14-bit A/D converters. The three channel force signals were acquired by force dynamometer and sent to the corresponding A/D converters after being amplified. The digital communication between the DSP controller board and the BA-20 amplifiers can be established via the 16–bit digital I/O interface on the DS1102 controller board. This allows the DSP controller to monitor and control the BA20 amplifier's operational status.

The generated reference trajectories consist of only straight line acceleration / deceleration, and a constant velocity straight line. The position, velocity and acceleration constraints are applied and

the algorithm is developed in S-function. A careful trajectory planning system using position, velocity, acceleration and jerk constraints as proposed in (Erkorkmaz and Altintas 2001) was also explored. However, the dSPACE is found to be incapable of handling this complicated and computationally demanding algorithm in real time. Therefore, it was not utilized for real time trajectory generation.

4.2 Modeling

A current-controlled three phase linear motor BLM-142-A is considered for the controller design. Figure 4.5 shows a model of a single axis linear motor feed drive for a grinding application. In Figure 4.5, u is the control signal; K_a is the current amplifier gain, K_f is the motor force constant, and the mass is the equivalent mass of the whole drive.

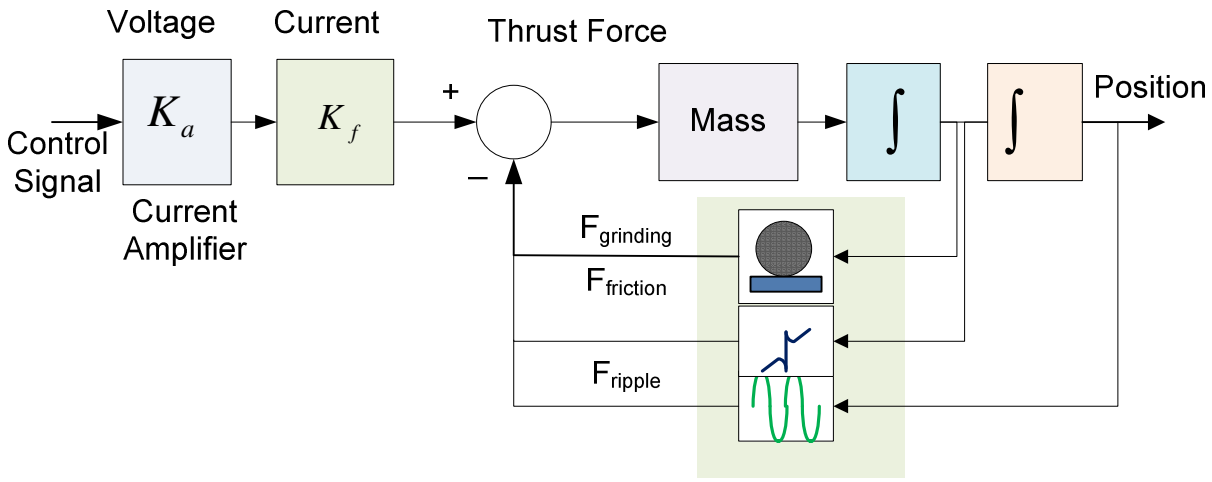

Figure 4.5 Block diagram of linear motor model.

According to Newton's law, the following equation can be obtained

$$F(t) = M\ddot{x} + f_{friction} + f_{ripple} + f_{grinding} \tag{4-1}$$

where M is the moving thrust mass, f_{ripple}, $f_{friction}$, and $f_{grinding}$ are force ripple, friction force and grinding force, respectively. Ignoring electrical dynamics, $F(t)$, the thrust force, is expressed as

$$F(t) = ku(t) \tag{4-2}$$

where $k = K_f K_a$

A classical friction model (Armstrong-Helouvry et al. 1994) that will be employed in this paper, is expressed as:

$$f_{friction}(\dot{x}) = \text{sgn}(\dot{x})(F_c + (F_s - F_c)e^{-(\dot{x}/v_s)^2}) + B\dot{x} \tag{4-3}$$

where F_s is stiction force , F_c is Coulomb friction force, B is the equivalent viscous friction coefficient , and v_s is the Stribeck velocity.

For the non-iron core motor that is used, the force ripple components associated with an iron-core motor do not exist. Although the force ripple component caused by self-commuting still exists, it will not remain a big issue because of the introduction of the modified six-step algorithm. Therefore, explicit modeling of force ripple will not be pursued. The system equation of motion can be thus obtained as

$$M\ddot{x} + B\dot{x} + D = Ku(t) \tag{4-4}$$

where the lumped term $D = \text{sgn}(\dot{x})(F_c + (F_s - F_c)e^{-(\dot{x}/v_s)^2}) + f_{ripple} + f_{grinding}$

Considering only linear terms, the simplified system equation of motion is basically a second-order system

$$M\ddot{x} + B\dot{x} = ku(t) \tag{4-5}$$

4.3 System Parameter Identifications

Once the model structure is determined, system identification can be carried out to determine its parameters. For an open loop linear time invariant system, many approaches have been suggested to fulfill the task of identification (Ljung 1999). For the linear motor feed drive, an open-loop approach will easily lead to collisions with physical limits. Hence, the closed–loop identification has to be performed.

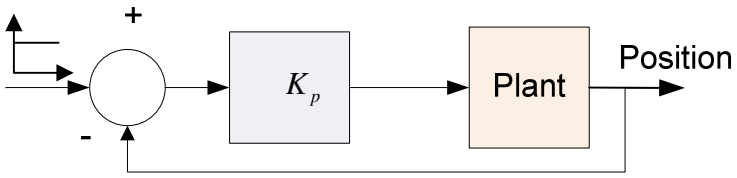

Figure 4.6 Closed-loop identification

4.3.1 Identification for linear dynamics

A direct approach (Ljung 1999) is applied for closed-loop identification. The loop is closed by a simple P controller as shown in Figure 4.6. A step signal was used an excitation. The step response of the closed-loop system is presented in Figure 4.7.

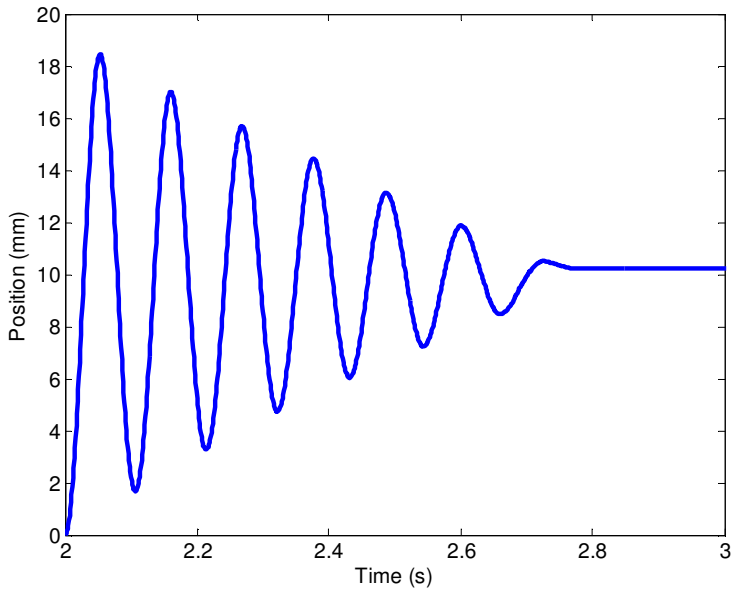

Figure 4.7 Step response of the linear motor feed drive under P control

For second order systems, the time response of a step input can be used to derive system parameters (Ogata 1992). The combination of the *2%* settling time, t_s, which is

$$t_s = \frac{4}{\zeta \omega_n} \tag{4-6}$$

where ζ is damping ratio and ω_n is undamped natural frequency, and the log decrement, δ, which is

$$\delta = \frac{1}{n}\ln(\frac{x_0}{x_n}) = \frac{2\pi\zeta}{\sqrt{1-\zeta^2}} \tag{4-7}$$

serves as a reliable means to determine the damping ratio and the undamped natural frequency. Once ζ and ω_n are determined, K/M and B/M will be determined to be 22,474 and 10.8, respectively.

4.3.2 Identification for friction

The static parameters can be estimated by construction of a friction-velocity map obtained from constant velocity motion. In this research, closed loop experiments under velocity PD control will be carried out. The measured velocity and input force values will be averaged to minimize the effect of velocity noise and force ripple to obtain friction-velocity data.

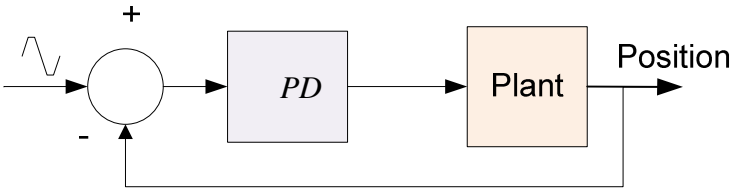

Figure 4.8 PD control for friction compensation

Experiments will be conducted for different constant velocities in a reasonable range. Within this range, a large number of average points will be collected at low velocity to improve identification of the Stribeck curve. A nonlinear optimization algorithm, as provided in the MATLAB optimization toolbox, will be used to fit the experimental data with the equation to minimize

$$\sum_{i=1}^{n}(F_{ss}(\dot{x}_i)-\hat{F}_{ss}(\dot{x}_i))^2 \tag{4-8}$$

where $F_{ss}(\dot{x}_i)$ are friction values measured during constant velocity motion and

$$\hat{F}_{ss}(v_i)=\mathrm{sgn}(\dot{x}_i)(\hat{F}_c+(\hat{F}_s-\hat{F}_c)e^{-|\dot{x}_i/\hat{V}_s|^2})+\hat{B}\dot{x}_i \tag{4-9}$$

where $\hat{F}_s$, $\hat{F}_c$, $\hat{B}$, and $\hat{V}_s$ are estimated friction parameters.

The Coulomb friction and stiction were found to be 0.22 and 0.24 volts, respectively. The calibrated relation between friction and velocity is presented in Figure 4.9.

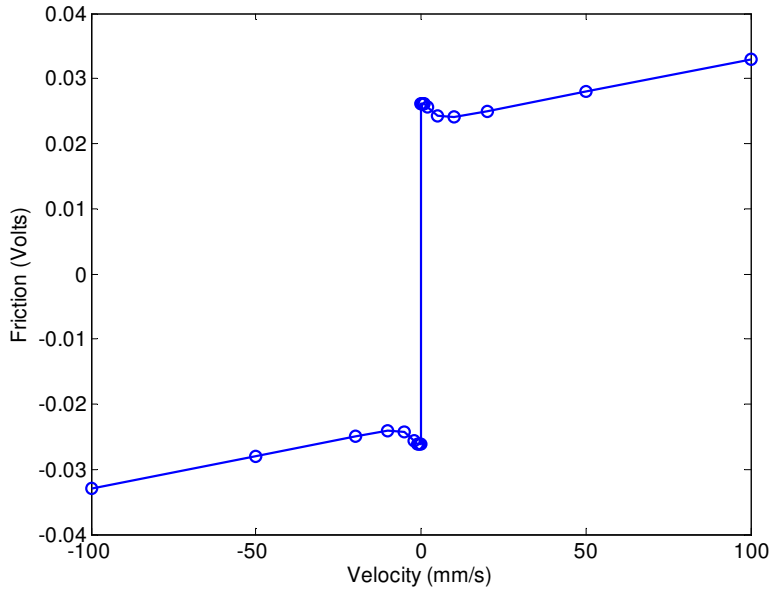

Figure 4.9 Friction model: friction force versus velocity

4.4 Model Validation

To validate the friction model, a PD controller law will be designed. Two tests will be performed: the first test is with a PD control only; the second test is with both PD feedback and friction feedforward compensation. The diagram for controller design is presented in Figure 4.10.

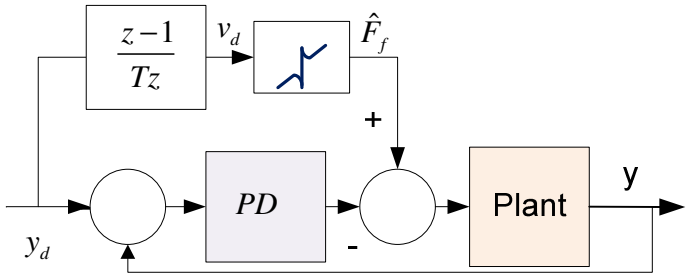

Figure 4.10 PD control with friction compensation

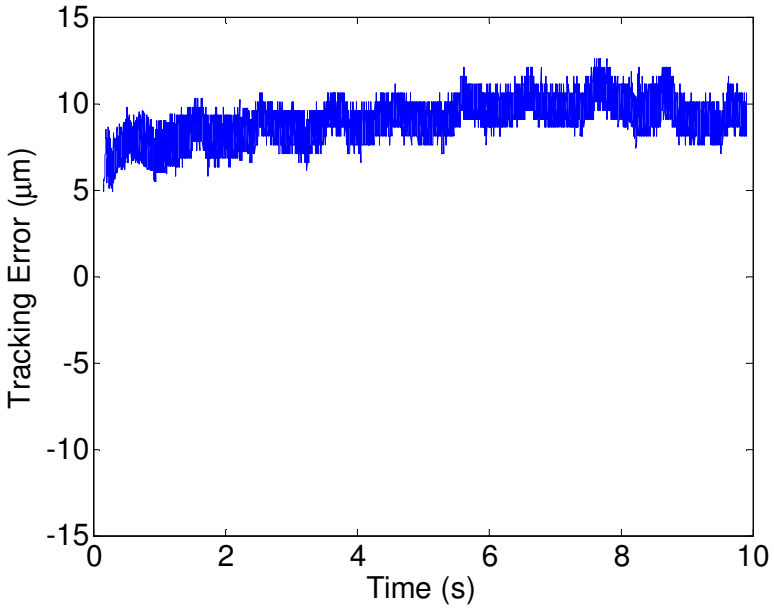

Figure 4.11 Tracking error without friction compensation

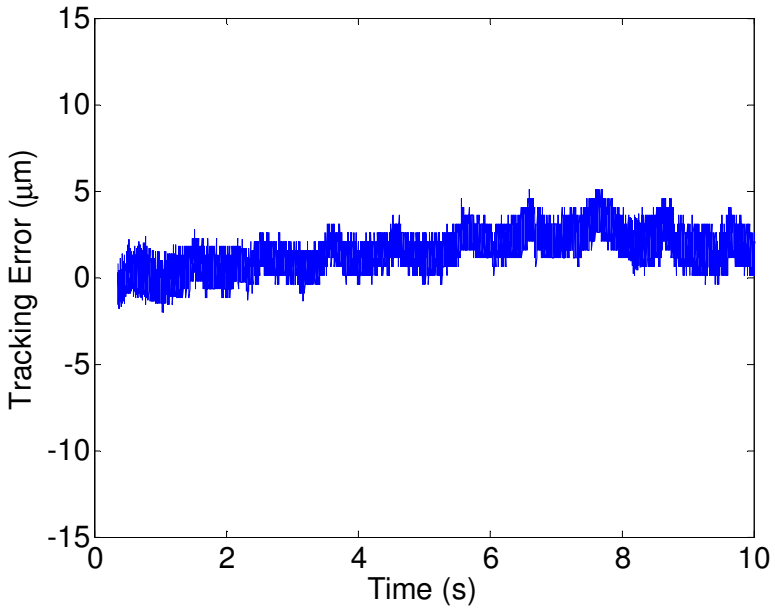

Figure 4.12 Tracking error with friction compensation

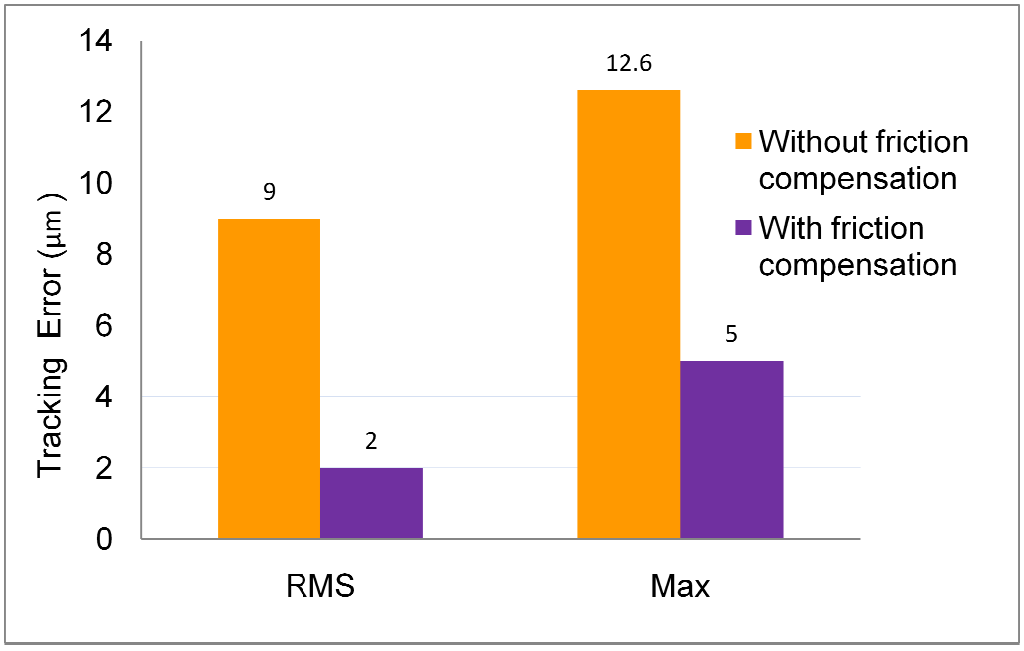

Figure 4.13 The comparison between the case without friction and the case with friction compensation

A reference trajectory with a feed rate of 10mm/s was employed for both tests. The tracking error for the case with a PD controller only is shown in Figure 4.11. It was determined that the axis tracking errors reach a value of 12.6 μm and there is steady state error due to the feedback controller not having integral action. On the other hand in Figure 4.12, it is seen that by injecting the predicted friction values into the control signal, both the tracking and the contour errors are reduced significantly, to a maximum value of about 5 μm. Furthermore, there is now no steady state error, in spite of the absence of integral action. Figure 4.13 presents the comparison between the case without friction compensation and the case with friction compensation. From this figure, it can be determined that friction compensation led to significant improvement of tracking performance, as the tracking error decreased about 80% in terms of the RMS value, and 60% in terms of the maximum value. These results demonstrate that the identified friction model can be used to successfully represent the actual friction, and to counteract its degrading effect on the tracking accuracy.

4.5 Summary

The chapter has two major parts. The first part, including Section 4.1, is the experimental setup. In this part, the mechanical and electrical aspects of the experimental setup are discussed. The motion control architecture which is employed for this study is also presented. The second part, including Sections 4.1-4.3, is concerned with modeling the identification for the linear motor feed drive. In this part, a linear servo model has been determined via the step response of the system under a simple P control. The parameters of the friction model have also been identified using a series of constant velocity experiments, and they have been verified in a trajectory with a

feed rate of 10mm/s. Experimental results showed that the identified friction model was very effective in counteracting the actual friction and preventing it from degrading the tracking and contouring performance. Hence, the axis dynamics and stiction characteristics required to design the high performance have been accurately modeled and identified.

CHAPTER 5

CONTROL OF LINEAR MOTOR FEED DRIVES FOR GRINDING MACHINES

This study investigates the application of a direct drive linear motor as the feed mechanism in a grinding machine. The goal is to achieve a higher level of positioning accuracy than can be obtained using traditional feed drive systems while avoiding insufficient dynamic stiffness, which is often encountered in control of linear motors for machining applications. This chapter proposes a robust motion control framework which combines the merits of a reaching law based sliding mode control and the disturbance estimation using either disturbance observer or adaptive on-line estimation for precision tracking to address the practical issues of friction, force ripple, and grinding force disturbances. The proposed control algorithm maintains the robustness of sliding mode control to parameter variations and external disturbances while attenuating the chattering which is often a major obstacle to practical implementation of sliding mode control. In this chapter, first a reaching law based sliding mode control system is presented. Next, a disturbance observer will be discussed. Then, a hybrid sliding mode control, which combines the sliding mode control and disturbance observer, is presented. After that, an adaptive sliding mode control system will be studied.

A linear motor feed drive will be subjected to external disturbances such as friction, force ripple and machining force. Due to the lack of a transmission unit, the tracking behavior of a linear motor feed drive is prone to be affected by external disturbances and model parameter variations

In this chapter, a hybrid sliding mode control (HSMC) which combines the reaching law based sliding mode control (RSMC) and disturbance observer (DOB) will be proposed. There are a few works (Kawamura et al. 1994; Kwon and Chung 2002) closely related to this approach, where a DOB based disturbance rejection was employed to improve the robustness of SMC. The HSMC is distinct from these approaches in these aspects:

(1) The RSMC in the proposed approach is also superior to that used in other approaches (Kawamura et al. 1994) in terms of chattering suppression performance and freedom in tuning to reach mode characteristics. Also, there exists a simple but systematic way to design a reaching law based SMC.
(2) In some approaches (Kwon and Chung 2002), however, because of the elimination of the discontinuous term, a finite reaching time cannot be obtained (Hung et al. 1993).
(3) The combination of DOB with RSMC is not simply putting two of them together; it is aimed at the best performance as a whole, instead. To facilitate this goal, a tuning mechanism will be introduced for DOB to achieve the best system performance.
(4) In addition, model-based friction compensation will be implemented to compensate for the shortcomings of DOB, therefore, enhancing the system tracking performance further.

A unique adaptive sliding mode control presented is also developed. Distinct from that presented by Altintas (2000), a reaching law based sliding mode control was utilized in order to provide a systematic way to design the sliding mode part. Meanwhile, it will guarantee asymptotic tracking error within a finite time. In addition, the discontinuous term will offer an option to handle the external disturbances and uncertainties without relying on a very high gain.

5.1 Introduction to Sliding Mode Control

Control problem solutions are usually based on a plant model, explicitly or implicitly. However, the plant model may not be a full description of the real plant, due for example to, the simplification in the modeling method, time varying plant model parameters, etc. The difference between the plant model and the real plant is called the model uncertainty. Moreover, the real plant always suffers from some external disturbances during operation. It is very important for a designed control system to ensure the desired performance in the presence of model uncertainty and disturbances.

This requirement calls for the robust control design method to be applied to the controller design. The sliding mode control (SMC) technique is a robust controller design method based on the linear model in state space.

It is often valid to address a machine tool feed drive as a linear single-input-single-output (SISO) system subject to model uncertainties and external disturbances. The linear plant model in state space for a (SISO) n-th order continuous-time system is given in Equation (5-1)

$$\begin{aligned} \dot{x}(t) &= Ax(t) + Bu(t) \\ y(t) &= Cx(t) \end{aligned} \tag{5-1}$$

with state vector $x \in R^n$, $C \in R^n$ is the output vector, u and y are the input and output variables, B is the input vector, C is the output vector, $A \in R^{n \times n}$ is the system matrix.

Sliding mode control is a particular type of variable structure control (VSC), in which the control system uses a switching function to provide different control laws according to different situations. The sliding mode control technique has its root in relay control and bang-bang control. It was developed in the former Soviet Union by S. V. Emelyanov, U. Itkis and several other researches in the 1950s, and only came to the attention of the whole control society in the 1970s (Utkin 1977).

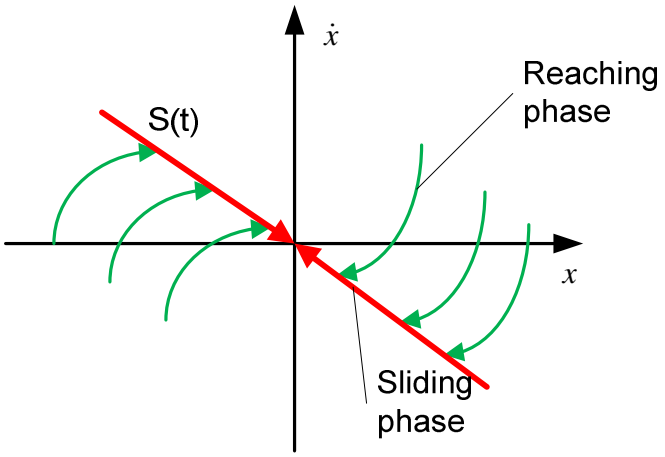

Figure 5.1 Two phases of sliding mode control

As shown in Figure 5.1, the motion of trajectory under sliding mode control consists of two phases. The first phase is the reaching phase, during which motion trajectories move toward a pre-defined switching surface and reach it in finite time. In the reaching phase, the dynamics of the closed-loop system is called the reaching mode. Following the reaching phase, the motion undergoes a sliding phase, during which the motion is confined to the sliding surface. In the sliding phase, the dynamic behavior of the closed-loop system is described as an ideal sliding mode.

Correspondingly, the sliding mode design approach consists of two steps. The first involves the design of the switching surface (or switching function) so that the sliding motion satisfies design specifications. The second is concerned with the selection of a control law, which may drive the system states onto the pre-defined switching surface in the state space, and may retain the system states on the surface once it is reached (Edwards and Spurgeon 1998). The condition under which the state will move toward and reach a sliding surface is called a reaching condition.

Suppose the pre-defined switching surface in state space has the form:

$$s(t) = cx(t), c \in R^n \tag{5-2}$$

control signal that is needed to maintain the system states in the ideal sliding mode can be determined using the method of equivalent control (Utkin et al. 1999). Suppose at t_0 the state trajectory of the plant intercepts the switching surface and a sliding mode exists for $t \geq t_0$. The existence of a sliding mode implies $\dot{s}(x(t)) = 0$ and $s(x(t)) = 0$ for all $t \geq t_0$.

From the chain rule $$\left[\frac{\partial s}{\partial x}\right]\dot{x} = \left[\frac{\partial s}{\partial x}\right]\left[Ax + Bu_{eq}\right] = 0 \tag{5-3}$$

where u_{eq} is the so called equivalent control which solves this equation. Assuming that the matrix product $\left[\frac{\partial s}{\partial x}\right]B$ is nonsingular for all t and x, u_{eq} can be computed as

$$u_{eq} = \left[\left[\frac{\partial s}{\partial x}\right]B\right]^{-1}\frac{\partial s}{\partial x}Ax \tag{5-4}$$

The total control law needed for both the reaching mode and the ideal sliding mode can be obtained by augmenting the equivalent control in Equation (5-4) such that:

$$u(t) = u_{eq} + u_{sw} \tag{5-5}$$

where u_{sw} is a discontinuous term, or so-called switching component, which can be expressed as

$$u_{sw} = -k_s \operatorname{sgn}(s) \tag{5-6}$$

where

$$\operatorname{sgn}(s) = \begin{cases} 1 & for\, s > 0 \\ 0 & for\, s = 0 \\ -1 & for\, s < 0 \end{cases} \tag{5-7}$$

5.2 Reaching Law Method for Sliding Mode Control

Three approaches for specifying the reaching condition have been proposed. The earliest one is the direct switching function approach, in which the reaching condition is described as

$$\begin{cases} \dot{s}_i < 0 & when \quad s_i > 0 \\ \dot{s}_i > 0 & when \quad s_i < 0 \end{cases} \tag{5-8}$$

This reaching condition is global but does not guarantee a finite reaching time. The Lyapunov function approach chooses a Lyapunov function candidate with a negative derivative as

$$\dot{V}(x,t) = (\frac{d}{dt})(s^2) < 0 \qquad s \neq 0 \tag{5-9}$$

A finite reaching time is guaranteed by modifying (5-9) to

$\dot{V}(x,t) < -\varepsilon$ where ε is positive (5-10)

For a SISO system, there is no difference between (5-8) and (5-9). Although approaches such as those presented in both (5-8) and (5-9) satisfy the reaching condition, no attention is paid to the transient performance of the reaching dynamics. As a result, the obtained control law is often unnecessarily large, which easily leads to saturation and thus the loss of the desired SMC characteristics. In addition to this, the solution procedures for the control law from (5-8) or (5-9) are not straightforward; and thus they often demand a great amount of time and effort, which is undesirable for practical implementation in motion control of a machine tool feed drive.

To overcome the shortcomings of the above approaches, a reaching law approach was developed (Gao and Hung 1993). It not only establishes the reaching condition but also specifies the dynamic characteristics of the system during the reaching phase. Additional merits of this approach include simplification of the solution for VSC and providing a measure for the reduction of chattering. The reaching law approach directly specifies the dynamics of the switching function. Let the dynamics of the switching function be specified by the differential equation

$$\dot{s} = -\eta \,\mathrm{sgn}(s) - qf(s) \tag{5-11}$$

The scalar function $f(s)$ satisfies the condition

$$sf(s) > 0 \tag{5-12}$$

Equation (5-11) is called the reaching law. Various choices of q and η specify different rates for s and yield different structures in the reaching law. One typical form is

$$\dot{s} = -\eta \,\mathrm{sgn}(s) - qs \tag{5-13}$$

The value of *s(t)* can be interpreted as a measurement of the distance of the system states to the switching surface, and the establishment of the sliding mode can be interpreted as the dynamic process by which the distance *s(t)* approaching to zero. To make sure that the switching surface can be reached under the sliding mode controller, it should be guaranteed with:

$q > 0$ (5-14)

To guarantee the finite reaching time, η should also be positive.

Having selected the reaching law, the control law can be determined as

$$u = -\left(\frac{\partial s}{\partial x}B\right)^{-1}\left[\left(\frac{\partial s}{\partial x}\right)Ax + \eta sgn(s) + qs\right] \quad (5\text{-}15)$$

which can be rewritten as

$$u = u_{eq} + u_{sw} \quad (5\text{-}16)$$

where $u_{eq} = -\left(\frac{\partial s}{\partial x}B\right)^{-1}\left[\left(\frac{\partial s}{\partial x}\right)Ax\right]$ and $u_{sw} = -\left(\frac{\partial s}{\partial x}B\right)^{-1}[\eta sgn(s) + qs]$.

5.3 SMC in the Presence of Model Uncertainty and External Disturbance

So far we have discussed the control law for establishing the sliding mode for a nominal continuous-time system. However, in the presence of plant model uncertainty and external disturbance, a sliding mode that can be established in finite time under the control law has to be verified.

Consider an uncertain and disturbed plant model as:

$$\dot{x} = (A + \Delta A)x(t) + (B + \Delta B)u(t) + f(t)$$

$$y(t) = Cx(t) \qquad (5\text{-}17)$$

With system matrix $A \in R^{n\times n}$, the multiplicative and additive uncertainties are lumped into the uncertainty matrix $\Delta A \in R^{n\times n}$, the input matrix $B \in R^{n\times r}$, and output matrix $C \in R^{m\times n}$. *x(t)* is the state vector, *u(t)* the input signal, f(t) $\in R^{r\times 1}$ the disturbance signal, *y(t)* $\in R^{m\times 1}$ the output signal, all with conformable dimension.

The plant presumes no statistical information on the uncertainties. To obtain some desirable properties, the plant uncertainties ΔA, ΔB and f are required to lie in the column space of B. This requirement is the so-called matching condition. Assuming the satisfaction of the matching condition, the min-max method (Corless and Leitmann 1981) provides a deterministic approach to the control of a class of uncertain systems as formulated in Equation (5-17) with bounded uncertainties.

The min-max approach leads to a discontinuous control law for the stabilization of the system with uncertainties. In this regard, the SMC shares a similarity. However, the SMC has an additional equivalent control term to accomplish the desired tracking performance.

Without the plant model uncertainty and external disturbance, an equivalent control can designed under the control law in Equation (5-4). In the presence of the model uncertainty and external disturbance, the equivalent control law can be derived as

$$u_{eq} = -(\frac{\partial s}{\partial x}(B + \Delta B))^{-1}\frac{\partial s}{\partial x}[(A + \Delta A)x + f] \qquad (5\text{-}18)$$

If the following matching condition is met

$$\begin{cases} \Delta A = B\tilde{A} \\ \Delta B = B\tilde{B} \end{cases}$$

$$f = B\tilde{f} \tag{5-19}$$

Equation (5-18) can be reformulated as

$$u_{eq} = -(I + \tilde{B})^{-1}(\frac{\partial s}{\partial x}B)^{-1}\frac{\partial s}{\partial x}[Ax + B(\tilde{A}x + \tilde{f})] \tag{5-20}$$

Substituting Equation (5-20) into Equation (5-17), the sliding mode is found to be

$$\dot{x} = Ax - B(\frac{\partial S}{\partial x}B)^{-1}\frac{\partial s}{\partial x}Ax \tag{5-21}$$

which is independent of perturbations and external disturbances. Basically this showed that, under matching conditions, the sliding mode is not affected by the system's perturbations and external disturbances, this property is called invariance (Drazenovic 1969). The invariance characteristic makes SMC an attractive robust control design method for uncertain and disturbed processes.

Suppose the controller structure is

$$u(t) = -\left(\frac{\partial s}{\partial x}B\right)^{-1}\left[\left(\frac{\partial s}{\partial x}\right)Ax + \eta sgn(s) + qs\right] \tag{5-22}$$

Applying the control law in (5-22) to the system described by (5-17), the reaching dynamics can be expressed as

$$\dot{s} = -qs - \eta\mathrm{sgn(s)} + \mathrm{cB}\left[\tilde{\mathrm{f}}(\mathrm{t}) + \tilde{\mathrm{A}}\mathrm{x}(\mathrm{t}) + \tilde{\mathrm{B}}\mathrm{u}(\mathrm{t})\right] \tag{5-23}$$

Let $\rho(x(t), u(t), t) = \tilde{f}(t) + \tilde{A}x(t) + \tilde{B}u(t)$

If the lumped disturbance is bounded with:

$$|\rho(x(t), u(t), t)| \leq F \tag{5-24}$$

To satisfy the reaching conditions, the following condition should be met

$$\begin{cases} \dot{s} < -\eta, s > 0 \\ \dot{s} > \eta, s < 0 \end{cases} \tag{5-25}$$

A conservative design can be obtained by modifying the control law as the following

$$u(t) = -\left(\frac{\partial s}{\partial x}B\right)^{-1}\left[\left(\frac{\partial s}{\partial x}\right)Ax + (\eta + F)sgn(s) + qs\right] \tag{5-26}$$

This finishes the derivation of the control law for the reaching law based SMC for a class of systems which undergo bounded disturbances and which satisfy the matching condition.

5.4 Reaching Based Sliding Mode Control for Linear Motor Feed Drives

The sliding mode control approach is very attractive for controlling systems with uncertainties such as the linear motor feed drives, because it is robust and in many cases it shows invariance characteristics, which means the system is complementally insensitive to parameter uncertainties and external disturbances (Hung et al. 1993).

So far, we have only discussed the regulation problem. For machine tool feed drives, the important problem is the tracking problem, which involves the design of a control law such that the system output follows a given reference trajectory. In this section, we will address the issue with direct application to the control of linear motor feed drives.

Assuming all the system states are available, the sliding mode control design can be derived as follows:

First, as in (Slotine and Li 1991) , the switching function can be defined as

$$s = \dot{e} + \lambda e \tag{5-27}$$

where e is the tracking error evaluated by the difference of x_d , the desired trajectory state and x , the actual state, as

$$e = x_d - x \tag{5-28}$$

Then, the reaching law method will be used to establish the reaching condition. The control law presented in (5-15) will be utilized. After some mathematical manipulations, the control law is found to be

$$u = \frac{m}{k}(\ddot{x}_d + \lambda(\dot{x}_d - \dot{x}) + \eta \,\mathrm{sgn}(s) + qs) \tag{5-29}$$

where *m* and *k* are the total mass and the whole amplification factor from the control signal to the generated force, respectively. From (5-30), it can be seen that a velocity signal is required for the implementation. Since no velocity sensor is used, the finite difference method will be applied to obtain the velocity information.

To prove the effectiveness of the reaching law that is used, the Lyapunov function is defined as

$$V = \frac{1}{2}s^2 \tag{5-30}$$

The time derivative of the above Lyapunov function can be evaluated by

$$\dot{V} = s\dot{s} = -\eta|s| - qs^2 \tag{5-31}$$

V is positive definite and $\dot{V}$ is negative definite (both η and q are positive). According to the second method of Lyapunov, the s will asymptotically tend to zero. Once on the sliding surface, the tracking error will be guaranteed to converge to zero.

The derived control law is implemented for the linear motor feed drive as shown in Figure 5.2,

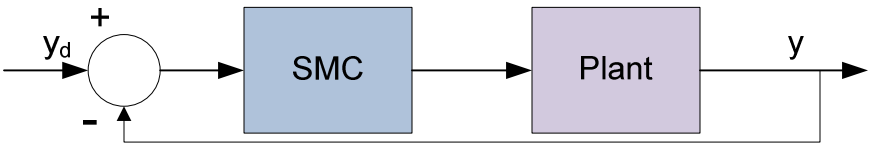

Figure 5.2 Block diagram of sliding mode control strategy

5.5 Disturbance Observer

DOB is one of several good approaches for handling disturbances in motion control (Umeno and Hori 1991; Ohnishi et al. 1996). The merit of the DOB is that it can estimate a disturbance and reject it without affecting performance. The separation property enables two independent design stages to be used for the overall controller design: one for performance and one for disturbance rejection. Another benefit of DOB is that it makes the real plant behave like the nominal plant for a certain frequency range and, thus, the robustness of the system is improved (Umeno and Hori 1991; Lee and Tomizuka 1996).

Figure 5.3 shows the general structure of a DOB for a SISO plant, where $P(s)$, $P_n(s)$, r, d, y and ξ are the actual plant transfer function, nominal plant transfer function, command input,

external disturbance, output, and sensor noise, respectively. The input-output relationship can be obtained as

$$y = \frac{P(s)P_n(s)}{\psi(s)} r + \frac{P(s)P_n(s)(1-Q(s))}{\psi(s)} d + \frac{P(s)Q(s)}{\psi(s)} \xi \tag{5-32}$$

where $\psi(s) = P_n(s) + Q(s)(P(s) - P_n(s))$.

$Q(s)$ is introduced as a low-pass filter to avoid direct plant inverse. Below the cutoff frequency, $Q(s) \approx 1$.Then, the input-output relation can be simplified as

$$y \approx P_n(s)r + \xi \tag{5-33}$$

Thus, the plant behaves the same as the nominal model. On the other hand, if $Q(s) \approx 0$, the input-output relation can be easily verified such that

$$y = P(s)r + P(s)d \tag{5-34}$$

Hence the high frequency measurement noise is attenuated and the system performs as an open loop system. Therefore, the design of the low-pass filter concerns the tradeoff between $1-Q(s)$ and $Q(s)$ to maintain insensitivity to both model uncertainty and measurement noise. Aiming at this goal, Ohnishi designed $Q(s)$ as a first-order filter (Murakami and Ohnishi 1990). Umeno and Hori suggested a binominal filter for $Q(s)$ (Umeno and Hori 1991). In this research, a third order binominal filter will be chosen.

$$Q(s) = \frac{3(\tau s)+1}{(\tau s)^3 + 3(\tau s)^2 + 3(\tau s) + 1} \tag{5-35}$$

where τ is a time constant.

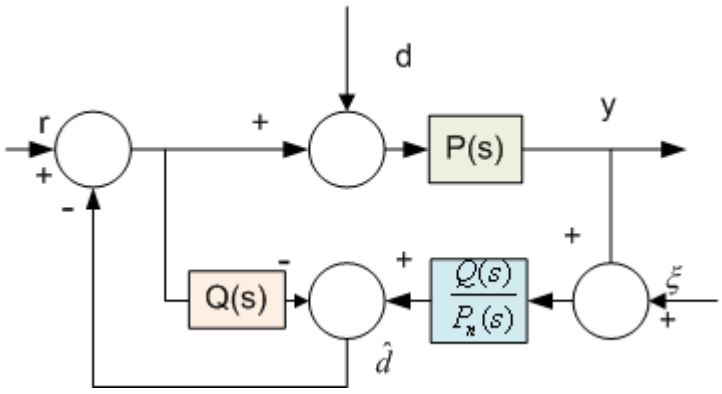

Figure 5.3 General structure of a DOB for a SISO plant

Figure 5.4 shows the equivalent structure to a two degree of freedom (TDOF) servo system with DOB as proposed in (Umeno et al. 1993).

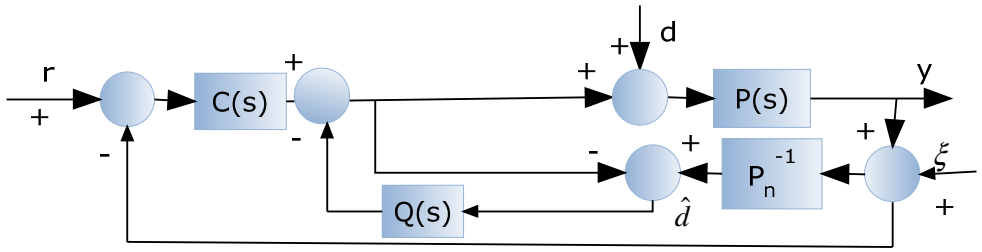

Figure 5.4 Block diagram of DOB control strategy.

5.6 Design of Robust Tracking Controllers

In this section, a robust tracking controller design framework will be proposed. First, the SMC design will be discussed. Then, the DOB will be examined. And finally the SMC will be combined with the DOB to further enhance the system tracking performance.

5.6.1 Hybrid Sliding Mode Control

In a SMC, the main purpose of the switching term is to reject disturbances and to desensitize against unknown parameter perturbations. If the disturbance is sufficiently compensated, the magnitude of the discontinuous control components can be reduced significantly, or the whole term can be discarded, to achieve a sliding mode. Thus, the issue of chattering could be minimized, or even eliminated. Motivated by this consideration, a robust tracking controller design framework which combines the reaching law based SMC and the disturbance observer (DOB) will be proposed. The schematic of the control structure is shown in Figure 5.5, where the SMC is employed. In this framework, the DOB is used to estimate a disturbance and to make system behave like the nominal plant for a certain frequency range. The proposed control algorithm maintains the robustness of sliding mode control to parameter variations and external disturbances while attenuating the chattering which is often a major obstacle to practical implementation of sliding mode control.

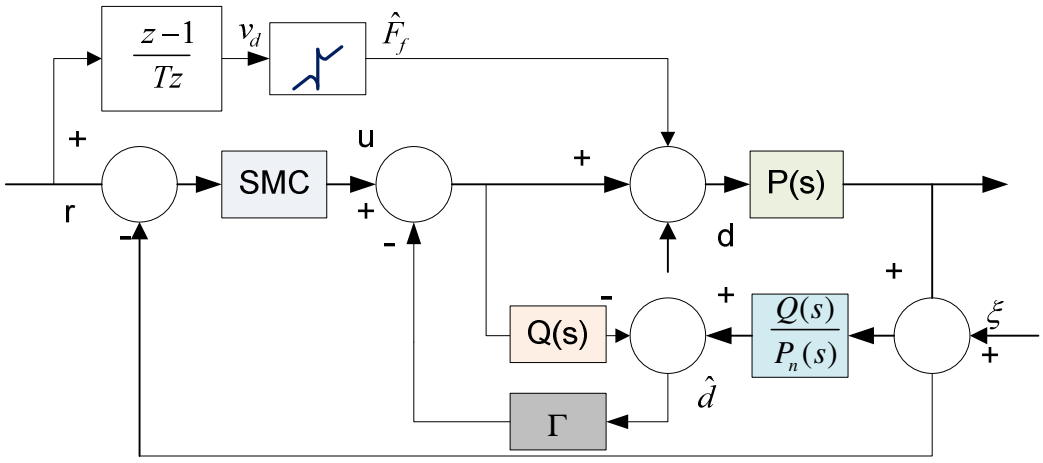

Figure 5.5 Hybrid SMC combining SMC with DOB.

5.6.2 Adaptive Sliding Mode Control

It is widely recognized that the accuracy of conventional approaches such as PID at high-speed or low speed is greatly affected by the parameter uncertainties and external disturbances. This sensitivity is especially severe for linear motor feed drives because of the elimination of the transmission system.

As shown in Figure 5.6, with the increase of the uncertainty of parameters and disturbances, the machine intelligence required should also enhance. Two classes of approaches are being actively studied to maintain the performance of the servo control in the presence of parameter uncertainties: robust control, to which class the SMC belongs, and adaptive control (Slotine and Li 1991). The adaptive approach improves the accuracy of a servo system with uncertainties over time, potentially holding the promise of consistent performance in the face of large uncertainties.

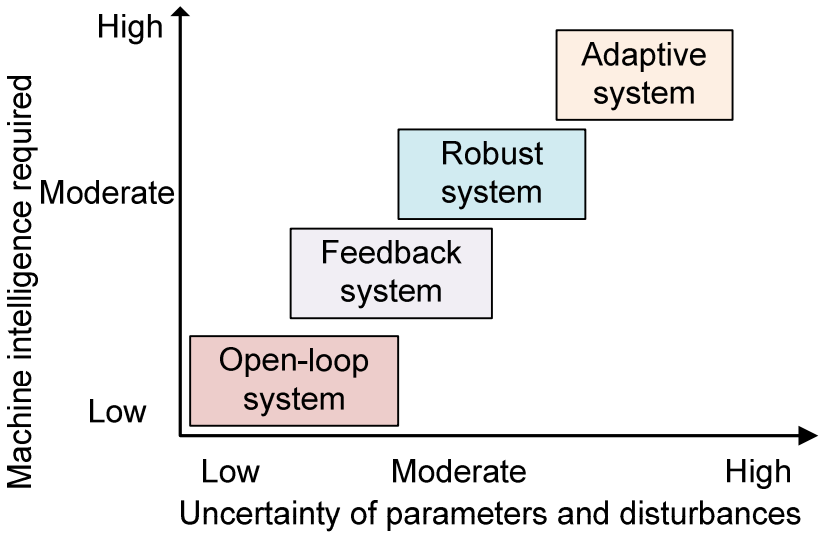

Figure 5.6 Intelligence required versus uncertainty for modern control system (Dorf and Bishop 2001)

An adaptive controller is formed by combining an adaptive mechanism, referred to as the adaptive law, to provide estimates of unknown parameters at each instant, with a control law that is motivated from the known parameter case (Ioannou and Sun 1996). The advantages of the adaptive algorithms lie in that the system can guarantee asymptotic stability when the system is subjected to parameter uncertainties only. However, they all have some significant drawbacks. One of them is that the transient performance of system controlled by an adaptive controller is hard to guarantee (Krstiâc et al. 1995); and even a poor initial parameter estimates may result in unacceptably bad transient behavior. Another shortcoming is that system may lose stability even when small disturbance appears because disturbances and unmodeled dynamics are not considered. In addition, determining the adaptation ceasing mechanism for an adaptive controller is an issue.

To obtain the advantages of both adaptive and robust control, more intelligent control, such as adaptive robust control (Slotine and Coetsee 1986; Yao et al. 1997) and robust adaptive control (Ioannou and Sun 1996) were developed.

The sliding mode control achieves effective tracking in the presence of disturbances, which may be time-varying, and parameter variations. In order to further improve performance, a more adaptive mechanism was added to the sliding mode control, enabling adaptation of unknown parameters with bounds, which leads to a so–called adaptive sliding mode controller. The progress was in large part due to the pioneering work of Slotine et al (Slotine and Coetsee 1986; Slotine and Li 1988; 1989). In these algorithms, all unknown plant parameters are estimated on-

line, which is not computationally efficient, especially for real-time implementation such as servo control of machine tool feed drives.

In order to facilitate the real time implementation, a computationally efficient adaptive sliding mode control algorithm will be introduced. The diagram of the algorithm is shown in Figure 5.7. In this approach, a reaching law based sliding mode control will be utilized to deal with model uncertainties to avoid unnecessary on-line estimation. Instead of the adaptation of unknown parameters, adaptation is conducted only for the unpredicted disturbances.

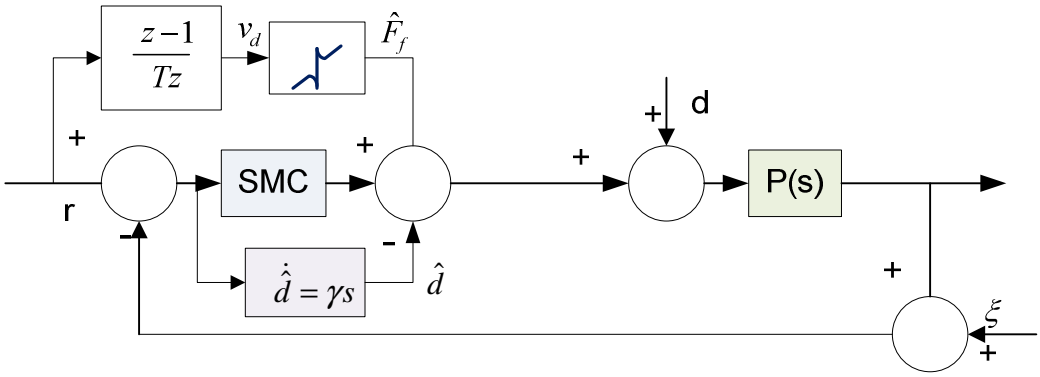

Figure 5.7 Diagram of the adaptive sliding mode control

In this approach, the variation in the external disturbance caused by grinding process and uncompensated friction is considered to be constant and bounded as

$$d \epsilon [d^-, d^+] \tag{5-36}$$

where $d^-$the lower is limit and d^+ is the upper limit of the external disturbance.

To estimate the disturbance, the following adaptation law (Yao et al. 1997) can be used

$$\dot{\hat{d}} = \begin{cases} 0, & if \begin{cases} \hat{d} = d^- \ and \ s > 0 \\ \hat{d} = d^+ \ and \ s < 0 \end{cases} \\ \gamma s, otherwise \end{cases} \tag{5-37}$$

where $\gamma > 0$ is the adaptation rate and s is the switching function as defined in (5-27).

The next step is to prove the stability of the controller. As in (Altintas et al. 2000), a Lyapunov function can be chosen as

$$V = \frac{1}{2}[ms^2 + \frac{(d-\hat{d})^2}{\gamma}] \tag{5-38}$$

Its derivative can be calculated as

$$\dot{V} = ms\dot{s} - \frac{(d-\hat{d})}{\gamma}\dot{\hat{d}} \tag{5-39}$$

By choosing a control law as

$$u = \frac{m}{k}(\ddot{x}_d + \lambda(\dot{x}_d - \dot{x}) + \eta\,\mathrm{sgn}(s) + qs) + u_a \tag{5-40}$$

where u_a is the adaptive control term, the equation can be rewritten as

$$ms(\eta\,\mathrm{sgn}(s) + qs) + (ku_a - \hat{d})s \tag{5-41}$$

By forcing $ku_a - \hat{d} = 0$

u_a can be computed as

$$u_a = \frac{\gamma\int sdt}{k} \tag{5-42}$$

So the total control effort can be described as

$$u = \frac{m}{k}(\ddot{x}_d + \lambda(\dot{x}_d - \dot{x}) + \eta\,\mathrm{sgn}(s) + qs) + \frac{\gamma\int sdt}{k} \tag{5-43}$$

With the above controller, the (4-40) can be calculated as

$$\dot{V} = ms(-\eta sgn(s) - qs) \tag{5-44}$$

which can be rewritten as

$$\dot{V} = -\eta m|s| - qms^2) \leq 0 \tag{5-45}$$

From the Lyapunov second law the asymptotic stability o f the presented algorithm will be ensured.

5.7 Summary

This chapter proposes a robust motion control framework for linear motor feed drives in grinding machines. The presented algorithms combine the merits of a reaching law based sliding mode control and disturbance estimation using either a disturbance observer or an adaptive mechanism for precision tracking. The result is that those algorithms address the practical issues of friction, force ripple, and grinding force disturbances. Compared to traditional SMC, HSMC maintains robustness to parameter variations and external disturbances while attenuating the chattering which is often a major obstacle to practical implementation of sliding mode control.

CHAPTER 6

EXPERIMENTAL RESULTS

The purpose of the experiments is to investigate the effectiveness of the proposed controllers. All of the experiments are performed on the linear motor feed drive test rig that is fabricated and implemented on a surface grinding machine. In these experiments, the design parameters of each controller are set to their best values, in terms of the conflicting requirements of tracking accuracy in the face of measurement noise, disturbances, and unmodeled high-frequency dynamics, so that the best performances of the controllers can be compared. A wide range of testing conditions has been pursued. These experimental results are used to validate the effectiveness and practicality of the proposed linear motor feed drive application for grinding machines.

6.1 Controller Parameters Tuning

Generally speaking, larger gains, k, result in smaller tracking errors. However, large gain values will excite unmodeled dynamics. So, there is a trade-off. A value of 3000 is found to be good for k. The selection of λ, which is the bandwidth of the sliding surface, is an important factor in the controller design. In general, a higher bandwidth will provide more accurate positioning

performance until high-frequency dynamics that are neglected in the course of modeling, such as resonant structural modes, neglected actuator time-delays, or sampling effects, are excited. To obtain a good λ ,a guideline suggested by Slotine (1991) will be followed. In this study, a value of 300 is found to be good. The selection of a discontinuous term is in accordance with the requirements of the reaching condition under the effects of model uncertainties and external disturbances. Since both *HSMC* and *ASMC* provide additional disturbance rejection capabilities, η was set to zero in order to reduce chattering. The adaption factor, $\boldsymbol{\gamma}$, for *ASMC*, the coefficient of DOB, Γ, for HSMC, and the gains of the *PD* controller are all tuned for their best performance. The time constant of the Q filter as presented in Chapter 5 is gradually reduced until the best tacking performance is obtained.

6.2 Comparative Experiments Results for Non-grinding

In order to compare the performances of different controller algorithms, four sets of experiments were carried out. In Set 1, all four controllers ran without friction compensation, whereas in Set 2, all of them were combined with friction compensation using the fiction model as presented in Chapter 4. In Set 3, we conducted experiments to compare low feed rate performance among all of the four controllers, for which a feed rate of 0.1mm/s was utilized. On the other hand, high feed rate capacities are desired for high productivity. To compare high feed rate performance, experiments with feed rate of 100mm/s will be conducted. For all four sets, the profiles of desired trajectories are similar to Figure 6.1 except that the feed rates may vary from case to case.

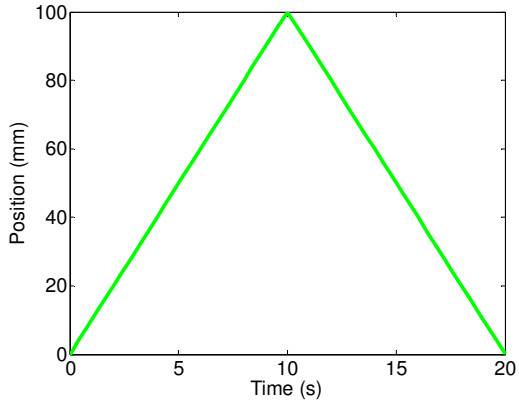

Figure 6.1. Desired trajectory with a feed rate of 10mm/s

Table 6.1 Comparative experimental results for a feed rate of 10mm/s without friction compensation

Controllers	PD	SMC	HSMC	ASMC
Max Error (μm)	12.6	10.6	2.2	3.6
Error RMS (μm)	9	6.3	0.8	1.4

Table 6.2 Comparative experimental results for a feed rate of 10mm/s with friction compensation

Controllers	PD	SMC	HSMC	ASMC
Max Error (μm)	5.1	4.6	3.4	4.1
Error RMS (μm)	2	1.7	1.1	1.6

Table 6.3 Comparative experimental results for a feed rate of 0.1mm/s

Controllers	PD	SMC	HSMC	ASMC
Max Error (μm)	2.4	5.4	1.4	1.8
Error RMS (μm)	1.3	1.6	0.3	1

Table 6.4 Comparative experimental results for a feed rate of 100mm/s

Controllers	PD	SMC	HSMC	ASMC
Max Error (μm)	5.7	6	3	3.2
Error RMS (μm)	2.3	2.4	1.2	1.3

For Set 1, the experimental results are listed in Table 6.1. In this Table, Max error refers to the maximum absolute tracking error, while Error RMS means the root mean square of tracking error.

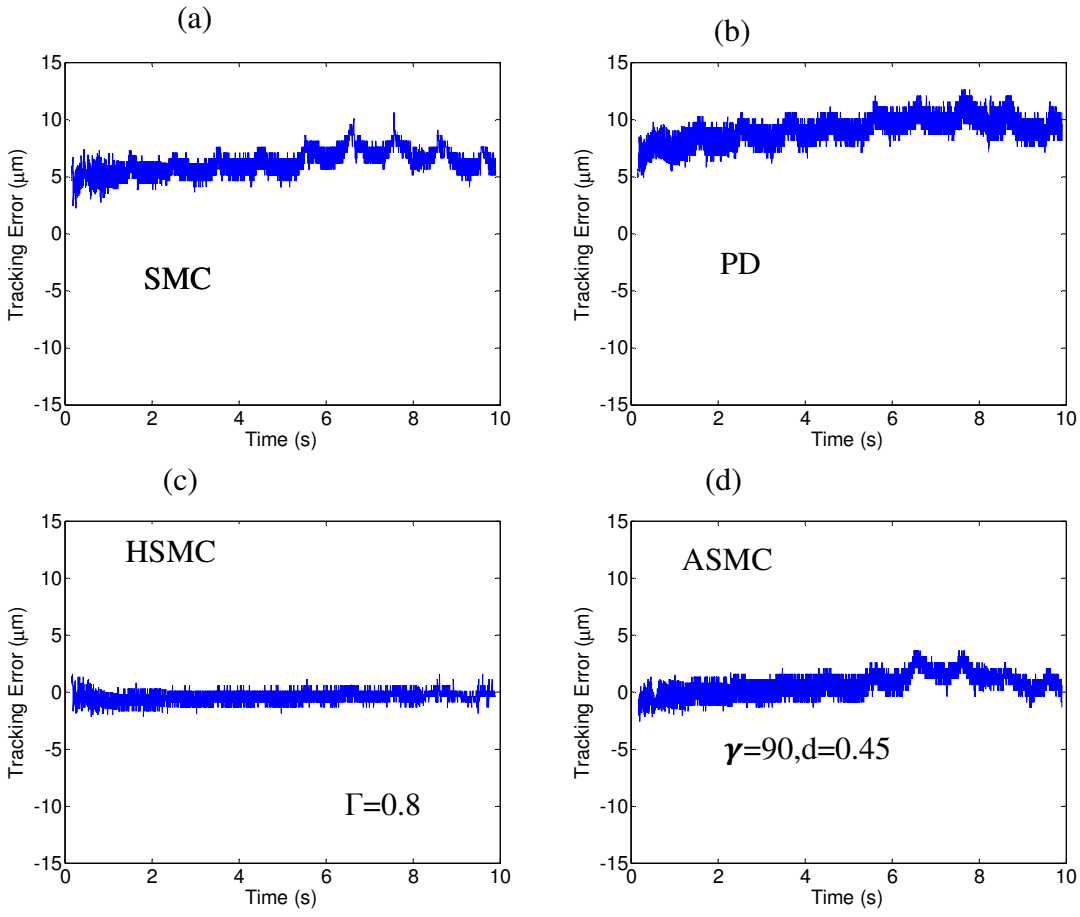

Figure 6.2 Tracking errors without friction compensation

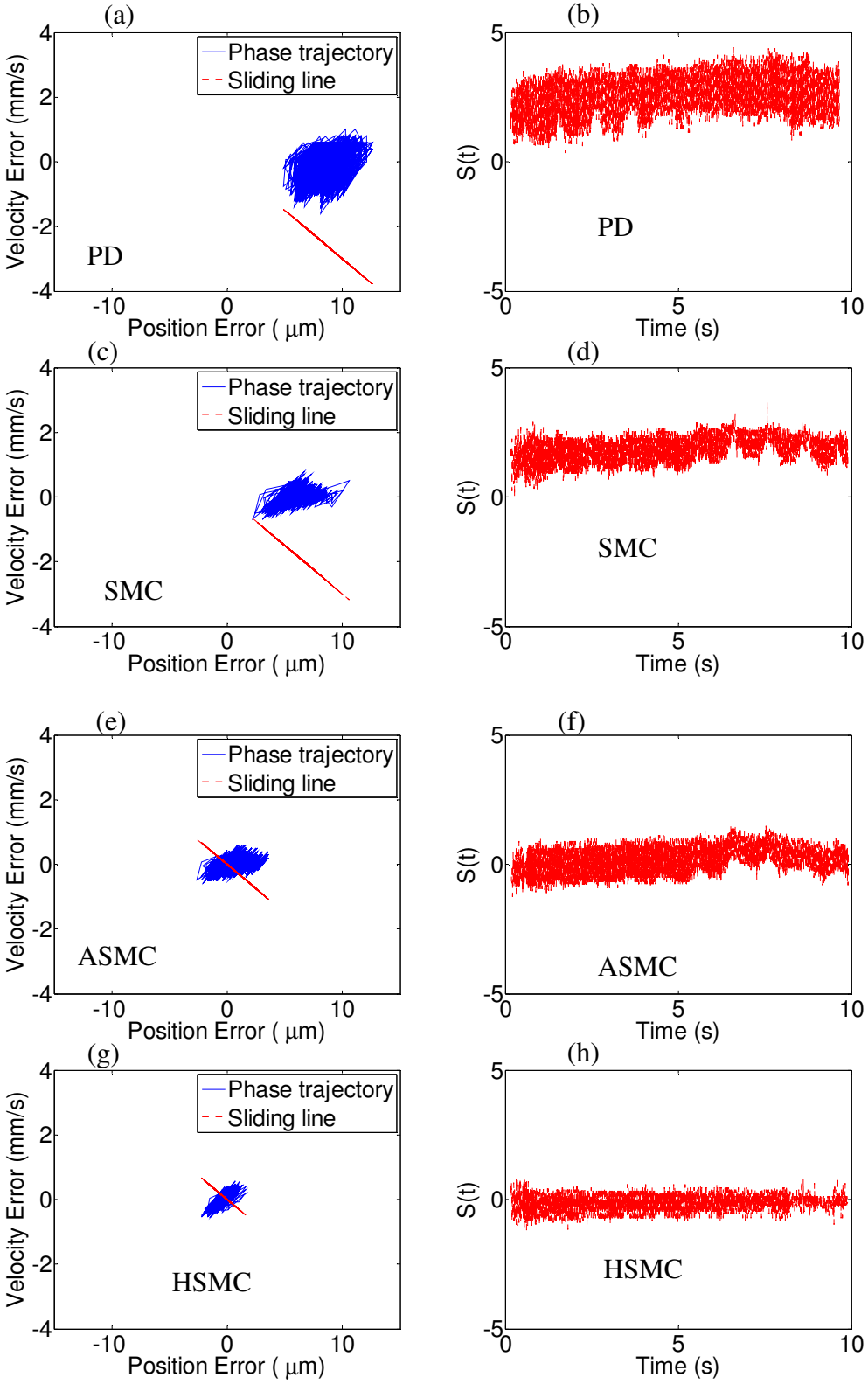

Figure 6.3 Sliding dynamics without friction compensation

Figure 6.2, for tracking errors, and Figure 6.3, for sliding dynamics, show the experimental results for SMC following the desired trajectory as shown in Figure 6.1. From both figures, it can be seen that the HSMC has the best performance, the next is ASMC, the third is SMC, and the PD has the worst performance. For the latter two, the existence of steady state errors is very evident. For PD, the steady state errors were caused due to the absence of integral action. More information can be gained from the plots of the phase portrait and switching function as shown in Figure 6.3(a) and (b), respectively. It can be seen from Figure 6.3(a) that the state trajectory deviated significantly from the sliding line. The plot of the switching function shows the existence of state errors indirectly, because zero steady sate error demands a zero steady state switching function, although no sliding mode controller is used. For SMC, the tracking error is diminished compared to the PD case because the switching term can handle the friction to some extent. From Figure 6.3(c), it can be seen that the state trajectory is not bounded to the sliding line. Meanwhile, Figure 6.3(d) also shows that the reaching mode is not as desired. A larger switching term would aid in satisfying the reaching condition; however, a larger switching term has an adverse impact on the tracking performance, which is expressed in state space.

By contrast, there is no steady state errors associated with HSMC and ASMC although no friction compensations are applied. This demonstrates their learning capabilities. However, they use different approaches to learning. For the HSMC, a modified disturbance observer, which is factored by a tuning parameter of 0.8 in this case, is utilized to estimate external disturbances, such as friction, and then cancel it immediately. In this way, a steady state error of zero is obtained. Meanwhile, the root mean square of the tacking errors is well controlled, leading to a value of 0.8 μm. From Figure 6.3(g), it can be seen that the phase trajectory is bounded with the

sliding line. And thus the closed-loop system stayed in sliding mode, as is also indicated by Figure 6.3(h). For the ASMC, an adaptation was used to estimate external disturbances. The adaption mechanism kept learning in order to get a good estimate of disturbances. In this way, the influence of the external disturbances on tracking errors will be minimized. From Figure 6.3(e), it can be seen that the phase trajectory is largely bounded with the sliding surface because of the adaption procedure involved; this can be seen from the variation of switching function with time in Figure 6.3(f). From this figure, we can know that the switching function was dynamically approaching a steady state of zero, meaning the system will stay in sliding mode. It should be noted that, because of the adaptation mechanism, a good transient performance is often hard to guarantee.

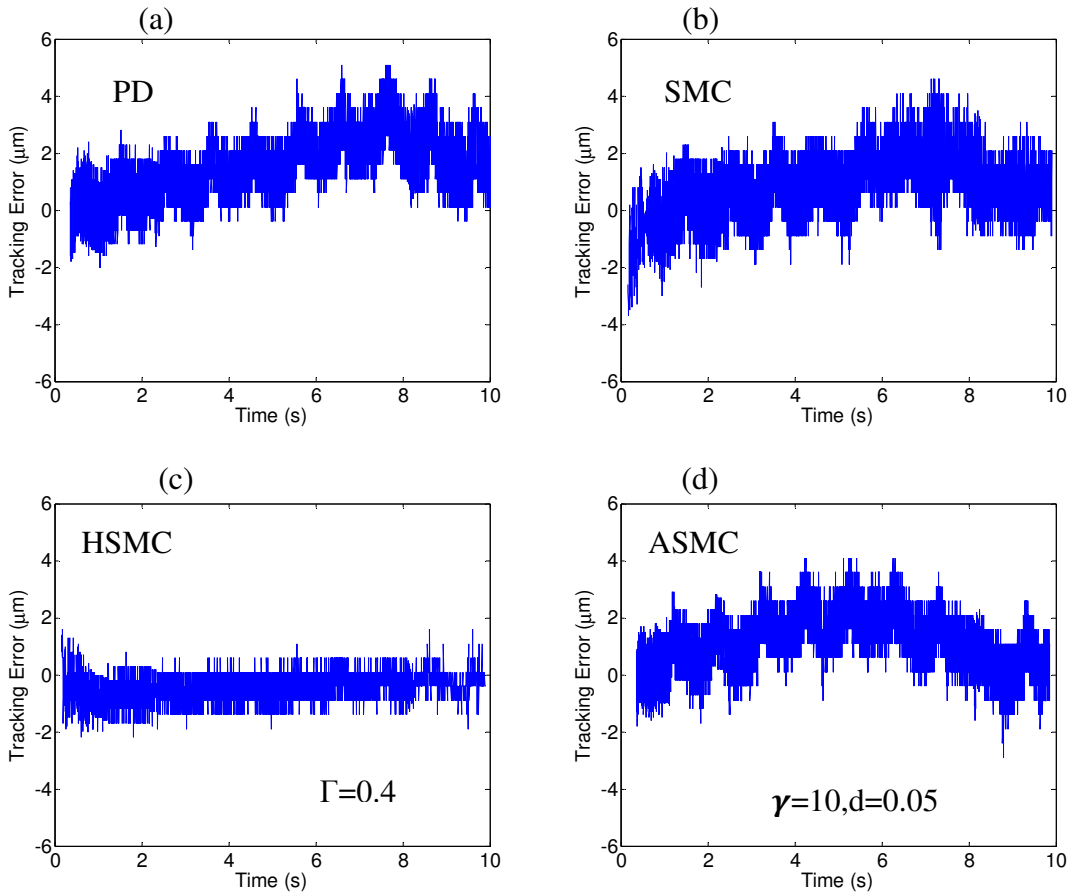

Figure 6.4 Tracking errors with friction compensation

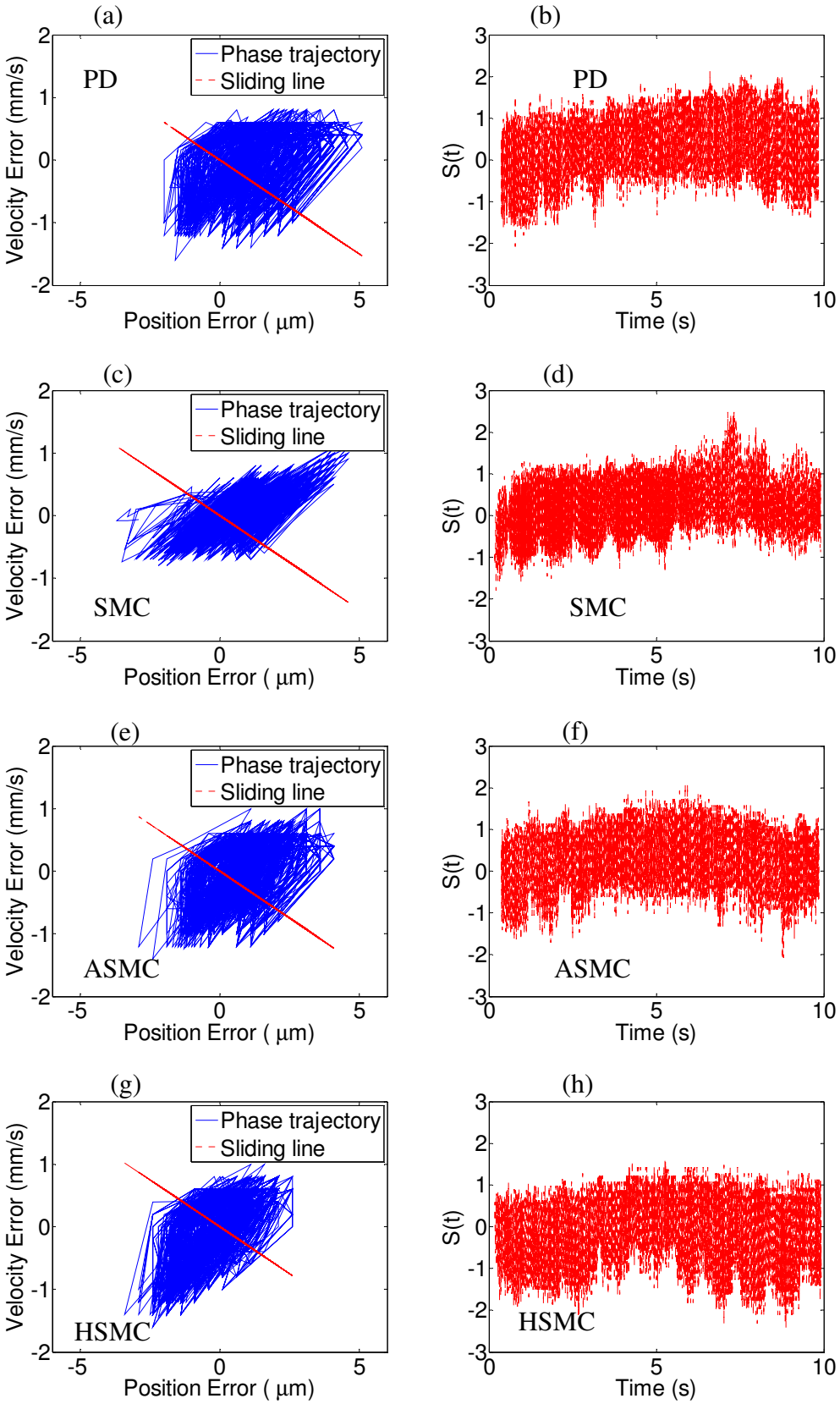

Figure 6.5 Sliding dynamics with friction compensation

The tracking errors for Set 2 are presented in Table 6.2. From this table, it can be seen that the tracking errors improved significantly over the non friction compensation cases for both PD and SMC. For the case of PD, the tracking error, in terms of the maximum tracking error, dropped from 12.6 μm to 5.1 μm, with a decrease of almost 60%; the root mean square of the tracking error declined almost 80%, from 9 μm to 2 μm. The experimental results for Set 2 are shown in Figures 6.4 and 6.5. When the feedfoward friction compensation was implemented, the phase trajectory was bounded to the sliding line, which is demonstrated in Figure 6.5 (a), and indicated by Figure 6.5(b) as well. Despite the significant improvement over the non friction compensation case, Figure 6.4(a) suggests the presence of a slight steady state error. This means that the friction model is not perfect although it is good enough. The slight steady state error is thus caused by the uncompensated friction component and other disturbances or model uncertainties. As for the PD controller, the implementation of feedfoward friction compensation SMC enhanced the tracking performance significantly. As can be seen from Table 6.2, there is a more than 56% decrease in terms of the maximum tracking error, from 10.6 μm to 4.6 μm. At the same time, the RMS of tracking error dropped over 70% to 1.7 μm. There is no steady state error associated with SMC although the friction model may not be perfect. This is because the discontinuous term is dealing with the uncompensated friction and other disturbances. Figure 6.5(c) shows the phase trajectory was bounded to the sliding line. Figure 6.5(d) shows that the switching function is able to achieve a steady state of zero.

The cases of HSMC and ASMC did not show improvements in tracking performance from the introduction of the feedfoward friction compensation. One possible reason is that the disturbance estimations are performed well enough for both cases so that friction compensation was not

providing any help. For ASMC, another possible reason for the lack of improvement is that the adaptation mechanism functioned without ceasing throughout even when a good tracking performance was already reached. From Figure 6.4(d), it can be seen that the tracking error was small enough at the very early stage of the cycle. Beyond that point, it will be desired that the adaptation be turned off to maintain this good performance. Since there is no mechanism for stopping adaptation for this case, the tracking error gradually increases until a point is reached beyond which the adaptation could improve the tracking performance. For HSMC, this may imply the existence of a better factor.

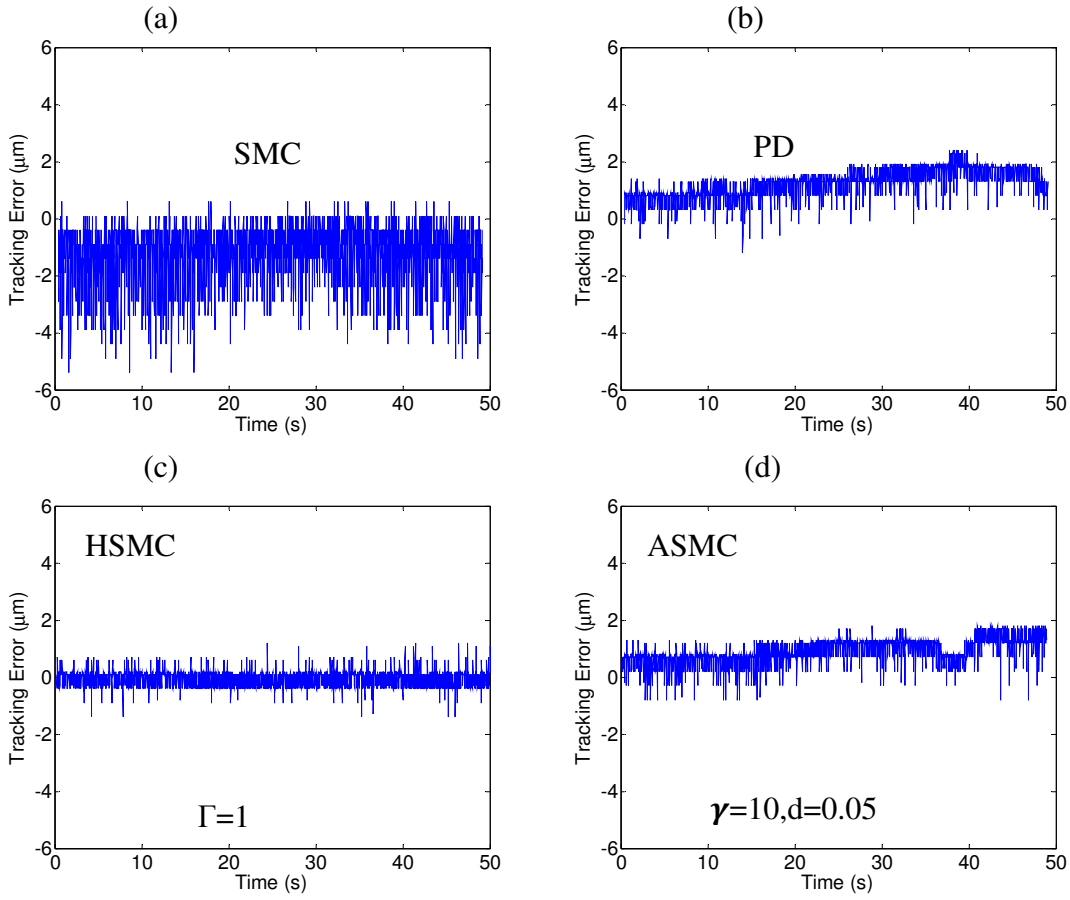

Figure 6.6 Tracking error for 0.1mms/ feed rate

The tracking errors are listed in Table 6.3 and shown in Figure 6.6 as well. From Table 6.3, it can be shown that the best controller for this experiment is HSMC, the second is the ASMC, the third is the PD, and the last one is SMC. However, the differences among the latter three are not significant. For the HSMC, the disturbance factor is determined to be one for the best performance, which is 0.3μm in terms of the RMS value, which is below the 0.5 μm resolution of the linear encoder. This means that HSMC is very effective in dealing with low-frequency disturbances such as stiction and force ripple.

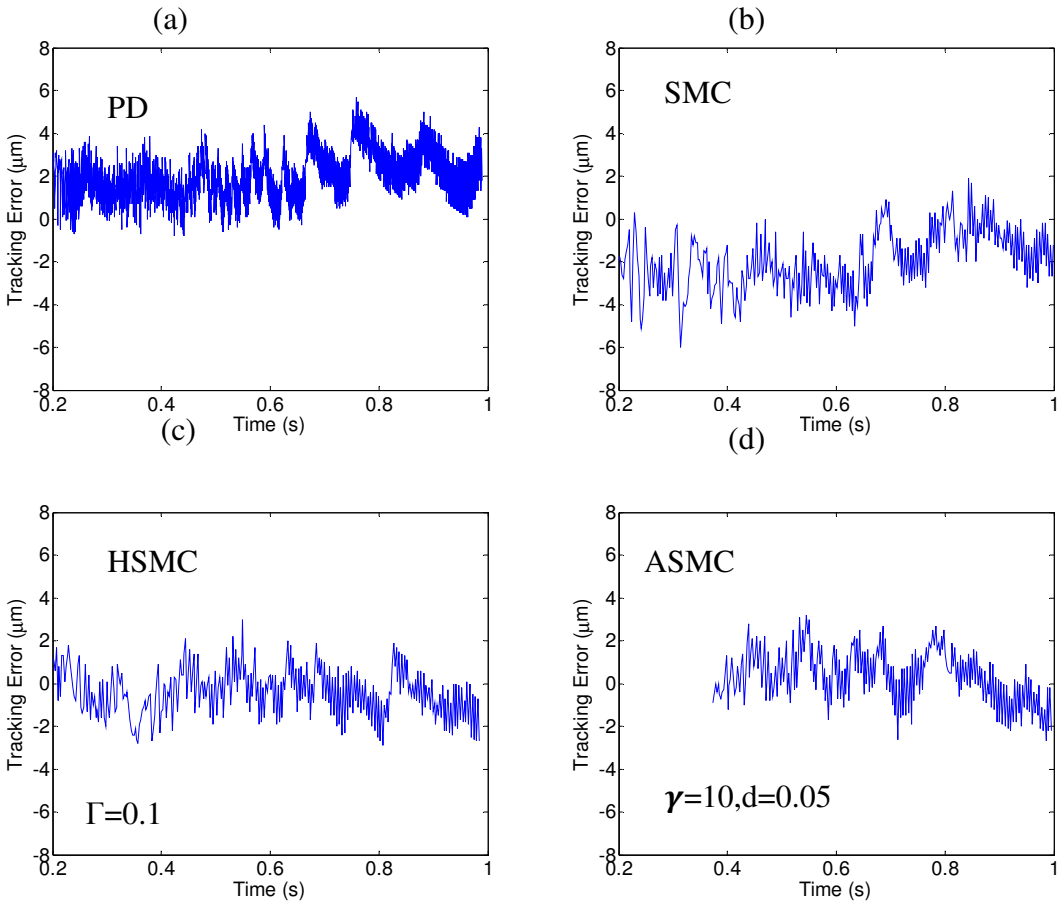

Figure 6.7 Tracking error for 100mms/ feed rate

Table 6.4 lists the tracking errors for Set 4. From this table, it can be seen that there are almost no differences between the tracking performances of HSMC and ASMC; in both of them the tracking errors are around $1\mu m$ in terms of the RMS value. This coincidence also happens for the cases of PD and SMC, for both of them the presence of steady state errors can be seen from Figure 6.7.

6.3 Comparative Experiments for Air Grinding

A step type response (an electrical signal) simulating grinding force is added at t = 5 s and removed at t = 6 s to test performance robustness for all of the four controllers. The experimental disturbance response is shown in Figure 6.8. From this figure, it can be seen that all controllers increased tracking error due to the existence of disturbance. With the exception of ASMC, feedfoward compensation is implemented. For the HSMC case, however, the influence of disturbance acts only at the time instances when the disturbance starts and stops, simulating points at which the grinding tool enters and leaves the workpiece. The controller resumes the normal tracking performance without undergoing any evident transient phase. For the PD case, there is an evident transient caused by the disturbance. Compared to the PD case, the transient response for ASMC is greatly improved but still exists. It can be seen from Figure 6.8 that the HSMC has the best tracking performance among all the three controllers. By employing the HSMC, the disturbance can be handled while minimizing chattering and without evident loss of the tracking performance.

Figure 6.9 shows the sliding dynamics in the course of the test. For the PD case, it can be seen that the presence of the simulated disturbance led the deviation of phase trajectory from the sliding line. By contrast, the ASMC controller managed to maintain the phase trajectory around the sliding line. For the HSMC case, the phase trajectory was not lying around the sliding line perfectly, which means the switching function is non zero. However, the value of the switching function is still the smallest overall among all the cases, which leads to the best tracking performance.

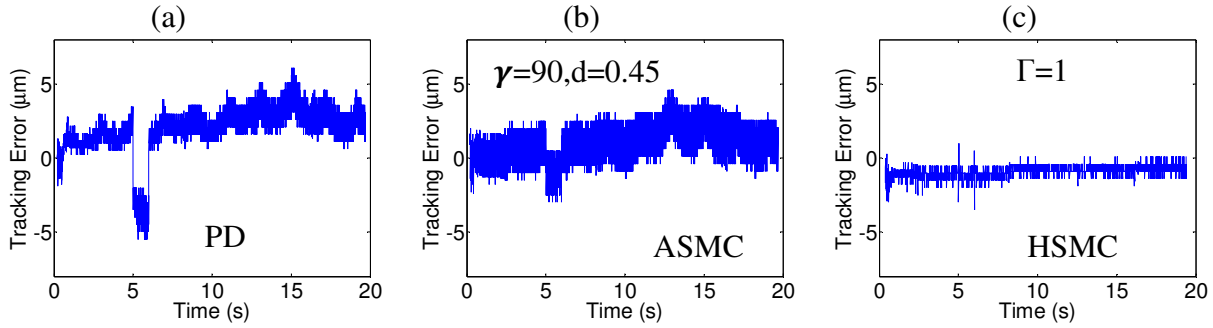

Figure 6.8 Tracking errors for air grinding tests

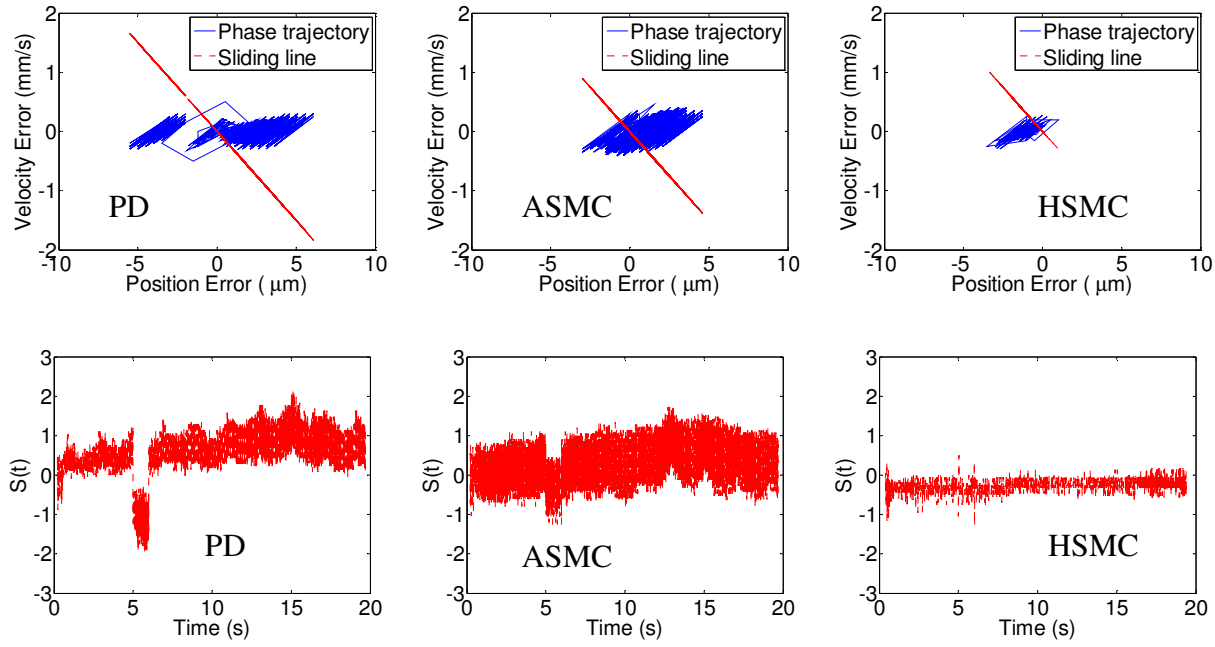

Figure 6.9 Sliding dynamics for air grinding tests

6.4 Grinding Experiments

The primary purpose of this part grinding test is to verify the control strategy's ability to maintain the desired positioning performance in the presence of grinding force disturbance. Only the HSMC controller will be tested, because it always has the best overall performance among all the controllers that we compared. Mild carbon steel ALSI 1018 is chosen for the test. The grinding wheel is a Norton tool specified as 32A80KVBE with a diameter of 14 inches and a width of 2 inches. Figures 6.10 shows the desired the trajectory and tracking errors for a feed rate of 1mm/s. It can be seen the majority of the tracking error lie between minus one micron and positive half a micron, which means that the algorithm worked very well in the presence of unmodeled grinding force.

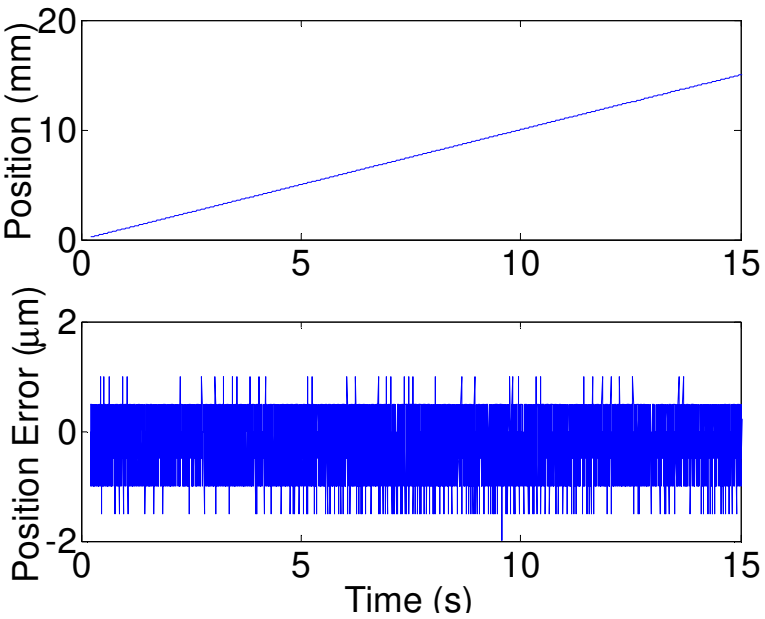

Figure 6.10 desired trajectory and tracking errors for a feed rate of 1mm/s

A feed rate of 5mm/s is commanded without friction compensation. Figure 6.11(a) shows the tracking errors. It is noticed there is a steady state error, which can be eliminated by tuning the DOB factor. Figure 6.11(b) shows the measured grinding force in three directions, where F_X

denotes tangential force, Fz denotes the normal force, and F_y denotes the force component perpendicular to both F_X and Fz .

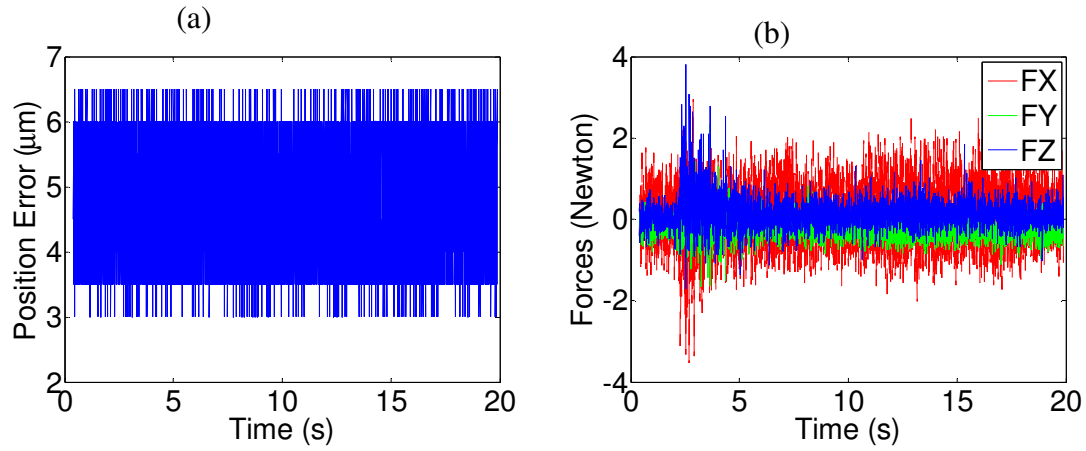

Figure 6.11 Grinding experiment with a feed rate of 5mm/s (Γ=1)

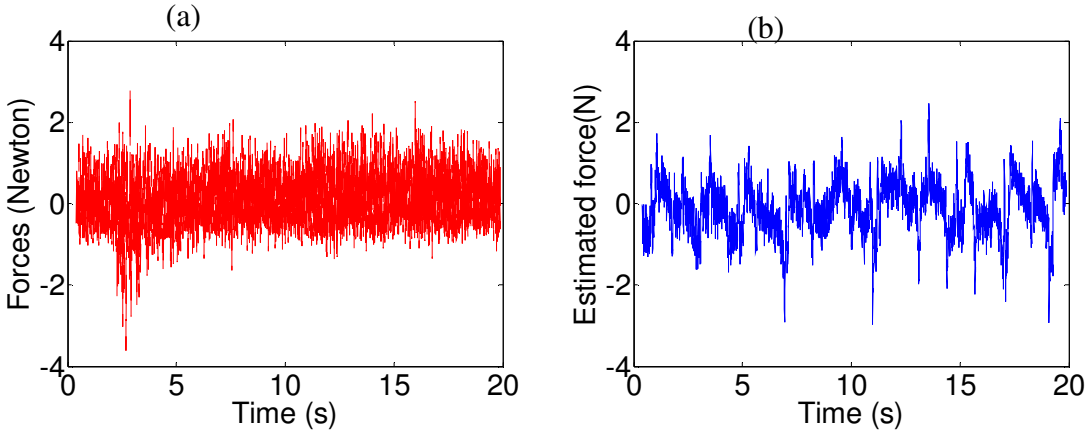

Figure 6.12 Grinding force in feed direction (a) measured (b) estimated using DOB

In HSMC, there is disturbance estimation mechanism using DOB. As discussed in Chapter 5, DOB can estimate lumped disturbance. Compared to non grinding case, the grinding case will have one more terms incorporated into its DOB output, which is grinding force in the feed direction. Hence, the discrepancy between the DOB output of grinding and that of non grinding case represents the grinding force in the feed direction. And therefore, a sensor-less grinding

force estimation can be realized by the DOB output. To verify this idea, a trajectory with a feed rate of 5mm/s was used for both non-grinding and grinding cases. The dynamometer and workpiece are mounted for both cases to ensure the same plant dynamics. We recorded the DOB output for both cases, and estimated the grinding force from their differences. It can be seen the estimated grinding force, as shown in Figure 6.12, can capture the grinding force reasonably well in this case. However, more works should be done to ensure that this sensor-less monitoring approach is reliable.

6.5 Summary

To validate the proposed control strategy, a linear motor feed drive test rig is fabricated and implemented on a surface grinding machine. A wide range of testing conditions has been pursued. Extensive comparative experimental tests were performed to validate the effectiveness and practicality of the proposed controller algorithm in a linear motor feed drive application for grinding machines. It was shown that the proposed control algorithm can achieve high tracking performance while attenuating friction and grinding force disturbances.

CHAPTER 7

CONCLUSIONS AND FUTURE WORK

7.1 Dissertation Overview

This dissertation presents a modeling and control methodology for the design of a CNC system to be implemented on grinding machines with linear motor feed drives. A comprehensive model of a linear motor feed drive for a class of grinding applications was suggested for a simulation study of the whole system; this model provided a basis for controller design. In this work, the LuGre dynamic friction model is used to capture not only observed static friction phenomena but also dynamic friction phenomena; such as the presliding displacement that is the prevailing friction phenomenon for high precision applications. Force ripple is also incorporated into the comprehensive model to examine its effect in smoothing the velocity output. An analytical modeling is either too complicated or it requires too many physical parameters, which are often not available to control engineers. In view of this, a simple but still very effective empirical model is utilized. To examine the effects of grinding force on the whole dynamics, an analytical grinding force model proposed by Hahn and Lindsay is employed. Both friction and force ripple model were validated.

A linear motor feed drive test rig was implemented on a surface grinding machine for experiments. It was found that the developed comprehensive model is too complicated and demanding for real time implementation. A simplified second order model with friction was

determined by system parameter identification via the step response and a series of constant velocity experiments.

This dissertation proposes a general robust motion control framework for the CNC design to achieve high speed/high precision as well as low speed/high precision. An application to the linear motor feed drives in grinding machines was carried out. One of the developed algorithms, HSMC, combines the merits of a reaching law based sliding mode control and a modified disturbance observer for precision tracking to address the practical issues of friction, force ripple, and grinding force disturbances. Another algorithm presented is ASMC, which combines the reaching law based sliding mode control with adaptive disturbance estimation to achieve an adaptive robust motion control.

To further validate the proposed control strategy, a linear motor feed drive test rig is fabricated and implemented on a surface grinding machine. A wide range of testing conditions has been pursued. Extensive comparative experimental tests were performed to validate the effectiveness and practicality of the proposed controller algorithm in linear motor feed drive application for grinding machines. It was shown that the proposed control algorithm can achieve high tracking performance while attenuating friction and grinding force disturbances.

7.2 Conclusions and Contributions

The contributions and conclusions from Chapter 3 are as follows:

- Developed a comprehensive model for the simulation study of the open-loop dynamics of liner motor feed drives for grinding machines.

- Friction behaviors under step input and sinusoidal input were investigated.
- It was found that the simulated position output is very close to that obtained for the bristle deflection in the stiction regime. This is not the case for macroscopic motion, though.
- The varying breakaway phenomena are captured by simulation. It has been found that larger force rate will result in a smaller breakaway point.
- To validate the force ripple model, the simulation result has been compared with the measured open velocity response of a linear motor motion system. The effectiveness of the model has been shown by obtaining good agreement between the simulation and the experimental results. The friction model has also been validated by the good agreements obtained between the simulation results and the measured response obtained by frequency domain identification on an electromechanical motion system.

Experimental setup and system parameter identifications were discussed in Chapter 4 and some of the contributions and conclusions are listed below.

- Since there are no commercially available linear motors driven grinding machines, a linear motor feed drive test rig was implemented on a surface grinding machine for this study and worked very well
- The friction model was validated by the feedfoward cancellation of the obtained friction model.

The controller design and experimental results are presented in Chapter 5 and Chapter 6, respectively, and some of the contributions and conclusions are listed below.

- The advantages of the developed HSMC are validated by a large variety of experiments
  - There is no steady state errors associated with HSMC although no friction compensation is applied.
  - The HSMC achieved a tracking error of $0.3\mu m$, which is below the linear encoder resolution in tracking a trajectory with a feed rate of 0.1mm/s.
- The advantages of the developed ASMC are also validated by a large variety of experiments
  - There is no steady state errors associated with ASMC although no friction compensations are applied.
  - The HSMC achieved good tracking performance by on-line learning of disturbance
- Grinding tests were performed with the HSMC
  - The grinding force did not show any evident effects on the tracking performance when the HSMC algorithm was used
  - Sensor-less monitoring was realized by using the DOB output information

7.3 Recommendations for Future Work

The research presented in this dissertation would aid in the CNC design for a linear motor feed drive for grinding machines. However, the developed modeling and control strategies are not

limited to grinding machines; they can be applied to general machine tools and extended to more general motion control. The effectiveness of the developed control algorithms are discussed and validated by a large variety of experiments. The trial-and-error tuning to get the optimal parameters for performance is required; this occurs for both HSMC and ASMC. To become a viable controller that can be implemented in CNC, a thorough and rigorous mathematical analysis is required to get a proper tuning rule.

Although the LuGre friction model was employed for the simulation study, it was not implemented. There are at least two reasons for this. First, the resolution of the linear encoder that was used is not fine enough to capture the dynamics in the presliding regime. Second, LuGre includes a dynamics for immeasurable state and is therefore too computationally demanding, due to the computational limit of the DSP that was used, which is a dSPACE1102 marketed a decade ago. In these years, we have seen the revolution in computer technology. New DSPs provide powerful computational capacities for real-time implementation of control algorithms. Likewise, force ripple compensation can also be performed on more powerful DSP. Another way to reduce force ripple is to employ sinusoidal computation instead of the six-step commutation used here.

The developed control algorithms are state-space based, for the implementation of which a velocity signal is required. When a velocity sensor is not available, a finite difference method was utilized to get velocity information; however, a high frequency noise is resulted from this action. To avoid a direct derivative, a Luenberger type state observer could be utilized to get velocity information for feedback.

In this study, the dynamics coupling between the infeed motion and the grinding force dynamics was not considered. This should be considered to avoid the occurrences of the chattering phenomena.

For grinding application, only tracking performance is tested. This is inadequate because our ultimate goal is to improve quality to which many factors contribute. To gain a thorough understanding of the developed control algorithms, the product quality, such as surface finish, should be compared among different controllers.

Both HSMC and ASMC can estimate disturbances, from which useful process parameters such as grinding information can be derived. And therefore, sensor-less process monitoring can be realized. To obtain reliable sensor-less monitoring, many experiments should be performed to find the correlation between estimated disturbances and measured grinding forces.

The implementation of the above improvements would result in an improvement in tracking performances; they will also aid the controllers to gain reliable grinding process knowledge and therefore facilitate the sensor-less force monitoring.

REFERENCES

Aerotech, I. (2000). BA10/20/30 series user's manual

Aerotech, I. (2002). "U" channel linear motors user's manual.

Aerotech, I. (2006). ALS20000 / ALS25000 Series Stage.

Alter, D. M. and T. Tsu-Chin (1996). "Control of linear motors for machine tool feed drives: design and implementation of H infinity optimal feedback control." Transactions of the ASME. Journal of Dynamic Systems, Measurement and Control **118**(4): 649-56.

Alter, D. M. and T. Tsu-Chin (1998). "Control of linear motors for machine tool feed drives: experimental investigation of optimal feedforward tracking control." Transactions of the ASME. Journal of Dynamic Systems, Measurement and Control **120**(1): 137-41.

Altintas, Y., K. Erkorkmaz and W. H. Zhu (2000). "Sliding mode controller design for high speed feed drives." CIRP Annals - Manufacturing Technology **49**(1): 265-270.

Armstrong-Hâelouvry, B. (1991). *Control of machines with friction*. Boston, Kluwer Academic Publishers.

Armstrong-Helouvry, B. (1991). *Control of machines with friction*, Kluwer Academic Publishers.

Armstrong-Helouvry, B., P. Dupont and C. Canudas De Wit (1994). "A survey of models, analysis tools and compensation methods for the control of machines with friction." Automatica **30**(7): 1083-138.

Bhateja, C. and R. Lindsay (1982). Grinding, theory, techniques, and troubleshooting. Dearborn, Mich., Society of Manufacturing Engineers, Marketing Services Dept.

Boldea, I. and S. A. Nasar (1997). *Linear electric actuators and generators*. Cambridge ; New York, Cambridge University Press.

Boucher, P., D. Dumur and A. U. Ehrlinger (1990). "Generalized predictive cascade control (GPCC) for machine tools drives." Annals of the CIRP **39**: 357-360.

Boucher, P., D. Dumur and H. P. Kurzweil (1993). "Polynomial-predictive functional control (PPFC) for motor drives." CIRP Annals **42**(1): 453-456.

Byrne, G., D. Dornfeld and B. Denkena (2003). "Advancing cutting technology." CIRP Annals - Manufacturing Technology **52**(2): 483-507.

Canudas de Wit, C., H. Olsson, K. J. Astrom and P. Lischinsky (1995). "A new model for control of systems with friction." IEEE Transactions on Automatic Control **40**(3): 419-25.

Choi, C. and T.-C. Tsao (2005). "Control of linear motor machine tool feed drives for end milling: Robust MIMO approach." Mechatronics **15**(10): 1207-1224.

Corless, M. J. and G. Leitmann (1981). "Continuous state feedback guaranteeing uniform ultimate boundedness for uncertain dynamic systems." IEEE Transactions on Automatic Control **AC-26**(5): 1139-44.

Dahl, P. R. (1976). "Solid friction damping of mechanical vibrations." AIAA Journal **14**(12): 1675-82.

De Wit, C. C. and P. Lischinsky (1997). "Adaptive friction compensation with partially known dynamic friction model." International Journal of Adaptive Control and Signal Processing **11**(1): 65-80.

DeCarlo, R. A., S. H. Zak and G. P. Matthews (1988). "Variable structure control of nonlinear multivariable systems: a tutorial." Proceedings of the IEEE **76**(3): 212-32.

Denkena, B., H. K. Tonshoff, X. Li, J. Imiela and C. Lapp (2004). "Analysis and control/monitoring of the direct linear drive in end milling." International Journal of Production Research **42**(24): 5149-66.

Dorf, R. C. and R. H. Bishop (2001). *Modern control systems*. Upper Saddle River, NJ, Prentice Hall.

Doyle, J. C., B. A. Francis and A. Tannenbaum (1992). *Feedback control theory*. New York, Macmillan Pub. Co. .

Drazenovic, B. (1969). "The invariance conditions in variable structure systems." Automatica **5**: 9.

Dumur, D. and P. Boucher (1994). "New predictive solutions to very high speed machining." CIRP Annals **43**(1): 363-366.

Dumur, D., P. Boucher and A. U. Ehrlinger (1996). "Constrained predictive control for motor drives." CIRP Annals - Manufacturing Technology **45**(1): 355-358.

Edwards, C. and S. K. Spurgeon (1998). *Sliding mode control : theory and applications*. London, Taylor & Francis.

Elfizy, A. T., G. M. Bone and M. A. Elbestawi (2004). "Model-based controller design for machine tool direct feed drives." International Journal of Machine Tools & Manufacture **44**(5): 465-77.

Elmali, H. and N. Olgac (1992). "Sliding mode control with perturbation estimation (SMCPE): a new approach." International Journal of Control **56**(4): 923-41.

Erkorkmaz, K. and Y. Altintas (2001). "High speed CNC system design. Part I: Jerk limited trajectory generation and quintic spline interpolation." International Journal of Machine Tools and Manufacture **41**(9): 1323-1345.

Friedland, B. (1996). *Advanced control system design*. Englewood Cliffs, N.J., Prentice Hall.

Futami, S., A. Furutani and S. Yoshida (1990). "Nanometer positioning and its micro-dynamics." Nanotechnology **1**(1): 31-7.

Gao, W., S. Dejima, H. Yanai, K. Katakura, S. Kiyono and Y. Tomita (2004). "A surface motor-driven planar motion stage integrated with an surface encoder for precision positioning." Precision Engineering **28**(3): 329-337.

Gao, W. and J. C. Hung (1993). "Variable structure control of nonlinear systems: a new approach." IEEE Transactions on Industrial Electronics **40**(1): 45-55.

Green, M. and D. J. N. Limebeer (1995). *Linear robust control*. Englewood Cliffs, N.J., Prentice Hall.

Hensen, R. H. A., M. R. J. G. Van De Molengraft and M. Steinbuch (2002). "Frequency domain identification of dynamic friction model parameters." IEEE Transactions on Control Systems Technology **10**(2): 191-196.

Hung, J. Y., W. Gao and J. C. Hung (1993). "Variable structure control: a survey." IEEE Transactions on Industrial Electronics **40**(1): 2-22.

Inasaki, I. (1999). "Surface grinding machine with a linear-motor-driven table system: development and performance test." CIRP Annals - Manufacturing Technology **48**(1): 243-246.

Ioannou, P. A. and J. Sun (1996). *Robust adaptive control*. Upper Saddle River, NJ, PTR Prentice-Hall.

Kalpakjian, S. (2001). *Manufacturing engineering and technology*. Upper Saddle River, NJ, Prentice Hall.

Karnopp, D. (1985). "Computer simulation of stick-slip friction in mechanical dynamic systems." Journal of Dynamic Systems, Measurement and Control, Transactions ASME **107**(1): 100-103.

Kawamura, A., H. Itoh and K. Sakamoto (1994). "Chattering reduction of disturbance observer based sliding mode control." IEEE Transactions on Industry Applications **30**(2): 456-61.

Khalil, H. K. (2002). *Nonlinear systems*. Upper Saddle River, NJ, Prentice Hall.

Kistler. (2007). "Cutting force measurement." from http://www.kistler.com, 11/2007.

Kopac, J. and P. Krajnik (2006). "High-performance grinding-A review." Journal of Materials Processing Technology **175**(1-3): 278-284.

Koren, Y. (1997). "Control of machine tools." Journal of Manufacturing Science and Engineering, Transactions of the ASME **119**(4(B)): 749-755.

Koren, Y. and C. C. Lo (1992). "Advanced controllers for feed drives." CIRP Annals **41**(2): 689-698.

Krstiâc, M., I. Kanellakopoulos and P. V. Kokotoviâc (1995). *Nonlinear and adaptive control design*. New York, Wiley.

Kwon, S. and W. K. Chung (2002). "A robust tracking controller design with hierarchical perturbation compensation." Journal of Dynamic Systems, Measurement and Control, Transactions of the ASME **124**(2): 261-271.

Lampaert, V., J. Swevers and F. Al-Bender (2004). Comparison of model and non-model based friction compensation techniques in the neighbourhood of pre-sliding friction, Boston, MA, USA, IEEE.

Lee, H. S. and M. Tomizuka (1996). "Robust motion controller design for high-accuracy positioning systems." IEEE Transactions on Industrial Electronics **43**(1): 48-55.

Liang, S. Y., R. L. Hecker and R. G. Landers (2004). "Machining process monitoring and control: The state-of-the-art." Journal of Manufacturing Science and Engineering, Transactions of the ASME **126**(2): 297-310.

Ljung, L. (1999). *System identification : theory for the user*. Upper Saddle River, NJ, Prentice Hall PTR.

Malkin, S. (1989). *Grinding technology : theory and applications of machining with abrasives*. Chichester, New York, E. Horwood ;J. Wiley.

Marinescu, I. D. (2004). *Tribology of abrasive machining processes*. Norwich, NY, William Andrew Pub.

Marinescu, I. D. (2007). *Handbook of machining with grinding wheels*. Boca Raton, FL, CRC / Taylor & Francis Group.

McLean, G. W. (1988). "Review of recent progress in linear motors." IEE Proceedings, Part B: Electric Power Applications **135**(6): 380-416.

Murakami, T. and K. Ohnishi (1990). Advance motion control in mechatronics-a tutorial, Istanbul, Turkey, IEEE.

Ninness, B. and G. C. Goodwin (1995). "Estimation of model quality." Automatica **31**(12): 1771-1797.

Ogata, K. (1992). *System dynamics*. Englewood Cliffs, N.J., Prentice-Hall.

Ohnishi, K., M. Shibata and T. Murakami (1996). "Motion control for advanced mechatronics." IEEE/ASME Transactions on Mechatronics **1**(1): 56-67.

Olsson, H., K. J. Astrom, C. Canudas de Wit, M. Gafvert and P. Lischinsky (1998). "Friction models and friction compensation." European Journal of Control **4**(3): 176-95.

Otten, G., T. J. A. de Vries, J. van Amerongen, A. M. Rankers and E. W. Gaal (1997). "Linear motor motion control using a learning feedforward controller." IEEE/ASME Transactions on Mechatronics **2**(3): 179-187.

Pritschow, G. (1998). "Comparison of linear and conventional electromechanical drives." CIRP Annals - Manufacturing Technology **47**(2): 541-548.

Pritschow, G., Y. Altintas, F. Jovane, Y. Koren, M. Mitsuishi, S. Takata, H. Van Brussel, M. Weck and K. Yamazaki (2001). "Open controller architecture - Past, present and future." CIRP Annals - Manufacturing Technology **50**(2): 463-470.

Radke, A. and Z. Gao (2006). A survey of state and disturbance observers for practitioners, Minneapolis, MN, United States, Institute of Electrical and Electronics Engineers Inc., Piscataway, NJ 08855-1331, United States.

Ro, P. I. and P. I. Hubbel (1993). "Model reference adaptive control of dual-mode micro/macro dynamics of ball screws for nanometer motion." Journal of Dynamic Systems, Measurement and Control, Transactions of the ASME **115**(1): 103-108.

Ro, P. I., W. Shim and S. Jeong (2000). "Robust friction compensation for submicrometer positioning and tracking for a ball-screw-driven slide system." Precision Engineering **24**(2): 160-173.

Schrijver, E. and J. van Dijk (2002). "Disturbance observers for rigid mechanical systems: equivalence, stability, and design." Transactions of the ASME. Journal of Dynamic Systems, Measurement and Control **124**(4): 539-48.

Schuffenhauer, U. (1996). Path control of a linear direct drive for the submicrometer-range, Bremen, Germany, AXON Technologie Consult GmbH.

Siemens. (2007). "Linear Motor Direct drive." from http://www2.sea.siemens.com, 11/2007.

Slocum, A. H. (1992). *Precision machine design*. Englewood Cliffs, N.J., Prentice Hall.

Slotine, J.-J. E. and W. Li (1988). "Adaptive manipulator control: A case study." IEEE Transactions on Automatic Control **33**(11): 995-1003.

Slotine, J. J. E. and J. A. Coetsee (1986). "Adaptive sliding controller synthesis for non-linear systems." International Journal of Control **43**(6): 1631-51.

Slotine, J. J. E. and W. Li (1991). *Applied nonlinear control*. Englewood Cliffs, N.J., Prentice Hall.

Slotine, J. J. E. and L. Weiping (1989). "Composite adaptive control of robot manipulators." Automatica **25**(4): 509-19.

Srinivasan, K. and P. K. Kulkarni (1990). "Cross-coupled control of biaxial feed drive servomechanisms." Journal of Dynamic Systems, Measurement and Control, Transactions ASME **112**(2): 225-232.

Srinivasan, K. and T. C. Tsao (1997). "Machine tool feed drives and their control-a survey of the state of the art." Transactions of the ASME. Journal of Manufacturing Science and Engineering **119**(4B): 743-8.

Tan, K. K., S. N. Huang and T. H. Lee (2002). "Robust adaptive numerical compensation for friction and force ripple in permanent-magnet linear motors." IEEE Transactions on Magnetics **38**(1 II): 221-228.

Toenshoff, H. K., B. Karpuschewski, T. Mandrysch and I. Inasaki (1998). "Grinding process achievements and their consequences on machine tools challenges and opportunities." CIRP Annals - Manufacturing Technology **47**(2): 651-668.

Tomizuka, M. (1987). "Zero phase error tracking algorithm for digital control." Transactions of the ASME. Journal of Dynamic Systems, Measurement and Control **109**(1): 65-8.

Tung, E. D., G. Anwar and M. Tomizuka (1993). "Low velocity friction compensation and feedforward solution based on repetitive control." Journal of Dynamic Systems, Measurement and Control, Transactions of the ASME **115**(2A): 279-284.

Tung, E. D. and M. Tomizuka (1993). "Feedforward tracking controller design based on the identification of low frequency dynamics." Transactions of the ASME. Journal of Dynamic Systems, Measurement and Control **115**(3): 348-56.

Tung, E. D., Y. Urushisaki and M. Tomizuka (1993). Low velocity friction compensation for machine tool feed drives, San Francisco, CA, USA, American Autom. Control Council.

Umeno, T. and Y. Hori (1991). "Robust speed control of DC servomotors using modern two degrees-of-freedom controller design." IEEE Transactions on Industrial Electronics **38**(5): 363-8.

Umeno, T., T. Kaneko and Y. Hori (1993). "Robust servosystem design with two degrees of freedom and its application to novel motion control of robot manipulators." IEEE Transactions on Industrial Electronics **40**(5): 473-85.

Utkin, V. I. (1977). "Variable structure systems with sliding modes." IEEE Transactions on Automatic Control **AC-22**(2): 212-22.

Utkin, V. I., J. Guldner and C.-h. Shih (1999). *Sliding mode control in electromechanical systems*. London ; Philadelphia, PA, Taylor & Francis.

Van Brussel, H. and P. Van den Braembussche (1998). "Robust control of feed drives with linear motors." CIRP Annals - Manufacturing Technology **47**(1): 325-328.

Van den Braembussche, P., J. Swevers and H. Van Brussel (2001). "Design and experimental validation of robust controllers for machine tool drives with linear motor." Mechatronics **11**(5): 545-562.

Van Den Braembussche, P., J. Swevers, H. Van Brussel and P. Vanherck (1996). "Accurate tracking control of linear synchronous motor machine tool axes." Mechatronics **6**(5): 507-521.

Webster, J. and M. Tricard (2004). "Innovations in abrasive products for precision grinding." CIRP Annals - Manufacturing Technology **53**(2): 597-617.

Weck, M. and G. Ye (1990). "Sharp Corner Tracking Using the IKF Control Strategy." CIRP Annals - Manufacturing Technology **39**(1): 437-441.

Weidner, C. and D. Quickel (1999). "High-speed machining with linear motors." Manufacturing Engineering **122**(3): 80-90.

Wikipedia. (2007). "Linear motor." from http://en.wikipedia.org, 11/2007.

Xie, Q., S. Y. Liang and R. Chen (2006). "Modelling of linear motor feed drives for grinding machines." International Journal of Manufacturing Research **1**(1): 41-58.

Yang, S. and M. Tomizuka (1988). "Adaptive pulse width control for precise positioning under the influence of stiction and Coulomb friction." Journal of Dynamic Systems, Measurement and Control, Transactions ASME **110**(3): 221-227.

Yao, B., M. Al-Majed and M. Tomizuka (1997). "High-performance robust motion control of machine tools: An adaptive robust control approach and comparative experiments." IEEE/ASME Transactions on Mechatronics **2**(2): 63-76.

Yao, B. and L. Xu (2002). "Adaptive robust motion control of linear motors for precision manufacturing." Mechatronics **12**(4): 595-616.

Youcef-toumi, K. and S. Reddy (1992). "Analysis of Linear Time Invariant Systems With Time Delay." Journal of Dynamic Systems Measurement and Control-Transactions of the Asme **114**(4): 544-555.

Young, K. D., V. I. Utkin and U. Ozguner (1999). "A control engineer's guide to sliding mode control." IEEE Transactions on Control Systems Technology **7**(3): 328-42.

Zames, G. (1996). "Input output feedback stability and robustness, 1959-85." IEEE Control Systems Magazine **16**(3): 61-66.

Zhou, K. and J. C. Doyle (1998). *Essentials of robust control*. Upper Saddle River, N.J., Prentice Hall.